Nonlinear network wave equations : periodic solutions and graph characterizations

Imene Khames

Normandie Université

THESE

Pour obtenir le diplôme de doctorat

Spécialité Mathématiques

Préparée au sein de l'Institut National des Sciences Appliquées de Rouen Normandie

Nonlinear Network Wave Equations: Periodic Solutions and Graph Characterizations

Présentée et soutenue par
Imene KHAMES

Thèse soutenue publiquement le 27 septembre 2018 devant le jury composé de		
Mme. Irene SCIRIHA	Professeur, University of Malta	Rapporteur
M. Mads-Peter SØRENSEN	Professeur, Technical University of Denmark	Rapporteur
M. Jean-Guy CAPUTO	Maître de conférences HDR, INSA Rouen Normandie	Directeur de thèse
M. Arnaud KNIPPEL	Maître de conférences, INSA Rouen Normandie	Co-Encadrant de thèse
M. Aziz ALAOUI	Professeur, Université du Havre Normandie	Examinateur
M. Panayotis PANAYOTAROS	Professeur, Universidad Nacional Autónoma de México	Examinateur
M. Christophe PICOULEAU	Professeur, Conservatoire National des Arts et Métiers	Examinateur

Thèse dirigée par M. Jean-Guy CAPUTO et co-encadrée par M. Arnaud KNIPPEL, Laboratoire de Mathématiques de l'INSA de Rouen Normandie - LMI (EA 3226)

INSA INSTITUT NATIONAL DES SCIENCES APPLIQUÉES ROUEN

MIIΣ

LMI - EA 3226

Cette thèse fait partie du projet XTerM (Systèmes compleXes, Intelligence Territoriale et Mobilité) cofinancé par l'Union Européenne à travers le Fonds Européen de Développement Régional (FEDER) et par la Région Normandie.

Résumé:

Dans cette thèse, nous étudions les équations d'ondes non-linéaires discrètes dans des réseaux finis arbitraires. C'est un modèle général, où le Laplacien continue est remplacé par le Laplacien de graphe. Nous considérons une telle équation d'onde avec une non-linéarité cubique sur les nœuds qui est le modèle Φ^4 discret, décrivant un réseau mécanique d'oscillateurs non-linéaires couplés ou un réseau électrique où les composants sont des diodes ou des jonctions Josephson. L'équation d'onde linéaire est bien comprise en termes de modes normaux, ce sont des solutions périodiques associées aux vecteurs propres du Laplacien de graphe. Notre premier objectif était d'étudier la continuation des modes normaux dans le régime non-linéaire et le couplage des modes en présence de la non-linéarité. Nous montrons que, en inspectant les modes normaux du Laplacien de graphe, nous identifions ceux qui peuvent être étendus à des orbites périodiques non-linéaires, pour l'équation Φ^4 discrète. Les modes normaux -dont les vecteurs propres du Laplacien sont composés uniquement de $\{1\}$, $\{+1,-1\}$ or $\{+1,-1,0\}$- donnent lieu à des orbites périodiques non-linéaires. Nous effectuons systématiquement une analyse de stabilité linéaire (Floquet) de ces orbites et montrons le couplage des modes lorsque l'orbite est instable. Ensuite, nous caractérisons les graphes ayant des vecteurs propres du Laplacien dans $\{+1,-1\}$ et $\{+1,-1,0\}$, en utilisant la théorie spectrale des graphes. Dans la deuxième partie, nous étudions des solutions périodiques localisées exponentiellement (spatialement), résultant de l'interaction entre la non-linéarité et la discrétisation. En supposant une condition initiale de grande amplitude localisée sur un nœud du graphe, nous approchons son évolution par l'équation de Duffing. Le reste du réseau satisfait un système linéaire forcé par le nœud excité. Cette approximation est validée en réduisant l'équation Φ^4 discrète à l'équation de Schrödinger non-linéaire discrète et par l'analyse de Fourier. Les résultats de cette thèse relient la dynamique non-linéaire à la théorie spectrale des graphes.

This thesis is part of the XTerM project, co-financed by the European Union with the European Regional Development Fund and by the Normandie Regional Council.

Abstract:

In this thesis, we study the discrete nonlinear wave equations in arbitrary finite networks. This is a general model, where the usual continuum Laplacian is replaced by the graph Laplacian. We consider such a wave equation with a cubic on-site nonlinearity which is the discrete Φ^4 model, describing a mechanical network of coupled nonlinear oscillators or an electrical network where the components are diodes or Josephson junctions. The linear graph wave equation is well understood in terms of normal modes, these are periodic solutions associated to the eigenvectors of the graph Laplacian. Our first goal was to investigate the continuation of normal modes in the nonlinear regime and the modes coupling in the presence of nonlinearity. We show that, inspecting the normal modes of the graph Laplacian, we identify which ones can be extended into nonlinear periodic orbits, for the discrete Φ^4 equation. Normal modes -whose Laplacian eigenvectors are composed uniquely of $\{1\}$, $\{+1,-1\}$ or $\{+1,-1,0\}$- give rise to nonlinear periodic orbits. We perform a systematic linear stability (Floquet) analysis of these orbits and show the modes coupling when the orbit is unstable. Then, we characterize graphs having Laplacian eigenvectors in $\{+1,-1\}$ and $\{+1,-1,0\}$, using graph spectral theory. In the second part, we investigate periodic solutions that are exponentially (spatially) localized, arising from the interplay between nonlinearity and discreteness. Assuming a large amplitude localized initial condition on one node of the graph, we approximate its evolution by the Duffing equation. The rest of the network satisfies a linear system forced by the excited node. This approximation is validated by reducing the discrete Φ^4 equation to the discrete nonlinear Schrödinger equation and by Fourier analysis. The results of this thesis relate nonlinear dynamics to graph spectral theory.

Acknowledgments

The completion of this doctoral thesis would not have been possible without the support of several people for whom I would like to express my sincere gratitude.

My deepest appreciation goes to my thesis committee members, the referees: Prof. Irene SCIRIHA and Prof. Mads-Peter SØRENSEN; and the examiners: Prof. Aziz ALAOUI, Prof. Panayotis PANAYOTAROS and Prof. Christophe PICOULEAU. Thank you for spending time reading, reviewing and commenting my work. It is my honor to present my work to you.

I am extremely grateful to my Ph.D. advisors Prof. Jean-Guy CAPUTO and Prof. Arnaud KNIPPEL for their patience, availability, continuous support, consistent encouragement, suggestions and productive ideas. Your valuable guidance helped me in all the time of research and in writing this thesis. It was and it will always be an honor to work with you.

The thesis would not come to a successful completion, without the collaborations with Prof. Alejandro ACEVES and Prof. Panayotis PANAYOTAROS. I gained a lot from you, through your scientific interactions and valuable suggestions.

A very special gratitude goes to all the members of "Laboratoire de Mathématiques de l'INSA Rouen Normandie (LMI)". Special acknowledgments to Prof. Nicolas FORCADEL and Prof. Christian GOUT, the directors of LMI, for their welcome, availability and support. I am grateful to Ms. Brigitte DIARRA, the secretary of LMI and to Prof. Carole LE GUYADER. Thank you for your availability, advice, help, support and kindness. In addition, I express a special thanks to the Ph.D. students of LMI who shared this experience with me. Noémie and Yahao, thanks a lot for your listening, encouragement, help and kindness.

Lastly and most importantly, a special thanks to my family. Words cannot express how grateful I am to my grandparents "Benyebka and Kheira" for all their unconditional love and continuous encouragement.
To the memory of my mother, I dedicate this thesis.

Contents

Introduction

This thesis is devoted to the study of complex systems, in particular nonlinear dynamical systems on networks. These are systems of nonlinear ordinary differential equations (ODEs) represented on graphs where the nodes are the components and the edges their interactions. Discreteness and nonlinearity are inherent to many systems in nature *e.g.* Josephson junction arrays, optical waveguides, diodes coupled by inductances and molecular crystals, to name some. Historically when studying discrete models, comparisons are regularly made with related continuum models. These comparisons go both ways; one can think of network nonlinear equations as discretizations of nonlinear partial differential equations (PDEs). Similarly, a nonlinear PDE may be seen as an approximation of a network model when one considers slow variations along the discrete variables.

In the linear theory, Newton's second law for coupled harmonic oscillators leads to the graph wave equation where the standard continuous Laplacian is replaced by the graph Laplacian. This formulation is very useful because the graph Laplacian is a symmetric matrix, so that its eigenvalues are real and we can choose a basis of orthogonal eigenvectors. It is then natural to describe the dynamics of the network by projecting it on a basis of the eigenvectors, which reduces the dynamical equations to an eigenvalue problem. This parallels Fourier transform in continuum systems, and gives rise to orbits (phase curves) which are time-periodic, also called normal modes. These are bound states of the Hamiltonian which is a quadratic, symmetric function of positions and velocities. Because of the orthogonality, normal modes do not couple and the harmonic theory is well understood and can be analyzed in terms of normal modes, by using their linear combinations.

However, when nonlinearity is present in the equations of motion, normal modes will couple. Natural questions are: how do they couple? Is there any trace of them in the nonlinear regime? We investigate which normal modes of the linear theory can or cannot be extended to the full nonlinear theory. This study leads us to consider the theory of graph spectra. The possibility of continuing normal modes into nonlinear periodic orbits (nonlinear normal modes) depends on whether the nonlinearity is on-site (on nodes) as in the discrete Φ^4 model or intersite (on edges) as in the Fermi-Pasta-Ulam model. This study leads us to ask: what kind of graph admits Laplacian eigenvectors yielding nonlinear normal modes ?

Coupled nonlinear oscillators can give rise to another type of periodic vibrations that are typically exponentially (spatially) localized solutions. These are labeled "intrinsic localized modes" and come from the interplay between nonlinearity and discreteness. It is important to ask: how can we approximate this type of nonlinear periodic solutions?

In the literature, nonlinear normal modes and localized modes in discrete models are studied in the particular case of lattices. The contribution of this thesis consist of the study of nonlinear normal modes and localized modes in general networks of arbitrary topology, by the formulation of the discrete models using the graph Laplacian, this leads to relate the nonlinear dynamics to the graph spectral theory.

The thesis is organized as follows:

In the introductory chapter 1, we recall how conservation laws lead to the graph wave equation. This is illustrated in two different physical contexts: a network of inductances and capacities and its equivalent mechanical analogue represented by masses and springs.

In Chapter 2, we consider the nonlinear graph wave equation with a cubic on-site nonlinearity (the discrete Φ^4 model) and show that inspecting the normal modes of the graph Laplacian, we can identify which ones extend into nonlinear periodic orbits. Three different types of periodic orbits were found, the monovalent (the so-called Goldstone) mode that exists in all graphs, and what we call bivalent and trivalent modes, depending on whether the corresponding eigenvectors are composed of 1 or $-1, +1$ or $-1, 0, +1$ (respectively). Then, we perform a systematic linear stability (Floquet) analysis of these orbits and show how a small nonlinearity will couple the normal modes when the orbit is unstable. Later, we consider the nonlinear graph wave equation with a cubic intersite nonlinearity (the FPU model) and show that in addition to the monovalent, bivalent and trivalent modes, there are other classes of nonlinear periodic orbits stemming from normal modes.

In Chapter 3, we characterize graphs having Laplacian eigenvectors in $\{-1, 1\}$ or $\{-1, 0, 1\}$, that we call bivalent and trivalent graphs respectively. This characterization is done using transformations of graphs based on Laplacian eigenvectors.

In Chapter 4, we present our first exploration, of applying the averaging method for the discrete Φ^4 equation. We average over the fastest oscillation corresponding to a possible resonance. This averaging is difficult because of the presence of the Goldstone mode which needs to be treated separately.

In Chapter 5, we consider exponentially localized periodic solutions for the discrete Φ^4 model. To obtain them we introduce a large amplitude localized initial condition on one node of the network. Then, we can approximate these nonlinear localized solutions. We validate the approximation by Fourier analysis and using modulation theory which reduces the nonlinear graph wave equation to the discrete nonlinear Schrödinger equation.

Chapter 1

Wave equations on networks

In this introductory chapter, we consider the graph wave equation where the Laplacian is replaced by the graph Laplacian. This is a natural model for describing miscible flows on a network since it arises from conservation laws. The graph wave equation is well understood in terms of normal modes, which are periodic solutions associated to the eigenvectors of the graph Laplacian. To study the extension of the normal modes into nonlinear periodic orbits, we consider a cubic nonlinear graph wave equations. These are the discrete Φ^4 model which has on-site nonlinearity and the Fermi-Pasta-Ulam model which has intersite nonlinearity.

1.1 The graph wave equation

Let $\mathcal{G}(\mathcal{V}, \mathcal{E})$ be a graph with vertex set $\mathcal{V}$ of cardinality N and edge set $\mathcal{E}$ of cardinality M. The branches are oriented with an arbitrary but fixed orientation. We consider finite and undirected graphs with no loops or multiple edges. Notice that we use bold-face capitals for matrices and bold-face lower-case letters for vectors.

The basic tool for expressing a flux is the $N \times M$ incidence matrix $\mathbf{Q}$ (with respect to the given orientation) defined as

$$Q_{je} = \begin{cases} -1 & \text{if edge } e \text{ starts from node } j, \\ 1 & \text{if edge } e \text{ finishes at node } j, \\ 0 & \text{otherwise.} \end{cases} \tag{1.1}$$

In this section, we present the conservation laws and derive the graph wave equation using as an example the star graph S_3 shown in Figure 1.1 (the star graph S_{N-1} is a tree on N nodes having one vertex of degree $N-1$, and $N-1$ pendant (degree 1) vertices). This can be easily generalized to any graph.

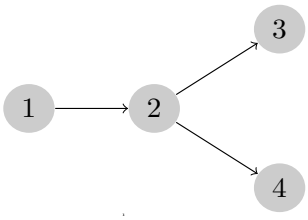

Figure 1.1 – The star graph S_3.

For the example shown in Figure 1.1, we have

$$\mathbf{Q} = \begin{pmatrix} -1 & 0 & 0 \\ 1 & -1 & -1 \\ 0 & 1 & 0 \\ 0 & 0 & 1 \end{pmatrix}. \tag{1.2}$$

The transpose $\mathbf{Q}^T = \boldsymbol{\nabla}$ is a discrete differential operator called gradient of graph. To see this consider a real-valued vector indexed by the graph's vertices $\mathbf{f} = (f_1, f_2, \ldots, f_N)$. The vector $\boldsymbol{\nabla}\mathbf{f}$ has as e component the difference of the values of $\mathbf{f}$ at the end points of the branch e (with orientation). In the example above, we have

$$\boldsymbol{\nabla}\mathbf{f} = \begin{pmatrix} -1 & 1 & 0 & 0 \\ 0 & -1 & 1 & 0 \\ 0 & -1 & 0 & 1 \end{pmatrix} \begin{pmatrix} f_1 \\ f_2 \\ f_3 \\ f_4 \end{pmatrix} = \begin{pmatrix} f_2 - f_1 \\ f_3 - f_2 \\ f_4 - f_2 \end{pmatrix}, \tag{1.3}$$

which is the discrete gradient of $\mathbf{f}$ associated with the graph. In many applications as we show below, the branches e_{ij} carry a weight m_{ij}. Then in expression (1.3) of the discrete gradient the $+1$ (resp. -1) should be replaced by m_{ij} (resp. $-m_{ij}$), so that we obtain a weighted discrete gradient. The discrete gradient and the incidence matrix appear in the theory of electrical currents and flows, it can be found in the famous Kirchhoff laws. As a reference we give the classical Kirchhoff's paper [1].

We will first write conservation laws using the $\boldsymbol{\nabla}$ operator and its transpose. From there we establish the relevant wave equation. These derivations are shown for the example of Figure 1.1 and can be generalized to any graph.

For the specific inductance-capacity electrical network shown in the left panel of Figure 1.2, the equations of motion in terms of the (node) voltages and (branch) currents are the conservation of current and voltage

$$\begin{aligned} \mathbf{C}\frac{\mathrm{d}\mathbf{v}}{\mathrm{d}t} + \boldsymbol{\nabla}^T\boldsymbol{\iota} &= \mathbf{s}, \\ \mathbf{L}\frac{\mathrm{d}\boldsymbol{\iota}}{\mathrm{d}t} - \boldsymbol{\nabla}\mathbf{v} &= 0, \end{aligned} \tag{1.4}$$

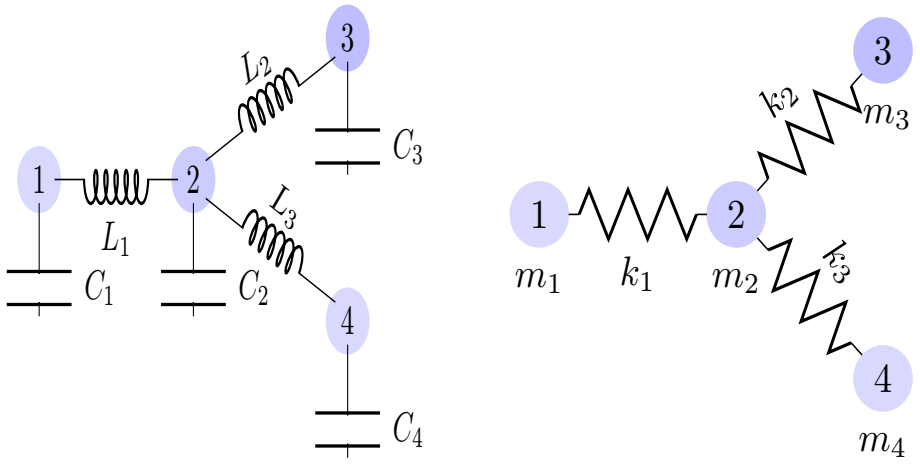

Figure 1.2 – Two different physical networks corresponding to the graph shown in Figure 1.1. The left panel shows a network of inductances and capacitances and the right panel shows the mechanical analogue in terms of masses and springs.

where $\mathbf{v} = (v_1, v_2, v_3, v_4)$ is the voltage field, $\boldsymbol{\iota} = (\iota_1, \iota_2, \iota_3)$ is the current field, $\mathbf{C} = \mathrm{diag}\,(C_1, C_2, C_3, C_4)$ and $\mathbf{L} = \mathrm{diag}\,(L_1, L_2, L_3)$ are respectively the diagonal matrix of capacitances and the diagonal matrix of inductances and where $\mathbf{s}$ represents the currents applied to each node (similar to boundary conditions in the continuum case). Note that equations (1.4) also describe in the linear limit, fluid flow in a pipe network [2], where $\mathbf{v}$ corresponds to the pressure and $\boldsymbol{\iota}$ to the flux. From the two equations (1.4) one obtains the generalized wave equation. For this, take the derivative of the first equation and substitute the second to obtain the node wave equation

$$\mathbf{C}\ddot{\mathbf{v}} + \boldsymbol{\nabla}^T\mathbf{L}^{-1}\boldsymbol{\nabla}\ \mathbf{v} = \dot{\mathbf{s}}, \tag{1.5}$$

where $\ddot{\mathbf{v}} = \frac{\mathrm{d}^2\mathbf{v}}{\mathrm{d}t^2}$, $\dot{\mathbf{s}} = \frac{\mathrm{d}\mathbf{s}}{\mathrm{d}t}$ (Newton's notation), and where

$$\boldsymbol{\nabla}^T\mathbf{L}^{-1}\boldsymbol{\nabla} = \begin{pmatrix} L_1^{-1} & -L_1^{-1} & 0 & 0 \\ -L_1^{-1} & L_1^{-1} + L_2^{-1} + L_3^{-1} & -L_2^{-1} & -L_3^{-1} \\ 0 & -L_2^{-1} & L_2^{-1} & 0 \\ 0 & -L_3^{-1} & 0 & L_3^{-1} \end{pmatrix}. \tag{1.6}$$

There is a corresponding branch wave equation for the currents that involves the link Laplacian in the terminology of [3]. Taking the time derivative of the second equation and substituting into the first we get

$$\mathbf{L}\ddot{\boldsymbol{\iota}} + \boldsymbol{\nabla}\mathbf{C}^{-1}\boldsymbol{\nabla}^T\ \boldsymbol{\iota} = \boldsymbol{\nabla}\mathbf{C}^{-1}\mathbf{s}. \tag{1.7}$$

In the rest we will only consider the node graph wave equation of type (1.5).

A similar graph wave equation arises when describing the other physical system shown in the right panel of Figure 1.2, the collection of four masses $m_i,\ i \in \{1,\dots,4\}$, connected by springs of stiffness $k_i,\ i \in \{1,2,3\}$. Here the variables are the displacements $u_i,\ i \in \{1,\dots,4\}$, of each mass. The equations of motion are

$$\begin{aligned} m_1\ddot{u}_1 &= k_1(u_2-u_1),\\ m_2\ddot{u}_2 &= k_1(u_1-u_2)+k_2(u_3-u_2)+k_3(u_4-u_2),\\ m_3\ddot{u}_3 &= k_2(u_2-u_3),\\ m_4\ddot{u}_4 &= k_3(u_2-u_4), \end{aligned} \tag{1.8}$$

which can be written

$$\ddot{\mathbf{u}} = -\mathbf{M}^{-1}\mathbf{K}\mathbf{u}, \tag{1.9}$$

where $\mathbf{u} = (u_1,u_2,u_3,u_4)^T$, $\mathbf{M} = \mathrm{diag}\,(m_1,m_2,m_3,m_4)$ is the diagonal matrix of masses and where

$$\mathbf{K} = \begin{pmatrix} k_1 & -k_1 & 0 & 0\\ -k_1 & (k_1+k_2+k_3) & -k_2 & -k_3\\ 0 & -k_2 & k_2 & 0\\ 0 & -k_3 & 0 & k_3 \end{pmatrix}. \tag{1.10}$$

Notice the correspondence capacitances/masses and inverse inductances/stiffnesses. The matrix (1.10) is symmetric just like the matrix (1.6). In the following, we assume that the masses are equal, this preserves the symmetry of the right hand side operator in (1.9). For simplicity we choose $k_1 = k_2 = k_3 = k_4 = k$. Then we normalize times by the natural frequency $w = \sqrt{\frac{k}{m}}$, $t' = wt$. Omitting the primes, the equations can be written in matrix form as

$$\begin{pmatrix} \ddot{u}_1\\ \ddot{u}_2\\ \ddot{u}_3\\ \ddot{u}_4 \end{pmatrix} = -\begin{pmatrix} 1 & -1 & 0 & 0\\ -1 & 3 & -1 & -1\\ 0 & -1 & 1 & 0\\ 0 & -1 & 0 & 1 \end{pmatrix}\begin{pmatrix} u_1\\ u_2\\ u_3\\ u_4 \end{pmatrix}, \tag{1.11}$$

which we will write formally as

$$\ddot{\mathbf{u}} = -\boldsymbol{\Delta}\mathbf{u}, \tag{1.12}$$

where $\mathbf{u} = (u_1,u_2,\dots,u_N)^T$ is the field amplitude and $\boldsymbol{\Delta}$ is the graph Laplacian [4], the equivalent of (1.6) and (1.10) for the star graph S_3. The $N \times N$ Laplacian matrix of a graph $\mathcal{G}$ is defined by

$$\boldsymbol{\Delta} = \boldsymbol{\nabla}^T\boldsymbol{\nabla} = \mathbf{D} - \mathbf{A}, \tag{1.13}$$

where $\mathbf{A}$ is the adjacency matrix such that $A_{ij} = 1$ if nodes i and j are connected ($i \neq j$) and $A_{ij} = 0$ otherwise, and $\mathbf{D}$ is the diagonal matrix where the entry $d_i = \sum_{j=1}^{N} A_{ij}$ is the degree of vertex i. Note that the graph Laplacian and the graph wave equation are independent of the orientation of the graph. In the theory of electrical networks, $\boldsymbol{\Delta}$ is referred to as a Kirchhoff matrix [1] or matrix of admittance [2] (*i.e.* conductivity, the reciprocal of impedance). Equation (1.11) is a finite difference discretization of the

continuous wave equation. This justifies the name of "Laplacian matrix" for $\mathbf{\Delta}$ since it is a discrete analogue of the Laplace differential operator. For an extensive survey on the Laplacian matrix see Merris [5].

Since the graph Laplacian $\mathbf{\Delta}$ is a real symmetric positive-semi definite matrix, it has real non negative eigenvalues and we can always build a basis of orthogonal eigenvectors $\mathbf{v}^j$ such that

$$\mathbf{\Delta}\mathbf{v}^j = \omega_j^2 \mathbf{v}^j, \tag{1.14}$$

where $j \in \{1, \ldots, N\}$. The vectors $\mathbf{v}^j$ can be chosen to be orthonormal with respect to the scalar product in $\mathbb{R}^N$, *i.e.* $\left\langle \mathbf{v}^i, \mathbf{v}^j \right\rangle = \delta_{i,j}$ where $\delta_{i,j}$ is the Kronecker delta ($\delta_{i,j} = 1$ if $i = j$, else $\delta_{i,j} = 0$), so the matrix $\mathbf{P}$ formed by the columns $\mathbf{v}^j$ is orthogonal. Notice that $\mathbf{\Delta}$ is a singular matrix (all the row sums are zero). Therefore $\mathbf{\Delta}$ has a zero eigenvalue $\omega_1^2 = 0$ which corresponds to the eigenvector of all ones, that we call the monovalent eigenvector $\mathbf{v}^1 = \frac{1}{\sqrt{N}}(1, 1, \ldots, 1)^T$. The multiplicity of 0 as an eigenvalue of $\mathbf{\Delta}$ is equal to the number of connected components of $\mathcal{G}$. The relation (1.14) can be written

$$\mathbf{\Delta}\mathbf{P} = \mathbf{P}\mathbf{W}, \tag{1.15}$$

where $\mathbf{W}$ is a diagonal matrix with entries $\omega_1^2 = 0 \leq \omega_2^2 \leq \cdots \leq \omega_N^2$. It is well known that the second smallest Laplacian eigenvalue is positive $\omega_2^2 > 0$ if and only if $\mathcal{G}$ is connected. Fiedler termed this eigenvalue the algebraic connectivity [6]. The eigenvectors of $\mathbf{\Delta}$ corresponding to the algebraic connectivity are known as the Fiedler vectors of $\mathcal{G}$. Throughout all graphs are assumed to be connected.

It is natural, following [7], to write the equation of motion (1.12) in terms of the amplitudes of the normalized eigenvectors $\mathbf{v}^j$. We introduce the vector $\mathbf{a} = (a_1, a_2, .., a_N)^T$ such that

$$\mathbf{u} = \mathbf{P}\mathbf{a} = \sum_{j=1}^{N} a_j \mathbf{v}^j. \tag{1.16}$$

Substituting (1.16) into (1.12) and projecting on each eigenvector $\mathbf{v}^j$, we obtain the amplitude equations in terms of normal modes

$$\ddot{a}_j + \omega_j^2 a_j = 0, \quad j \in \{1, \ldots, N\}. \tag{1.17}$$

The normal modes are bound states of the Hamiltonian

$$\mathcal{H}_0 = \frac{1}{2} \sum_{j=1}^{N} \left[(\dot{a}_j)^2 + \omega_j^2 a_j^2 \right]. \tag{1.18}$$

Because of the orthogonality, normal modes do not couple and the system can be described solely in terms of the amplitude of each mode and its time second derivative. The solution of the linear evolution problem (1.12) is given in terms of the linearly independent normal modes

$$\mathbf{u}(t) = a_1(t)\mathbf{v}^1 + \sum_{j=2}^{N} \left[a_j(0) \cos(\omega_j t) + \frac{\dot{a}_j(0)}{\omega_j} \sin(\omega_j t) \right] \mathbf{v}^j. \tag{1.19}$$

The zero linear frequency mode associated to the monovalent eigenvector $\mathbf{v}^1$ is called Goldstone mode ([8] p.986). The solution $a_1(t) = \dot{a}_1(0)t + a_1(0)$ is different from the others since it is not an oscillation and can be fixed to a constant by setting $\dot{a}_1(0) = 0$.

When non linearity is present in the equations of motion, normal modes will couple. It is then natural to examine what happens to these normal modes in the presence of a nonlinearity, when the equation becomes

$$\ddot{\mathbf{u}} = -\boldsymbol{\Delta}\mathbf{u} + \mathbf{f}(\mathbf{u}), \tag{1.20}$$

where $\mathbf{f}(\mathbf{u}) = (f(u_1), f(u_2), \ldots, f(u_N))^T$ is the field of nonlinear components. We expand $\mathbf{u}$ using the eigenvectors $\mathbf{v}^j$ of $\boldsymbol{\Delta}$. In terms of the coordinates a_j, substituting (1.16) into (1.20) and projecting on each mode $\mathbf{v}^j$, we get the system of N-coupled ordinary differential equations

$$\ddot{a}_j = -\omega_j^2 a_j + \left\langle \mathbf{f}(\mathbf{u}), \mathbf{v}^j \right\rangle, \quad j \in \{1, ..., N\}, \tag{1.21}$$

where we have used the orthonormality of the eigenvectors of $\boldsymbol{\Delta}$. Note how the decomposition (1.21) is adapted to examine the couplings between modes. Below we show that some systems exhibit nonlinear periodic solutions that are continued from normal modes, these are nonlinear normal modes in the strict sense [9]. The situation differs whether the degrees of freedom are nonlinear and coupled linearly as in the discrete Φ^4 equation or whether they are linear oscillators coupled nonlinearly as in the Fermi-Pasta-Ulam model.

1.2 On-site nonlinearity : the discrete Φ^4 model

We consider the nonlinear graph wave equation with a cubic on-site nonlinearity $\mathbf{f}(\mathbf{u}) = -\mathbf{u}^3 = -(u_1^3, u_2^3, \ldots, u_N^3)^T$ in (1.20)

$$\ddot{\mathbf{u}} = -\left(\epsilon\boldsymbol{\Delta} + \omega^2\mathbf{I}\right)\mathbf{u} - \mathbf{u}^3, \tag{1.22}$$

where $\mathbf{I}$ is the $N \times N$ identity matrix. The parameters are the natural frequency ω and the linear coupling coefficient ϵ. With this cubic on-site nonlinearity, the equation (1.22) is well-posed, see [10] for a review of the well-posedness of the continuum model. The power of the nonlinearity is important to get a well-posed problem. This can be seen by omitting the Laplacian and looking at the differential equation $\ddot{u} = -u^m$ whose solutions are bounded for m odd.

This model is an extension to a graph of the Φ^4 well-known model in condensed matter physics ([8] p.299). In the literature [8], the discrete Φ^4 model was studied only in the particular case of lattices where the graph Laplacian $(\boldsymbol{\Delta}\mathbf{u})_i = u_{i+1} - 2u_i + u_{i-1}$ (for a one-dimensional lattice) is a finite difference discretization of the continuous Laplacian. We formulate the discrete Φ^4 model using the graph Laplacian to describe general networks

of arbitrary topology. The model can describe networks of nonlinear oscillators, such as Josephson junctions or diodes ([11] p.71-72, 187-189). In mechanical engineering, several aerospace structures e.g. turbine rotors or space antennas, are composed of weakly coupled sectors assembled in a cyclic and symmetric configuration. Such a complex system can be reduced to the Φ^4 model in one-dimensional lattice [12].

1.2.1 Amplitude equations

We expand $\mathbf{u}$ in terms of the amplitudes $\mathbf{a} = (a_1, a_2, .., a_N)^T$ of the normalized eigenvectors $\mathbf{v}^j$ of $\mathbf{\Delta}$ as $\mathbf{u} = \sum_{j=1}^{N} a_j \mathbf{v}^j$. The amplitude equations are

$$\ddot{a}_j = -\left(\epsilon\omega_j^2 + \omega^2\right) a_j - \sum_{m=1}^{N} u_m^3 v_m^j, \quad j \in \{1, ..., N\}.$$

The term u_m^3 can be written as $u_m^3 = \sum_{k,l,n=1}^{N} a_k a_l a_n \; v_m^k v_m^l v_m^n$. We get then a set of N second order inhomogeneous coupled differential equations

$$\ddot{a}_j + \left(\epsilon\omega_j^2 + \omega^2\right) a_j = -\sum_{k,l,n=1}^{N} \Gamma_{jkln} \; a_k a_l a_n, \tag{1.23}$$

where

$$\Gamma_{jkln} = \sum_{m=1}^{N} v_m^j \; v_m^k \; v_m^l \; v_m^n. \tag{1.24}$$

Notice that the graph geometry comes through the coefficients Γ_{jkln}. For a general graph, the spectrum needs to be computed numerically and these coefficients as well. For some special cases however, like cycles and chains, the eigenvalues and the eigenvectors of the Laplacian have an explicit formula (see Appendix A) so that Γ_{jkln} can be computed explicitly. Then, we obtain the amplitude equations coupling the normal modes.

1.2.2 Hamiltonian description

The Hamiltonian of model (1.22) is

$$\mathcal{H}(\mathbf{u}, \dot{\mathbf{u}}) = \frac{1}{2}\langle \dot{\mathbf{u}}, \dot{\mathbf{u}} \rangle + \frac{1}{2}\left\langle \mathbf{u}, \left(\epsilon\mathbf{\Delta}\mathbf{u} + \omega^2\mathbf{u}\right) \right\rangle + \frac{1}{4}\sum_{m=1}^{N} u_m^4. \tag{1.25}$$

The Hamiltonian in terms of normal modes $\mathbf{u} = \sum_{j=1}^{N} a_j \mathbf{v}^j$

$$\mathcal{H}(\mathbf{a}, \dot{\mathbf{a}}) = \frac{1}{2}\sum_{j=1}^{N}\left[(\dot{a}_j)^2 + \left(\epsilon\omega_j^2 + \omega^2\right) a_j^2\right] + \frac{1}{4}\sum_{m=1}^{N}\left(\sum_{j=1}^{N} a_j v_m^j\right)^4.$$

Thus,

$$\mathcal{H}\left(\mathbf{a},\dot{\mathbf{a}}\right)=\frac{1}{2}\sum_{j=1}^{N}\left[\left(\dot{a}_j\right)^2+\left(\epsilon\omega_j^2+\omega^2\right){a_j}^2\right]+\frac{1}{4}\sum_{j,k,l,n=1}^{N}\Gamma_{jkln}\ a_j a_k a_l a_n. \tag{1.26}$$

If we define the conjugate $q_j=a_j,\quad p_j=\dot{q}_j$, the expression $\mathcal{H}$

$$\mathcal{H}\left(\mathbf{q},\mathbf{p}\right)=\frac{1}{2}\sum_{j=1}^{N}\left[p_j^2+\left(\epsilon\omega_j^2+\omega^2\right){q_j}^2\right]+\frac{1}{4}\sum_{j,k,l,n=1}^{N}\Gamma_{jkln}\ q_j\ q_k\ q_l\ q_n. \tag{1.27}$$

The equations of motion are

$$\dot{q}_j=\frac{\partial\mathcal{H}}{\partial p_j},\quad \dot{p}_j=-\frac{\partial\mathcal{H}}{\partial q_j},$$

the second equation is equivalent to (1.23).

1.3 Intersite nonlinearity : the Fermi-Pasta-Ulam model

We consider the nonlinear graph wave equation with a cubic intersite nonlinearity, known as the Fermi-Pasta-Ulam equation [13]

$$\ddot{u}_i=-\sum_{j=1}^{N}\Delta_{ij}\ u_j-\sum_{k\sim i}(u_i-u_k)^3,\quad i\in\{1,\ldots,N\}, \tag{1.28}$$

where the notation $k\sim i$ indicates adjacency of vertices and the sum in the second term on the right hand side is taken over the neighbors k of i. This system was derived from nonlinear elastic network model describing protein vibrations [14]. The model (1.28) is an extension to a general graph of the Fermi-Pasta-Ulam lattice model [13].

1.3.1 Amplitude equations

We expand $\mathbf{u}$ in terms of the amplitudes of the Laplacian eigenvectors as $\mathbf{u}=\sum_{j=1}^{N}a_j\mathbf{v}^j$. The amplitude equations are

$$\ddot{a}_j=-\omega_j^2 a_j-\sum_{l,m,n=1}^{N}\Lambda_{jlmn}\ a_l a_m a_n,\quad j\in\{1,...,N\}, \tag{1.29}$$

where

$$\Lambda_{jlmn}=\sum_{i=1}^{N}\sum_{k\sim i}\left(v_i^j-v_k^j\right)\left(v_i^l-v_k^l\right)\left(v_i^m-v_k^m\right)\left(v_i^n-v_k^n\right). \tag{1.30}$$

1.3.2 Hamiltonian description

The Hamiltonian of model (1.28) is

$$\mathcal{H}\left(\mathbf{u},\dot{\mathbf{u}}\right)=\frac{1}{2}\left\langle \dot{\mathbf{u}},\dot{\mathbf{u}}\right\rangle +\frac{1}{2}\left\langle \mathbf{u},\mathbf{\Delta u}\right\rangle +\frac{1}{4}\sum_{i=1}^{N}\sum_{k\sim i}(u_{i}-u_{k})^{4}. \tag{1.31}$$

The Hamiltonian in terms of normal modes $\mathbf{u}=\sum_{j=1}^{N}a_{j}\mathbf{v}^{j}$

$$\mathcal{H}\left(\mathbf{a},\dot{\mathbf{a}}\right)=\frac{1}{2}\sum_{j=1}^{N}\left[\left(\dot{a}_{j}\right)^{2}+\omega_{j}^{2}a_{j}^{2}\right]+\frac{1}{4}\sum_{j,l,m,n=1}^{N}\Lambda_{jlmn}\ a_{j}a_{l}a_{m}a_{n}. \tag{1.32}$$

Then, Hamilton's equation for the zero frequency mode follows that

$$\ddot{a}_{1}=\frac{-\partial\mathcal{H}}{\partial a_{1}}=\frac{-1}{4}\frac{\partial}{\partial a_{1}}\left[\sum_{j,l,m,n=1}^{N}\Lambda_{jlmn}\ a_{j}a_{l}a_{m}a_{n}\right]\equiv0, \tag{1.33}$$

using that the components of $\mathbf{v}^{1}$ are all equal, we have $\Lambda_{1lmn}=\cdots=\Lambda_{jlm1}=0$, when at least one index is unity. We have that $\dot{a}_{1}$ is a constant. The zero mode corresponds to a translation of degree of freedom and can be eliminated by setting $\dot{a}_{1}=0$. The Hamiltonian (1.32) is then reduced to (see [15])

$$\mathcal{H}\left(\mathbf{a},\dot{\mathbf{a}}\right)=\frac{1}{2}\sum_{j=2}^{N}\left[\left(\dot{a}_{j}\right)^{2}+\omega_{j}^{2}a_{j}^{2}\right]+\frac{1}{4}\sum_{j,l,m,n=2}^{N}\Lambda_{jlmn}\ a_{j}a_{l}a_{m}a_{n}. \tag{1.34}$$

1.4 Continuation of normal modes

Nonlinear periodic orbits continued from normal modes have been studied for vibrating mechanical systems, see the extensive review by [16]. Classical approaches for proving the existence of periodic orbits in Hamiltonian systems rely on the Lyapunov center theorem [17] (see also [18] p.219) and Weinstein–Moser theorem [19, 20]. The elimination of zero frequency (Goldstone) mode in the FPU model, implies that the quadratic part of the Hamiltonian (1.34) is positive definite, and the existence of nonlinear normal modes that are continued from linear ones is guaranteed by the Weinstein-Moser theorem. However, Goldstone mode exist in the discrete Φ^{4} model as we will show in Chapter 2, then the Weinstein-Moser theorem cannot be invoked since the quadratic part in the Hamiltonian (1.27) is positive semidefinite.

We show in Chapter 2 that for the discrete Φ^{4} model (on-site nonlinearity), only normal modes associated to eigenvectors composed of $\{1,-1,0\}$ extend to nonlinear

periodic orbits. In addition to these eigenvectors, there are other eigenvectors giving rise to nonlinear normal modes for the Fermi-Pasta-Ulam model (intersite nonlinearity).

The results show the importance of nodes where the component of the eigenvector is zero. The authors in [7] show that at such nodes, any forcing or damping of the system is null for the corresponding eigenmode. We have the following definition

Definition 1 (Soft node [7])**.** *A node s of a graph is a soft node for an eigenvalue ω_j^2 of the graph Laplacian if there exists an eigenvector $\mathbf{v}^j$ for this eigenvalue such that $v_s^j = 0$.*

1.5 Intrinsic localized modes

Another type of nonlinear periodic orbits can exist, intrinsic localized modes, also called discrete breathers which are time periodic and (typically exponentially) spatially localized solutions that appear in nonlinear discrete systems arising in many physical, biological systems and networks. They were analytically studied first by Sievers and Takeno [21], Page [22]. Later, MacKay and Aubry [23] proved the existence of discrete breathers by considering a lattice model of coupled anharmonic oscillators in the limit of very weak interaction (anticontinuous limit). The existence of localized solutions in nonlinear networks is due to the interplay between nonlinearity and discreteness. In fact, non-resonance of the breather frequency with the linear spectrum is a necessary condition for obtaining a time-periodic localized state [24]. In order to avoid this resonance, we need the linear spectrum to be bounded from above. This explains why spatial discretisation is needed. In contrast, most spatially continuous field equations have an unbounded linear spectrum. That makes resonances unavoidable.

Localized modes have been investigated theoretically and numerically for a variety of physical systems [25]. Experimentally observed reports for various systems include Josephson-junction arrays [26], optical waveguides [27, 28], photonic crystals [29], DNA double strand [30], micromechanical oscillators [31] and electronic circuits [32].

Localized modes have been thoroughly studied in the Fermi-Pasta-Ulam lattice [33] and in the discrete nonlinear Schrödinger equation [34]. In Chapter 5, we study localized solutions for the discrete Φ^4 model and validate the approach by reducing the model to the discrete nonlinear Schrödinger equation.

In the literature, nonlinear normal modes and localized modes are studied in the particular case of lattices. The contribution of this thesis consist of the study of nonlinear normal modes and localized modes in general networks of arbitrary topology, invoking graph spectral theory.

Chapter 2

Periodic orbits in nonlinear wave equations on networks

Abstract. We consider the nonlinear graph wave equation with on-site cubic nonlinearity (the discrete ϕ^4 equation). We show that inspecting the normal modes of the graph Laplacian, we can immediately identify which ones can be extended into nonlinear periodic orbits (generalizing work of Aoki, 2016). We first define monovalent, bivalent and trivalent nonlinear periodic orbits depending on whether the components of the corresponding eigenvectors of the graph Laplacian are in $\{+1\}$, $\{-1,+1\}$ or $\{-1,0,+1\}$. Then, we perform a systematic linear stability (Floquet) analysis of these orbits. In particular, the linearized equations are decoupled for normal modes associated to eigenvectors without 0 (soft nodes), these modes are the monovalent (Goldstone) and the bivalent orbits. We find that for chains the Goldstone mode is stable for a wide range of parameters while the bivalent mode is unstable. Nevertheless, the linearized equations are coupled for modes with soft nodes. Numerical results for some graphs show that trivalent periodic orbits that continue nondegenerate linear modes are unstable below an amplitude threshold; orbits continued from modes with frequency degeneracy are unstable.

The chapter is organized as follows: In section 2.1, we generalize the criterion of Aoki that shows which linear normal modes extend to nonlinear periodic orbits, for the (on-site) nonlinear graph wave equation (discrete ϕ^4 model). Section 2.2 classifies these nonlinear normal modes for chains and cycles and gives other examples. Section 2.3 presents the variational equations obtained by perturbing the nonlinear normal modes. These are solved numerically for chains in section 2.4 for the Goldstone and the bivalent modes. Full numerical results are presented in section 2.5 for trivalent modes. Preliminary results on nonlinear quasi-periodic orbits are shown in section 2.6. In section 2.7, we clarify the extension of linear normal modes for the Fermi-Pasta-Ulam model.

2.1 Existence of periodic orbits

We consider a simplified version of the nonlinear graph wave equation (1.22) with a natural frequency $\omega = 0$ and a coupling coefficient $\epsilon = 1$

$$\ddot{\mathbf{u}} = -\boldsymbol{\Delta}\mathbf{u} - \mathbf{u}^3. \tag{2.1}$$

Expanding $\mathbf{u}$ in the basis of Laplacian eigenvectors, $\mathbf{u} = \sum_{k=1}^{N} a_k \mathbf{v}^k$, we obtain the amplitudes equations (1.23) in terms of normal modes

$$\ddot{a}_j + \omega_j^2 a_j = -\sum_{k,l,p=1}^{N} \Gamma_{jklp}\, a_k a_l a_p, \quad j \in \{1, \dots, N\}. \tag{2.2}$$

In [35], Aoki studied nonlinear periodic orbits for chain or cycle graphs, *i.e.* one dimensional lattices with free or periodic boundary conditions. He identified a criterion allowing to extend some linear normal modes into nonlinear periodic orbits for the discrete ϕ^4 model. In [36], we generalized Aoki's criterion to any graph.

Let us find the conditions for the existence of a nonlinear periodic solution of (2.1) of the form

$$\mathbf{u}(t) = a_j(t)\mathbf{v}^j, \tag{2.3}$$

the equations of motion (2.1) reduce to

$$\ddot{a}_j v_m^j = -\omega_j^2 a_j v_m^j - a_j^3 \left(v_m^j\right)^3. \tag{2.4}$$

These equations are satisfied for the nodes m such that $v_m^j = 0$ (the soft nodes).

For $v_m^j \neq 0$, we can simplify (2.4) by v_m^j and obtain

$$\ddot{a}_j = -\omega_j^2 a_j - a_j^3 \left(v_m^j\right)^2.$$

These equations should be independent of m and this imposes

$$\left(v_m^j\right)^2 = C, \tag{2.5}$$

where C is a constant. Remembering that $\left\|\mathbf{v}^j\right\| = 1$, we get

$$C = \frac{1}{N - S},$$

where S is the number of soft nodes, $S = \operatorname{card}\left\{m,\ v_m^j = 0\right\}$.

To summarize, for a general network, we identified nonlinear periodic orbits $\mathbf{u}^j(t)$ associated to a linear eigenvector $\mathbf{v}^j$ of the Laplacian; they are:

$$\begin{cases} \mathbf{u}^j(t) = a_j(t)\mathbf{v}^j, \\ \dfrac{1}{\sqrt{C}} v_m^j \in \{0, 1, -1\}, \quad \forall m \in \{1, \dots, N\}, \quad C = \dfrac{1}{N - S}, \\ \ddot{a}_j = -\omega_j^2 a_j - C a_j^3. \end{cases} \tag{2.6}$$

We distinguish three kinds of nonlinear periodic orbits monovalent, bivalent and trivalent depending on whether their components are $+1$ or $-1, +1$ or $-1, 0, +1$ up to a normalization constants. The monovalent orbit is the Goldstone mode $\mathbf{v}^1$, and exists for any graph. The bivalent orbits contain $-1, +1$ up to the normalization constant $\frac{1}{\sqrt{N}}$. Finally, the trivalent orbits are composed of $-1, 0, +1$; they possess soft nodes and the normalization constant is $\frac{1}{\sqrt{N-S}}$ where S is the number of soft nodes. We present in Chapter 3 a characterization of graphs having bivalent and trivalent Laplacian eigenvectors (see also [37]).

An important remark is that the criterion can be generalized to any odd power of the nonlinearity. We can use the condition (2.5) to systematically find periodic orbits for the discrete ϕ^4 model (1.22) and for a general nonlinear wave equation (1.20) with a polynomial on-site nonlinearity with odd powers $\mathbf{f}(\mathbf{u}) = -\mathbf{u}^3 - \mathbf{u}^5 \dots$.

2.2 Examples of nonlinear periodic orbits

We identify the bivalent and trivalent eigenvectors in chains and cycles, since the graph Laplacian Δ is tridiagonal matrix for chains and circulant matrix for cycles, and their spectrum is well-known (see Appendix A). We give other examples that are neither a chain or a cycle.

First, consider the modes without soft nodes.

- The monovalent mode, also named zero linear frequency mode or Goldstone mode

$$v_m^1 = \frac{1}{\sqrt{N}}, \quad \forall m \in \{1, \dots, N\},$$

  exists for any graph.

- The bivalent mode

$$v_m^j = \pm\frac{1}{\sqrt{N}}, \quad \forall m \in \{1, \dots, N\},$$

  exists for chains with N even and $j = \frac{N}{2} + 1$,

$$v_m^{\frac{N}{2}+1} = \frac{1}{\sqrt{N}} \begin{cases} (-1)^{\frac{m}{2}}, & \text{if } m \text{ even}, \\ (-1)^{\frac{m-1}{2}}, & \text{if } m \text{ odd}, \end{cases}$$

  corresponds to the frequency $\omega_{\frac{N}{2}+1} = \sqrt{2}$. For example, for a chain of $N = 4$ nodes, we have the following bivalent mode

- For cycles with N even, the bivalent mode $\mathbf{v}^N$ alternates, it is such that $v_m^N = -v_{m+1}^N$. It corresponds to the frequency $\omega_N = 2$

$$v_m^N = \frac{1}{\sqrt{N}} (-1)^{m-1}, \quad \forall m \in \{1, \ldots, N\}.$$

For a cycle of $N = 4$ nodes, we have the following bivalent mode

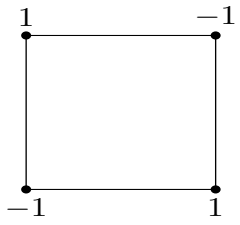

Other graphs can exhibit bivalent nonlinear modes. These are for example:

- the network

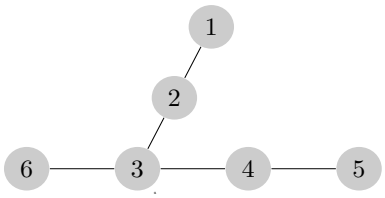

The nonlinear periodic orbit originates from the linear mode,

$$\omega_4^2 = 2, \ \mathbf{v}^4 = \frac{1}{\sqrt{6}} (1, -1, -1, -1, 1, 1)^T.$$

- the network

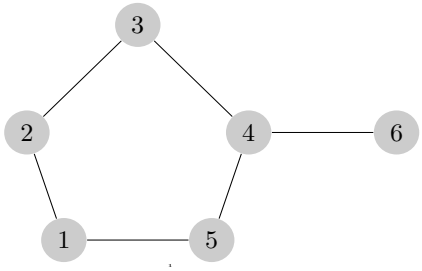

The nonlinear periodic orbit originates from the linear mode,

$$\omega_4^2 = 2, \ \mathbf{v}^4 = \frac{1}{\sqrt{6}} (-1, -1, 1, 1, 1, -1)^T.$$

Nonlinear modes containing soft nodes, or trivalent modes can be found in the following graphs:

- For chains with N multiple of 3, the trivalent mode $\mathbf{v}^{\frac{N}{3}+1}$ corresponds to the frequency $\omega_{\frac{N}{3}+1} = 1$

$$v_m^{\frac{N}{3}+1} = \sqrt{\frac{2}{N}} \cos\left(\frac{m\pi}{3} - \frac{\pi}{6}\right), \quad \forall m \in \{1, \ldots, N\}.$$

  Notice that $v_m^{\frac{N}{3}+1} = 0$ for $m = 3k+2$ and $k \in \{0, \ldots, \frac{N}{3} - 1\}$.

- For cycles with N multiple of 3, the trivalent mode $\mathbf{v}^{\frac{2N}{3}+1}$ corresponds to the double frequency $\omega_{\frac{2N}{3}} = \omega_{\frac{2N}{3}+1} = \sqrt{3}$

$$v_m^{\frac{2N}{3}+1} = \sqrt{\frac{2}{N}} \sin\left(\frac{2\pi}{3}(m-1)\right), \quad \forall m \in \{1, \ldots, N\}.$$

  Notice that $v_m^{\frac{2N}{3}+1} = 0$ for $m = 3k+1$ and $k \in \{0, \ldots, \frac{N}{3} - 1\}$.

- For cycles where N is multiple of 4, we have a double frequency $\omega_{\frac{N}{2}} = \omega_{\frac{N}{2}+1} = \sqrt{2}$ and two eigenvectors

$$v_m^{\frac{N}{2}} = \sqrt{\frac{2}{N}} \begin{cases} 0, & \text{if } m \text{ even}, \\ (-1)^{\frac{m-1}{2}}, & \text{if } m \text{ odd}. \end{cases}$$

$$v_m^{\frac{N}{2}+1} = \sqrt{\frac{2}{N}} \begin{cases} (-1)^{\frac{m}{2}+1}, & \text{if } m \text{ even}, \\ 0, & \text{if } m \text{ odd}. \end{cases}$$

- For cycles with N multiple of 6, the trivalent mode $\mathbf{v}^{\frac{N}{3}+1}$ corresponds to the double frequency $\omega_{\frac{N}{3}} = \omega_{\frac{N}{3}+1} = 1$

$$v_m^{\frac{N}{3}+1} = \sqrt{\frac{2}{N}} \sin\left(\frac{\pi}{3}(m-1)\right), \quad \forall m \in \{1, \ldots, N\}.$$

  Notice that $v_m^{\frac{N}{3}+1} = 0$ for $m = 3k+1$ and $k \in \{0, \ldots, \frac{N}{3} - 1\}$.

Other networks containing soft nodes have eigenvectors extending into nonlinear periodic orbits. These are for example:

- the butterfly graph [38]

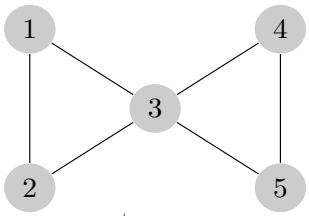

We have the following important parts of the spectrum

$$\omega_2^2 = 1,\ \mathbf{v}^2 = \frac{1}{2}(1,1,0,-1,-1)^T,$$
$$\omega_3^2 = 3,\ \mathbf{v}^3 = \frac{1}{\sqrt{2}}(-1,1,0,0,0)^T,$$
$$\omega_4^2 = 3,\ \mathbf{v}^4 = \frac{1}{\sqrt{2}}(0,0,0,-1,1)^T.$$

- the network

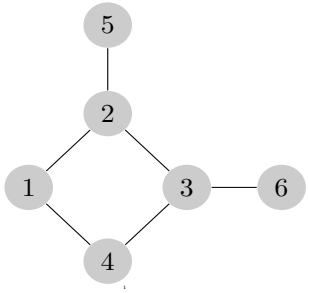

The nonlinear periodic orbit originates from the linear mode,

$$\omega_3^2 = 1,\ \mathbf{v}^3 = \frac{1}{2}(1,0,0,1,-1,-1)^T.$$

In [37], we have characterized the graphs having bivalent and trivalent eigenvectors. This characterization is presented in Chapter 3.

2.3 Linearization around the periodic orbits

We now analyze the stability of the nonlinear periodic orbits that we found by perturbation. This analysis reveals two main classes of orbits depending on whether they contain soft nodes or not.

To analyse the stability of (2.6), we perturb a nonlinear mode $\mathbf{w} = a_j(t)\mathbf{v}^j$ satisfying (2.6) and write

$$\mathbf{u} = \mathbf{w} + \mathbf{y}, \tag{2.7}$$

where $\|\mathbf{y}\| \ll \|\mathbf{w}\|$. Plugging the above expression into (2.1), we get for each coordinate i

$$\ddot{y}_i = -\sum_{p=1}^{N} \Delta_{ip} y_p - 3\ w_i^2 y_i - 3\ w_i y_i^2 - y_i^3, \tag{2.8}$$

where we have used the fact that $\mathbf{w}$ is a solution of (2.1).

Two situations occur here, depending on whether the eigenvector $\mathbf{v}^j$ contains zero components (soft nodes) or not. If there are no soft nodes, then $w_i \neq 0,\ \ \forall i \in \{1, \ldots, N\}$, like for the Goldstone mode or the bivalent mode, equation (2.8) can be linearized to

$$\ddot{\mathbf{y}} = -\mathbf{\Delta}\mathbf{y} - \frac{3}{N} a_j^2(t)\mathbf{y}. \tag{2.9}$$

Expanding $\mathbf{y}$ on the normal modes, $\mathbf{y} = \sum_{k=1}^{N} z_k(t)\mathbf{v}^k$, we decouple (2.9) and obtain N one dimensional Hill-like equations for each amplitude z_k

$$\ddot{z}_k = -\left[\omega_k^2 + \frac{3}{N} a_j^2(t)\right] z_k, \quad k \in \{1, \ldots, N\}. \tag{2.10}$$

Again we generalize the result, obtained by Aoki [35] for chains and cycles, to a general graph.

In the case where there are soft nodes, we can also write the linearized equations. First, let us assume for simplicity that there is only one zero component m of $\mathbf{v}^j$, then $w_m = 0$ so that we need to keep the cubic term y_m^3 in (2.8) for $i = m$, and we can linearize (2.8) for all $i \neq m$. The evolution of $\mathbf{y}$ is given by

$$\begin{aligned}
\ddot{y}_i &= -\sum_{p=1}^{N} \Delta_{ip} y_p - 3C a_j^2(t) y_i, \quad i \in \{1, \ldots, N\}, \quad i \neq m, \\
\ddot{y}_m &= -\sum_{p=1}^{N} \Delta_{mp} y_p - y_m^3.
\end{aligned}$$

Expanding $\mathbf{y}$ on the normal modes, $\mathbf{y} = \sum_{l=1}^{N} z_l(t)\mathbf{v}^l$, we get

$$\sum_{l=1}^{N} \ddot{z}_l v_i^l = -\sum_{l=1}^{N} \omega_l^2 z_l v_i^l - 3C a_j^2(t) \sum_{l=1}^{N} z_l v_i^l, \ i \neq m, \tag{2.11}$$

$$\sum_{l=1}^{N} \ddot{z}_l v_m^l = -\sum_{l=1}^{N} \omega_l^2 z_l v_m^l - \sum_{l,p,q=1}^{N} z_l z_p z_q v_m^l v_m^p v_m^q. \tag{2.12}$$

We now multiply (2.11) by v_i^k and sum over $1 \leq i \leq N$ with $i \neq m$ and multiply (2.12) by v_m^k. The two equations are

$$\begin{aligned}
\sum_{l=1}^{N} \ddot{z}_l \sum_{i \neq m} v_i^l v_i^k &= -\sum_{l=1}^{N} \left[\omega_l^2 z_l + 3\ Ca_j^2(t) z_l\right] \sum_{i \neq m} v_i^l v_i^k, \\
\sum_{l=1}^{N} \ddot{z}_l v_m^l v_m^k &= -\sum_{l=1}^{N} \omega_l^2 z_l v_m^l v_m^k - \sum_{l,p,q=1}^{N} z_l z_p z_q v_m^l v_m^p v_m^q v_m^k.
\end{aligned}$$

Adding the above equations and using the orthogonality condition $\sum_{i \neq m} v_i^l v_i^k = \delta_{l,k} - v_m^l v_m^k$, we obtain

$$\ddot{z}_k = -\left[\omega_k^2 + 3Ca_j^2(t)\right] z_k + 3Ca_j^2(t) \sum_{l=1}^{N} z_l v_m^l v_m^k - \sum_{l,p,q=1}^{N} z_l z_p z_q v_m^l v_m^p v_m^q v_m^k. \tag{2.13}$$

Equation (2.13) shows that the amplitudes z_k of the perturbation $\mathbf{y}$ around a nonlinear periodic orbit $\mathbf{w} = a_j(t)\mathbf{v}^j$ containing a soft node $v_m^j = 0$, are coupled linearly. Omitting the nonlinear term and keeping only the linear coupling term in (2.13), we obtain N one dimensional coupled equations for each amplitude z_k

$$\ddot{z}_k = -\left[\omega_k^2 + 3Ca_j^2(t)\right] z_k + 3Ca_j^2(t) \sum_{l=1}^{N} z_l v_m^l v_m^k.$$

In the general case, let us denote by $\mathcal{S}_j = \left\{m, \quad v_m^j = 0\right\}$ the set of the soft nodes of the trivalent mode $\mathbf{v}^j$, then the variational system can be written

$$\begin{cases}
\ddot{z}_k = -\left(\omega_k^2 + 3C\left(1 - \sum_{m \in \mathcal{S}_j} \left(v_m^k\right)^2\right) a_j^2(t)\right) z_k + 3Ca_j^2(t) \sum_{l \neq k} z_l \sum_{m \in \mathcal{S}_j} v_m^l v_m^k, \quad \forall k \neq j, \\
\ddot{z}_j = -\left(\omega_j^2 + 3Ca_j^2(t)\right) z_j.
\end{cases} \tag{2.14}$$

The linearized equations (2.14) show how the modes will couple. If $\mathcal{S}_j \subset \mathcal{S}_k$ for such a $k \in \{1, \ldots, N\}$, $k \neq j$, the nonlinear mode $\mathbf{v}^j$ will not couple with the mode $\mathbf{v}^k$ *i.e.* $\mathbf{v}^k$ will not be excited when exciting the mode $\mathbf{v}^j$. Another factor of the uncoupling is when the coupling coefficients $\sum_{m \in \mathcal{S}_j} v_m^l v_m^k = 0, \quad \forall\ l \neq k$.

To summarize, the stability of the Goldstone and the bivalent nonlinear periodic orbits, is governed by the N decoupled equations (2.10). For nonlinear periodic orbits containing soft nodes (trivalent modes), the stability is given by the coupled system (2.14). In all cases, the orbit will be stable if the solutions z_k are bounded for all k.

2.4 Stability of the Goldstone and the bivalent periodic orbits: Floquet analysis

The variational system corresponding to the Goldstone mode or the bivalent mode can be decomposed into the set of independent (uncoupled) equations (2.10) where $a_j(t)$ is the Goldstone or the bivalent periodic elliptic function solution of

$$\ddot{a}_j = -\omega_j^2 a_j - \frac{1}{N} a_j^3, \tag{2.15}$$

for proper initial conditions $a_j(0)$ and $\dot{a}_j(0)$.

In order for the Goldstone mode and the bivalent mode to be stable, the solutions of the differential equations (2.10) must be bounded $\forall k \in \{1, \ldots, N\}$. The equations (2.10) are uncoupled Hill-like equations and can be studied separately for each k. From the evolution of z_k in (2.10) we obtain the Floquet multipliers [39] (see Appendix B); this requires the integration of the first order variational equations

$$\begin{cases} \dot{\mathbf{M}} = \mathbf{A}_k(t)\mathbf{M}, \\ \mathbf{M}(0) = \mathbf{I_2}, \end{cases} \tag{2.16}$$

where $\mathbf{M}$ is a 2×2 matrix whose columns are the linearly independent solutions $(z_k(t), \dot{z}_k)^T$ of (2.10) for the initial conditions given by the columns of the identity matrix $\mathbf{I_2}$. The matrix A_k is

$$\mathbf{A}_k(t) = \begin{pmatrix} 0 & 1 \\ -\left[\omega_k^2 + \frac{3}{N} a_j^2(t)\right] & 0 \end{pmatrix}, \tag{2.17}$$

where $a_j(t)$ is the Goldstone or the bivalent periodic orbit solution of (2.15). The fundamental matrix solution of (2.16) is $\mathbf{M}(t)$. For $t = T$, the period of a_j, the matrix $\mathbf{M}(T)$ is called the monodromy matrix. The eigenvalues of $\mathbf{M}(T)$ are the Floquet multipliers and Floquet's theorem [39] states that all the solutions of (2.16) are bounded whenever the Floquet multipliers have magnitude smaller than one. To calculate the Floquet multipliers, we integrate over the period T the first order variational equations (2.16) simultaneously with the equation of motion (2.15). For this, we used a fourth order Runge-Kutta routine and the Matlab infrastructure [40].

2.4.1 Goldstone periodic orbit

For a general graph with N nodes, the Goldstone periodic orbit $a_1(t)$ solution of (2.15) for $j = 1$, $\omega_1 = 0$, can be written in terms of Jacobi elliptic functions [41] (see Appendix C). The solutions lie on the level curves of the energy

$$E = \frac{1}{2}(\dot{a}_1)^2 + \frac{1}{4N} a_1^4, \tag{2.18}$$

which is a constant of the motion. Therefore, the phase portrait is easily obtained by plotting the level curves Figure 4.19. The period of oscillations is (see Appendix D)

$$T = \frac{\sqrt{N}\ \Gamma^2\left(\frac{1}{4}\right)}{a_1(0)\sqrt{\pi}}, \tag{2.19}$$

where $\Gamma(.)$ is the gamma function $\Gamma(x) = \int_0^\infty y^{x-1}\mathrm{e}^{-y}\mathrm{d}y$, and $\Gamma\left(\frac{1}{4}\right) \approx 3.6256$. The frequency of oscillations is

$$\omega_{\mathrm{NL}} = \frac{2\pi}{T} = \frac{2\pi\sqrt{\pi}}{\sqrt{N}\ \Gamma^2\left(\frac{1}{4}\right)} a_1(0). \tag{2.20}$$

We set $\gamma = (4N\ E)^{\frac{1}{4}}$, then we can write the solution as

$$a_1(t) = \gamma\ \mathrm{cn}\left(\frac{\gamma}{\sqrt{N}}t, \frac{1}{\sqrt{2}}\right), \tag{2.21}$$

where $\mathrm{cn}\,(t,\kappa)$ is the cosine Jacobi elliptic function [41] with modulus κ and where we have chosen $\dot{a}_1(0) = 0$.

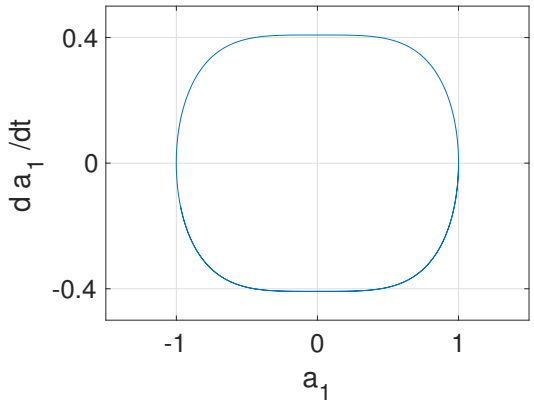

Figure 2.1 – Goldstone periodic orbit for $N = 3$, $a_1(0) = 1$ and $\dot{a}_1(0) = 0$.

For the Goldstone periodic orbit, the variational equations (2.10) can be written

$$\ddot{z}_k = -\left[\omega_k^2 + \frac{3}{N}\gamma^2 \mathrm{cn}^2\left(\frac{\gamma}{\sqrt{N}}t, \frac{1}{\sqrt{2}}\right)\right] z_k, \quad k \in \{1, \ldots, N\}. \tag{2.22}$$

Equations (2.22) are uncoupled Lamé equations in the Jacobian form [42] and can be studied separately for each k. Note that the stability domain of (2.22) was determined for example in [43]; it can be seen that there are instable bounds in the plane $\left(\gamma^2, \omega_k^2\right)$.

For chains, we studied the Floquet multipliers for the Goldstone periodic orbit.

2.4.2 Floquet analysis of Goldstone periodic orbit in chains

For chains with N nodes, the instability region of the Goldstone mode is shown in Figure 2.2 as a function of the amplitude $a_1(0)$. The points indicate instability. The plot shows the unstable intervals typical of the Mathieu or Lamé equations [43]. For small chain sizes, there are just a few very narrow unstable intervals, for example for $N = 4$, we have three intervals. As the chain gets longer, the number of the unstable intervals and their width increases. Note however that for large enough amplitude, the Goldstone mode is always stable.

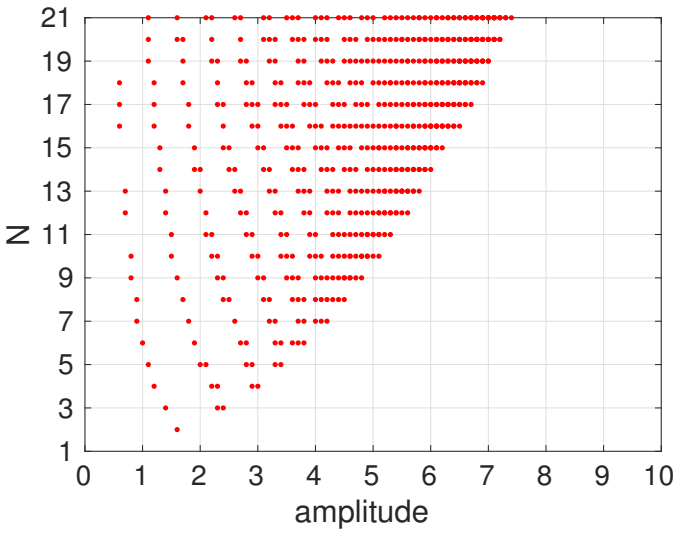

Figure 2.2 – Instability regions of the Goldstone periodic orbit for chains with N nodes for different initial amplitude $a_1(0)$.

2.4.3 The bivalent periodic orbit

The bivalent periodic orbit $a_j(t)$ solution of (2.15) can be expressed via Jacobi elliptic cosine [41]

$$a_j(t) = \gamma \, \mathrm{cn}\left(\Omega t, \kappa^2\right), \tag{2.23}$$

where $\gamma = a_j(0)$, $\dot{a}_j(0) = 0$ and $\Omega^2 = \frac{\omega_j^2}{1-2\kappa^2}$, while the modulus κ of the elliptic function is determined by $2\kappa^2 = \frac{\gamma^2}{N\omega_j^2+\gamma^2}$.

For the bivalent periodic orbit, the variational system are the uncoupled Lamé equations in the Jacobian form

$$\ddot{z}_k = -\left[\omega_k^2 + \frac{3}{N}\gamma^2 \mathrm{cn}^2\left(\Omega t, \kappa^2\right)\right] z_k, \quad k \in \{1, \ldots, N\}. \tag{2.24}$$

For chains, we studied the Floquet multipliers for the bivalent periodic orbit.

2.4.4 Floquet analysis of the bivalent periodic orbit in chains

Remember that the bivalent mode only exists for chains with an even number of nodes N. We calculate the instability region of the bivalent mode $\mathbf{v}^{\frac{N}{2}+1}$ and present it in Figure 2.3 as a function of the amplitude $a_{\frac{N}{2}+1}(0)$. The points indicate the unstable solutions of (2.24) with N even. For a narrow region starting from a zero amplitude, the bivalent mode is stable. Above a critical amplitude it is unstable. Notice the difference with the Goldstone mode which is mostly stable while the bivalent mode is mostly unstable.

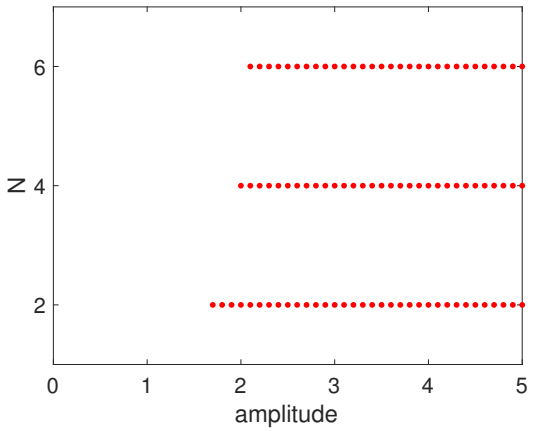

Figure 2.3 – Instability regions of the bivalent mode $\mathbf{v}^{\frac{N}{2}+1}$ for chains with an even number of nodes N for different amplitudes $a_{\frac{N}{2}+1}(0)$.

To illustrate the dynamics of the Goldstone and the bivalent modes, we solve (2.1) for a chain of length 1. We confirm the results of the Floquet analysis and show the couplings that occur in the instability regions.

2.4.5 Example: chain of length 1

For a chain of length 1,

the spectrum is

$$\omega_1^2 = 0,\ \mathbf{v}^1 = \frac{1}{\sqrt{2}}(1,1)^T,$$
$$\omega_2^2 = 2,\ \mathbf{v}^2 = \frac{1}{\sqrt{2}}(1,-1)^T.$$

The amplitude equations (2.2) are:

$$\begin{cases} \ddot{a}_1 = \dfrac{-1}{2}a_1^3 - \dfrac{3}{2}a_1 a_2^2, \\ \ddot{a}_2 = -2a_2 - \dfrac{1}{2}a_2^3 - \dfrac{3}{2}a_1^2 a_2. \end{cases} \tag{2.25}$$

First we consider the evolution of the Goldstone nonlinear periodic orbit. We solve numerically (2.1) for an initial condition $\mathbf{u}(0) = a_1(0)\mathbf{v}^1$ with $\dot{\mathbf{u}}(0) = 0$. The left panel of Figure 2.4 shows the amplitudes $a_1(t), a_2(t)$ for $a_1(0) = 1.6$. As expected from the Floquet analysis Figure 2.2 the orbit is unstable and gives rise to a coupling with the mode $\mathbf{v}^2$. On the other hand, for $a_2(0) = 2$ the amplitudes shown in the right panel of Figure 2.4 do not show any coupling. The Goldstone mode is stable as shown in Figure 2.2. Note that this evolution is similar for large times.

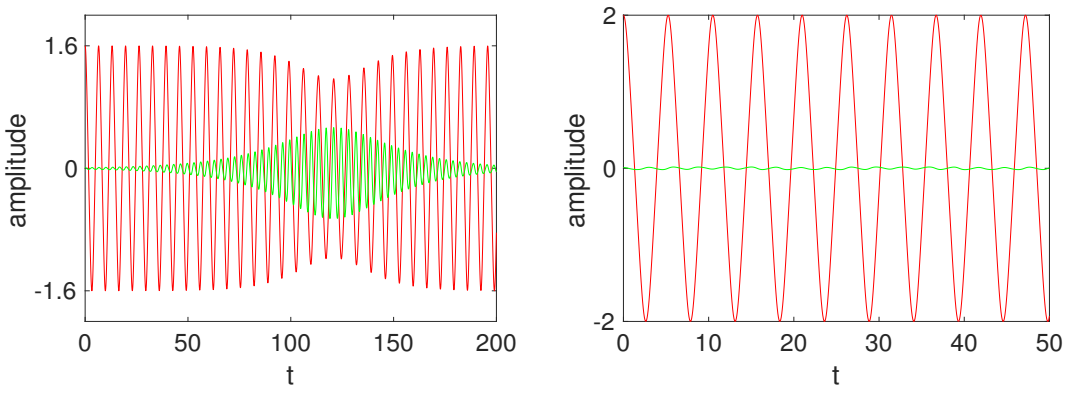

Figure 2.4 – Time evolution of the mode amplitudes a_1 (red online) and a_2 (green online) when exciting Goldstone mode $\mathbf{v}^1$ for $a_1(0) = 1.6$ (left) and $a_1(0) = 2$ (right) with $a_2(0) = 10^{-2}$.

We then consider the evolution of the bivalent mode $\mathbf{v}^2$. For that, we solve numerically (2.1) for an initial condition $\mathbf{u}(0) = a_2(0)\mathbf{v}^2$ and $\dot{a}_2(0) = 0$. For $a_2(0) = 1.5$, the amplitudes shown in the left panel of Figure 2.5 do not show any coupling. As expected from the Floquet analysis in Figure 2.3, the bivalent mode is stable for $a_2(0) < 1.7$ and

unstable for $a_2(0) \geq 1.7$. For $a_2(0) = 1.7$, we observe coupling to the Goldstone mode as shown in the right panel of Figure 2.5.

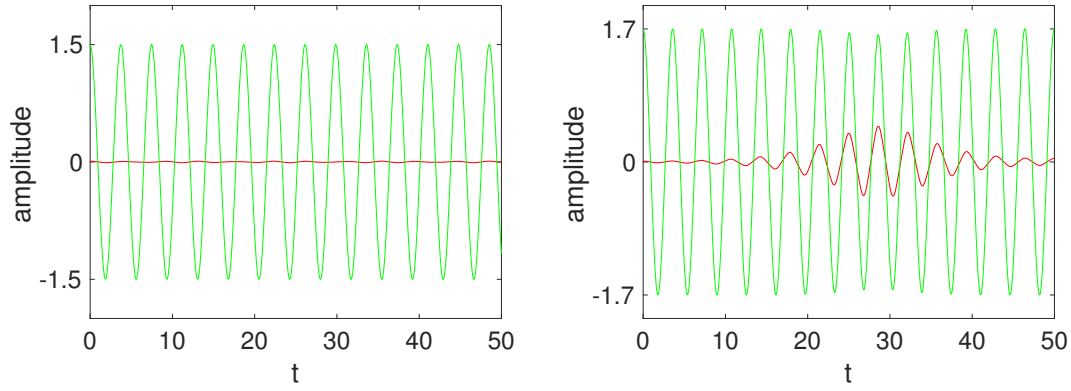

Figure 2.5 – Time evolution of the mode amplitudes a_1 (red online) and a_2 (green online) when exciting the bivalent mode $\mathbf{v}^2$ for $a_2(0) = 1.5$ (left) and $a_2(0) = 1.7$ (right) with $a_1(0) = 10^{-2}$.

2.5 Nonlinear modes containing soft nodes : Numerical simulations

To illustrate the dynamics of trivalent modes, we consider three examples. These are the single frequency mode in a chain of length 2, the double frequency mode of cycle 3, and the modes of the butterfly graph. The latter are the single frequency mode and two double frequency modes. We show the difference in the stability of a single frequency mode versus a double frequency mode.

2.5.1 Chain of length 2

For a chain of length 2,

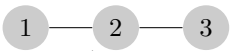

the spectrum is

$$\omega_1^2 = 0,\ \mathbf{v}^1 = \frac{1}{\sqrt{3}}(1,1,1)^T,$$
$$\omega_2^2 = 1,\ \mathbf{v}^2 = \frac{1}{\sqrt{2}}(1,0,-1)^T,$$
$$\omega_3^2 = 3,\ \mathbf{v}^3 = \frac{1}{\sqrt{6}}(1,-2,1)^T.$$

The amplitude equations (2.2) are:

$$\begin{cases} \ddot{a}_1 = \frac{-1}{3}a_1^3 - a_1\left(a_2^2 + a_3^2\right) + \frac{1}{\sqrt{18}}a_3^3 - \frac{1}{\sqrt{2}}a_2^2 a_3, \\ \ddot{a}_2 + a_2 = \frac{-1}{2}a_2^3 - a_2\left(a_1^2 + \frac{1}{2}a_3^2\right) - \sqrt{2}a_1 a_2 a_3, \\ \ddot{a}_3 + 3a_3 = \frac{-1}{2}a_3^3 - a_3\left(a_1^2 + \frac{1}{2}a_2^2\right) - \frac{1}{\sqrt{2}}a_1 a_2^2 + \frac{1}{\sqrt{2}}a_1 a_3^2. \end{cases} \tag{2.26}$$

When exciting the nonlinear mode $\mathbf{v}^2$ containing a soft node, with $a_2(0) = 2$, the modes $\mathbf{v}^1$ and $\mathbf{v}^3$ will be excited as shown in the left panel of Figure 2.6. This instability is explained by two factors. First the coupling terms in the linearized equations (2.14) do not vanish and the variational system is

$$\begin{pmatrix} \ddot{z}_1 \\ \ddot{z}_2 \\ \ddot{z}_3 \end{pmatrix} = \begin{pmatrix} -a_2^2 & 0 & -\frac{1}{\sqrt{2}}a_2^2 \\ 0 & -\left(1 + \frac{3}{2}a_2^2\right) & 0 \\ -\frac{1}{\sqrt{2}}a_2^2 & 0 & -\left(3 + \frac{1}{2}a_2^2\right) \end{pmatrix} \begin{pmatrix} z_1 \\ z_2 \\ z_3 \end{pmatrix}. \tag{2.27}$$

The second factor is the closeness of the nonlinear frequency $\omega_{NL} \approx 1.569$ (for $a_2(0) = 2$) to the linear frequencies of the graph. When the nonlinear frequency is far from the linear frequencies, for example when $a_2(0) \geq 3.12$ ($\omega_{NL} \geq 2.128$) the periodic orbit $\mathbf{v}^2$ is stable and no coupling with the other modes occurs as shown in the right panel of Figure 2.6.

Notice that the matrix in the variational equations (2.27) is the Jacobian matrix [39] of the system (2.26) calculated at the periodic orbit a_2 solution of $\ddot{a}_2 + a_2 = \frac{-1}{2}a_2^3$. Note that this evolution is recurrent for large times.

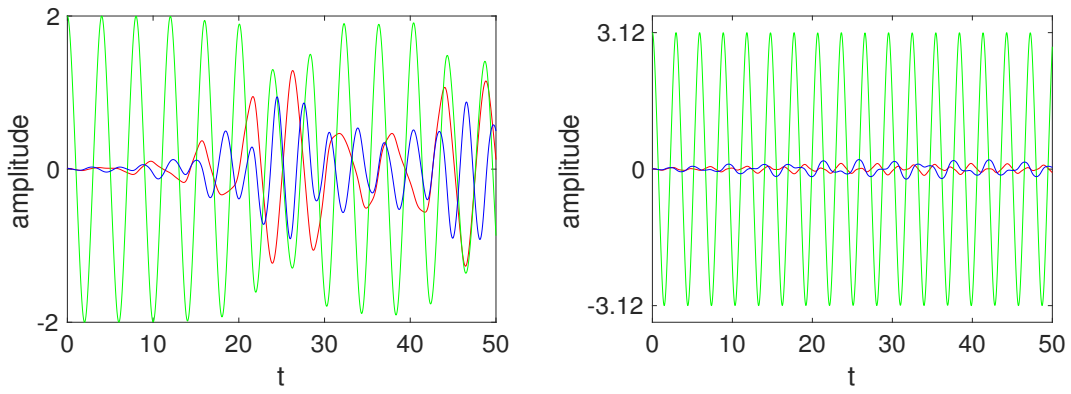

Figure 2.6 – Time evolution of the mode amplitudes a_1 (red online), a_2 (green online) and a_3 (blue online) when exciting the mode $\mathbf{v}^2$ with $a_2(0) = 2$ (left) and $a_2(0) = 3.12$ (right). The other initial amplitudes are $a_1(0) = a_3(0) = 10^{-2}$.

2.5.2 Cycle 3

For a cycle 3,

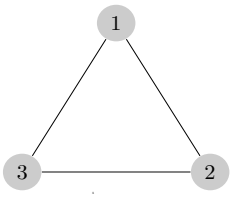

the spectrum is

$$\omega_1^2 = 0,\ \mathbf{v}^1 = \frac{1}{\sqrt{3}}(1,1,1)^T,$$
$$\omega_2^2 = 3,\ \mathbf{v}^2 = \frac{1}{\sqrt{6}}(2,-1,-1)^T,$$
$$\omega_3^2 = 3,\ \mathbf{v}^3 = \frac{1}{\sqrt{2}}(0,1,-1)^T.$$

The amplitude equations (2.2) are:

$$\begin{cases} \ddot{a}_1 = \dfrac{-1}{3}a_1^3 - a_1a_2^2 - a_1a_3^2 - \dfrac{1}{\sqrt{18}}a_2^3 + \dfrac{1}{\sqrt{2}}a_2a_3^2, \\ \ddot{a}_2 + 3a_2 = -a_1^2a_2 - \dfrac{1}{2}a_2^3 - \dfrac{1}{2}a_2a_3^2 - \dfrac{1}{\sqrt{2}}a_1a_2^2 + \dfrac{1}{\sqrt{2}}a_1a_3^2, \\ \ddot{a}_3 + 3a_3 = -a_1^2a_3 - \dfrac{1}{2}a_3^3 - \dfrac{1}{2}a_2^2a_3 + \sqrt{2}a_1a_2a_3. \end{cases} \tag{2.28}$$

The nonlinear mode $\mathbf{v}^3$ containing a soft node and corresponding to a double frequency, is unstable for all initial amplitudes $a_3(0)$. It couples with the modes $\mathbf{v}^1$ and $\mathbf{v}^2$ as shown in Figure 2.7. There, we show the evolution of the amplitudes for initial conditions $a_3(0) = 2$ (left) and $a_3(0) = 8$ (right). The coupling can be seen in the linearized equations (2.14)

$$\begin{pmatrix} \ddot{z}_1 \\ \ddot{z}_2 \\ \ddot{z}_3 \end{pmatrix} = \begin{pmatrix} -a_3^2 & \frac{1}{\sqrt{2}}a_3^2 & 0 \\ \frac{1}{\sqrt{2}}a_3^2 & -\left(3+\frac{1}{2}a_3^2\right) & 0 \\ 0 & 0 & -\left(3+\frac{3}{2}a_3^2\right) \end{pmatrix} \begin{pmatrix} z_1 \\ z_2 \\ z_3 \end{pmatrix}. \tag{2.29}$$

The instability observed for large initial amplitudes seems to be due to the degeneracy of the linear frequency as we discuss below.

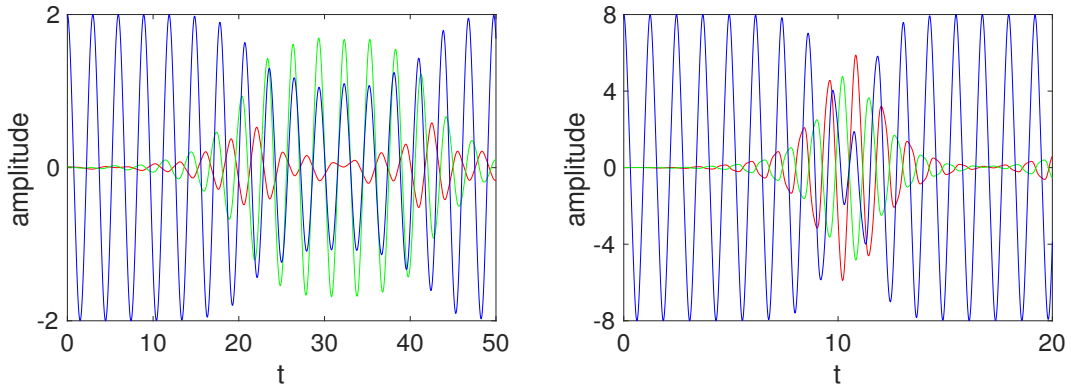

Figure 2.7 – Time evolution of the mode amplitudes a_1 (red online), a_2 (green online) and a_3 (blue online) when exciting the mode $\mathbf{v}^3$ for $a_3(0) = 2$ (left) and $a_3(0) = 8$ (right) with $a_1(0) = a_2(0) = 10^{-2}$.

2.5.3 Butterfly graph

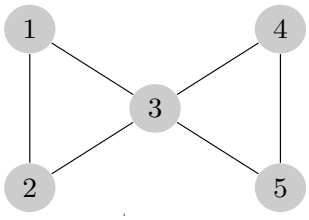

The butterfly graph contains nonlinear mode with soft node corresponding to a simple frequency, and two nonlinear modes with soft nodes corresponding to a double frequency.

The spectrum is

$$\omega_1 = 0,\ \mathbf{v}^1 = \frac{1}{\sqrt{5}}(1,1,1,1,1)^T,$$
$$\omega_2^2 = 1,\ \mathbf{v}^2 = \frac{1}{2}(1,1,0,-1,-1)^T,$$
$$\omega_3^2 = 3,\ \mathbf{v}^3 = \frac{1}{\sqrt{2}}(-1,1,0,0,0)^T,$$
$$\omega_4^2 = 3,\ \mathbf{v}^4 = \frac{1}{\sqrt{2}}(0,0,0,-1,1)^T,$$
$$\omega_5^2 = 5,\ \mathbf{v}^5 = \frac{1}{\sqrt{20}}(-1,-1,4,-1,-1)^T.$$

When exciting the nonlinear mode $\mathbf{v}^2$ containing a soft node and corresponding to a simple frequency $\omega_2 = 1$ for initial conditions $2.3 \leq a_2(0) \leq 3.37$, there is coupling with the modes $\mathbf{v}^1$ and $\mathbf{v}^5$ as shown in Table 2.1. There is no coupling with $\mathbf{v}^3$ and $\mathbf{v}^4$ since the soft node 3 of $\mathbf{v}^2$ is also soft for the modes $\mathbf{v}^3$ and $\mathbf{v}^4$, so that the coupling terms vanish in (2.14). For $a_2(0) \geq 3.38$ ($\omega_{NL} \geq 1.755$), the nonlinear mode $\mathbf{v}^2$ is stable; there is no coupling with the other modes.

The nonlinear modes $\mathbf{v}^3$ and $\mathbf{v}^4$ have soft nodes and correspond to the double frequency $\omega_3 = \omega_4 = \sqrt{3}$. When exciting $\mathbf{v}^3$ with a small amplitude $a_3(0) < 1.5$ we see no coupling with the other modes. Starting from $a_3(0) \geq 1.5$ ($\omega_{NL} \geq 1.958$) there is coupling with the modes $\mathbf{v}_1$, $\mathbf{v}_2$ and $\mathbf{v}_5$ as shown in Table 2.1 and no coupling with $\mathbf{v}^4$. This is because the coupling terms in (2.14) corresponding to the mode $\mathbf{v}^4$ vanish, $\sum_{m\in\mathcal{S}_3} v_m^4 v_m^k = 0,\ \ \forall\ k \neq 4$ where $\mathcal{S}_3 = \left\{m,\ \ v_m^3 = 0\right\}$ the set of the soft nodes of the trivalent mode $\mathbf{v}^3$. We observe similar effects when exciting $\mathbf{v}^4$ instead of $\mathbf{v}^3$, see Table 2.1.

Excited modes	ω_j	Nonlinear frequency	amplitude for instability	Activated modes
$\mathbf{v}_2$	1	$[1.404, 1.751]$	$[2.3, 3.37]$	$\mathbf{v}_2,\ \mathbf{v}_1,\ \mathbf{v}_5$
$\mathbf{v}_3$	$\sqrt{3}$	≥ 1.958	≥ 1.5	$\mathbf{v}_3,\ \mathbf{v}_1,\ \mathbf{v}_2,\ \mathbf{v}_5$
$\mathbf{v}_4$	$\sqrt{3}$	≥ 1.958	≥ 1.5	$\mathbf{v}_4,\ \mathbf{v}_1,\ \mathbf{v}_2,\ \mathbf{v}_5$

Table 2.1 – Excited modes and their associated linear frequencies, nonlinear frequencies depending on the initial amplitudes for instability regions, and the activated modes.

To summarize, we observe that a trivalent periodic orbit is stable for large amplitudes when the eigenvalue is simple. Conversely, when the eigenvalue is double, the periodic orbit is unstable. In fact, the criterion of Aoki [35] is realized only for a particular choice of eigenvectors. Rotating the eigenspace will break the criterion and destroy the periodic

orbits. In that sense, a trivalent periodic orbit for a multiple eigenvalue is structurally unstable.

2.6 Existence of two-mode solutions

We seek nonlinear solutions of (2.1) that involve two nonlinear normal modes. Substituting the ansatz,

$$\mathbf{u}(t) = a_j(t)\mathbf{v}^j + a_k(t)\mathbf{v}^k, \tag{2.30}$$

into the equation of motion (2.1) and projecting on each mode $\mathbf{v}^j$ and $\mathbf{v}^k$, we get

$$\begin{cases} \ddot{a}_j = -\omega_j^2 a_j - \sum_{m=1}^{N} u_m^3 v_m^j, \\ \ddot{a}_k = -\omega_k^2 a_k - \sum_{m=1}^{N} u_m^3 v_m^k, \end{cases}$$

where we have used the orthonormality of the eigenvectors. The term u_m^3 can be written as

$$u_m^3 = a_j^3 (v_m^j)^3 + 3a_j^2 a_k (v_m^j)^2 v_m^k + 3a_j a_k^2 v_m^j (v_m^k)^2 + a_k^3 (v_m^k)^3,$$

so that the above equations can be written

$$\ddot{a}_j = -\omega_j^2 a_j - a_j^3 \sum_{m=1}^{N} (v_m^j)^4 - 3a_j^2 a_k \sum_{m=1}^{N} (v_m^j)^3 v_m^k - 3a_j a_k^2 \sum_{m=1}^{N} (v_m^j)^2 (v_m^k)^2 - a_k^3 \sum_{m=1}^{N} (v_m^k)^3 v_m^j, \tag{2.31}$$

$$\ddot{a}_k = -\omega_k^2 a_k - a_k^3 \sum_{m=1}^{N} (v_m^k)^4 - 3a_j^2 a_k \sum_{m=1}^{N} (v_m^j)^2 (v_m^k)^2 - 3a_j a_k^2 \sum_{m=1}^{N} v_m^j (v_m^k)^3 - a_j^3 \sum_{m=1}^{N} (v_m^j)^3 v_m^k. \tag{2.32}$$

To have two periodic solutions for a_j and a_k, these equations should be uncoupled and this imposes

$$\sum_{m=1}^{N} (v_m^j)^3 v_m^k = 0, \tag{2.33}$$

$$\sum_{m=1}^{N} (v_m^j)^2 (v_m^k)^2 = 0, \tag{2.34}$$

$$\sum_{m=1}^{N} v_m^j (v_m^k)^3 = 0, \tag{2.35}$$

in which case the equations reduce to

$$\begin{cases} \ddot{a}_j = -\omega_j^2 a_j - \dfrac{1}{N - S_j} a_j^3, \\ \ddot{a}_k = -\omega_k^2 a_k - \dfrac{1}{N - S_k} a_k^3. \end{cases} \tag{2.36}$$

where S_j is the number of soft nodes of $\mathbf{v}^j$ and S_k is the number of soft nodes of $\mathbf{v}^k$.

The conditions (2.33, 2.34 and 2.35) are the criteria for the existence of two-mode solutions. It is clear that only trivalent eigenvectors can satisfy these conditions, because if one of the two eigenvectors is monovalent or bivalent, then the condition (2.34) is not satisfied. From the examples mentioned in section 2.2, only cycles where N is multiple of 4 exhibit nonlinear normal modes satisfying the conditions (2.33, 2.34 and 2.35), they are the nonlinear modes $\mathbf{v}^{\frac{N}{2}}$ and $\mathbf{v}^{\frac{N}{2}+1}$ corresponding to the double frequency $\omega_{\frac{N}{2}} = \omega_{\frac{N}{2}+1} = \sqrt{2}$.

2.7 Nonlinear periodic orbits in Fermi-Pasta-Ulam model on networks

For the Fermi-Pasta-Ulam model (cubic intersite nonlinearity), we show below that bivalent and trivalent eigenvectors give rise to nonlinear normal modes. In addition, we identify other eigenvectors giving such nonlinear normal modes.

We consider the Fermi-Pasta-Ulam equation on a general network (1.28)

$$\ddot{u}_i = -\sum_{j=1}^{N} \Delta_{ij}\ u_j - \sum_{k \sim i} (u_i - u_k)^3, \quad i \in \{1, \ldots, N\}. \tag{2.37}$$

Nonlinear normal modes have been investigated in the FPU lattice (for chain or cycle graphs) [44] using powerful group theoretical methods. Stability analysis has been performed explicitely for periodic orbits in the FPU model [45].

2.7.1 Existence of nonlinear normal modes

Let us find the conditions for the existence of a nonlinear periodic solution of (2.37), following [35], of the explicit form

$$\mathbf{u}(t) = a_j(t)\mathbf{v}^j,$$

the equations of motions (2.37) reduce to

$$\ddot{a}_j v_i^j = -\omega_j^2 a_j v_i^j - a_j^3 \sum_{k\sim i} \left(v_i^j - v_k^j\right)^3 . \tag{2.38}$$

These equations are satisfied for the nodes i such that $v_i^j = 0$ (soft nodes) if and only if $\sum_{k\sim i} \left(v_k^j\right)^3 = 0$. This condition is satisfied for trivalent eigenvectors, since $\sum_{k\sim i} v_k^j = \left(d_i - \omega_j^2\right) v_i^j = 0$ which implies (only for trivalent eigenvectors) that $\sum_{k\sim i} \left(v_k^j\right)^3 = 0$.

For $v_i^j \neq 0$, we can simplify (2.38) by v_i^j and obtain

$$\ddot{a}_j = -\omega_j^2 a_j - \left[\frac{1}{v_i^j} \sum_{k\sim i} \left(v_i^j - v_k^j\right)^3\right] a_j^3. \tag{2.39}$$

These equations should be independent of i and this imposes

$$\frac{1}{v_i^j} \sum_{k\sim i} \left(v_i^j - v_k^j\right)^3 = \gamma_j, \quad \forall i \in \{1, \ldots, N\}, \tag{2.40}$$

where γ_j is a constant. Bivalent and trivalent eigenvectors which are identified for the discrete Φ^4 model in section 2.1, satisfy the condition (2.40) and yield nonlinear normal modes also for the FPU model. This is because condition (2.5) implies condition (2.40). It is important to identify other eigenvectors that are not in $\{1, 0, -1\}$ satisfying the condition (2.40).

2.7.2 Other nonlinear periodic orbits for the FPU model

In addition to the bivalent and trivalent eigenvectors identified explicitely and generally for cycles and chains in section 2.2, we have the following eigenvectors satisfying (2.40) :

- For chains with N multiple of 3, the mode $\mathbf{v}^{\frac{2N}{3}+1}$

$$\mathbf{v}^{\frac{2N}{3}+1} = \frac{1}{\sqrt{2N}} \left(1, -2, 1, \mid 1, -2, 1, \mid \ldots, \mid 1, -2, 1\right)^T , \quad \omega^2_{\frac{2N}{3}+1} = 3, \quad \gamma_{\frac{2N}{3}+1} = \frac{3^3}{2N}. \tag{2.41}$$

- For cycles with N multiple of 3, the mode $\mathbf{v}^{\frac{2N}{3}}$

$$\mathbf{v}^{\frac{2N}{3}} = \frac{1}{\sqrt{2N}} \left(2, -1, -1, \mid 2, -1, -1 \mid \ldots, \mid 2, -1, -1\right)^T , \quad \omega^2_{\frac{2N}{3}} = 3, \quad \gamma_{\frac{2N}{3}} = \frac{3^3}{2N}. \tag{2.42}$$

- For star graphs S_{N-1} on N vertices, all the modes $\mathbf{v}^2, \ldots, \mathbf{v}^N$ extend to nonlinear periodic orbits. The normal modes and the corresponding constants γ_j are

$$\begin{aligned}
&\omega_2^2 = 1, \quad \mathbf{v}^2 = \frac{1}{\sqrt{2}}\,(0, 1, -1, 0, \ldots, 0)^T\,, \quad \gamma_2 = \frac{1}{2}, \\
&\omega_3^2 = 1, \quad \mathbf{v}^3 = \frac{1}{\sqrt{2}}\,(0, 0, 1, -1, 0, \ldots, 0)^T\,, \quad \gamma_3 = \frac{1}{2}, \\
&\omega_{N-1}^2 = 1, \quad \mathbf{v}^{N-1} = \frac{1}{\sqrt{2}}\,(0, 0, \ldots, 0, 1, -1)^T\,, \quad \gamma_{N-1} = \frac{1}{2}, \\
&\omega_N^2 = N, \quad \mathbf{v}^N = \frac{1}{\sqrt{N(N-1)}}\,(N-1, -1, \ldots, -1)^T\,, \quad \gamma_N = \frac{N^2}{N-1}.
\end{aligned} \tag{2.43}$$

2.8 Conclusion

We consider the graph wave equation with a cubic on-site nonlinearity on a general network. We identified a criterion allowing to extend some linear normal modes of the graph Laplacian into nonlinear periodic orbits. Three different types of periodic orbits were found, the monovalent, bivalent and trivalent ones depending on whether the corresponding eigenvectors contain 1 or $-1, +1$ or $-1, 0, +1$. For the monovalent and bivalent modes, the linearized equations decouple into N Hill-like equations. For chains, the monovalent mode is mostly stable while the bivalent is unstable. Trivalent modes contain soft nodes and the variational equations do not decouple. The stability is governed by a system of coupled resonance equations; they indicate which modes will be excited when the orbit is unstable. Modes that share a soft node with a trivalent orbit will not be excited. Numerical results show that trivalent modes with a single eigenvalue are unstable below a threshold amplitude. Conversely, trivalent modes with multiple eigenvalues seem always unstable. These results emphasize the importance of normal modes even in the nonlinear regime. They also show that soft nodes change the dynamics, a fact that was pointed out in [7].

In this chapter, we classified the bivalent and trivalent eigenvectors in chains and cycles. In Chapter 3, we characterize the graphs having such eigenvectors.

Chapter 3

On bivalent and trivalent graphs

Abstract. We define a bivalent graph as having a Laplacian eigenvector with components in $\{-1, +1\}$ (bivalent eigenvector) and a trivalent graph as having a Laplacian eigenvector with components in $\{-1, 0, +1\}$ (trivalent eigenvector). These graphs are important because they yield periodic orbits for nonlinear wave equations on networks. In this chapter, we characterize them by applying some graph transformations. Bivalent graphs are shown to be the regular bipartite graphs and their extensions obtained by adding edges between vertices with the same value for the given eigenvector. We define a soft regular graph as having a Laplacian eigenvector whose all non zero component vertices have the same degree. Trivalent graphs are shown to be extensions of these soft regular graphs via the transformations.

The chapter is organized as follows. In section 3.1, we introduce some preliminaries of the graph Laplacian. In section 3.2, we present transformations of graphs. Section 3.3 presents a characterization of bivalent graphs. Section 3.4 presents a similar characterization for trivalent graphs.

3.1 Preliminaries

For simplicity, we consider the eigenvectors $\mathbf{v}^j,\ j \in \{1, \ldots, N\}$ of $\mathbf{\Delta}$ without normalization and denote the eigenvalues by $\lambda_1 = 0 \leq \lambda_2 \leq \cdots \leq \lambda_N$. We note $\mathbf{\Delta}(\mathcal{G})$ instead of $\mathbf{\Delta}$, for a given graph $\mathcal{G}$. Thus, $\mathbf{v}$ is an eigenvector of $\mathbf{\Delta}(\mathcal{G})$ affording λ if and only if

$$(d_i - \lambda)\, v_i = \sum_{k \sim i} v_k, \quad \forall i \in \{1, \ldots, N\}. \tag{3.1}$$

It will be convenient to associate with the eigenvector $\mathbf{v}$ a labeling of $\mathcal{G}$ in which vertex i is labeled v_i. Such labelings are called valuations [46]. Formally, the (vertex)

valuation afforded by eigenvector $\mathbf{v}$ is the function $\mathbf{v} : \mathcal{V} \longrightarrow \mathbb{R}$ defined by $\mathbf{v}(i) = v_i, \;\; i \in \{1, \ldots, N\}$. As the notation indicates, we will feel free to confuse the eigenvector with its associated valuation.

In the following we give some useful definitions from the literature and we present our proper definitions (Def.3 and Def.6).

Definition 2 (Regular graph)**.** *A graph is d-regular if every vertex has the same degree d.*

Definition 3 (Soft regular graph)**.** *A graph is d-soft regular for an eigenvector* $\mathbf{v}$ *of the Laplacian if every non-soft node for* $\mathbf{v}$ *has the same degree d.*

The graph on the left of Figure 3.1 is 3-soft regular for the eigenvector $(0, 1, 1, 0, -1, -1)^T$ since all the non-zero vertices have the same degree 3. The graph on the right of Figure 3.1 is non-soft regular for the eigenvector $(0, 1, 1, 0, -1, -1, 0, 0)^T$ since the non-zero vertices have different degrees.

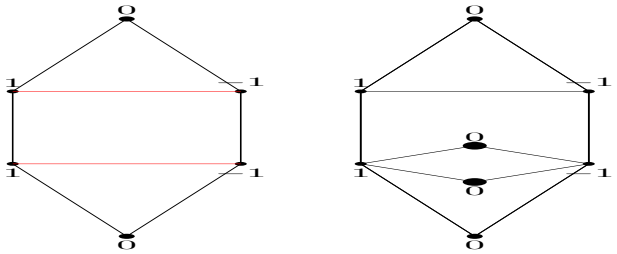

Figure 3.1 – 3-soft regular graph for the Laplacian eigenvector $(0, 1, 1, 0, -1, -1)^T$ (left). Non-soft regular graph for the Laplacian eigenvector $(0, 1, 1, 0, -1, -1, 0, 0)^T$ (right).

Definition 4 (k-partite graph)**.** *A k-partite graph is a graph whose vertices can be partitioned into k different independent sets so that no two vertices within the same set are adjacent.*

When $k = 2$ these are the bipartite graphs, and when $k = 3$ they are the tripartite graphs.

Definition 5 (Perfect matching)**.** *A perfect matching of a graph* $\mathcal{G}$ *is a matching (i.e. an independent edge set) in which every vertex of the graph is incident to exactly one edge of the matching.*

Definition 6 (Alternate perfect matching)**.** *An alternate perfect matching for a vector* $\mathbf{v}$ *on the nodes of a graph* $\mathcal{G}$ *is a perfect matching for the nonzero nodes such that edges* e_{ij} *of the matching satisfy* $v_i = -v_j \;\; (\neq 0)$.

The left of Figure 3.1 shows the alternate perfect matching (represented by red lines) for the vector $(0, -1, -1, 0, 1, 1)^T$ on the nodes of the 6-cycle.

3.2 Transformations of graphs

Merris [47] considers several transformations of graphs based on Laplacian eigenvectors. In the following we review some of them and we present another transformation (Thm.10).

3.2.1 Transformations preserving eigenvalues

Theorem 7 (**Link between two equal nodes** [47]). *Let* $\mathbf{v}$ *be an eigenvector of* $\mathbf{\Delta}(\mathcal{G})$ *affording an eigenvalue* λ. *If* $v_i = v_j$, *then* $\mathbf{v}$ *is an eigenvector of* $\mathbf{\Delta}(\mathcal{G}')$ *affording the eigenvalue* λ, *where* $\mathcal{G}'$ *is the graph obtained from* $\mathcal{G}$ *by deleting or adding the edge* e_{ij} *depending on whether* e_{ij} *is an edge of* $\mathcal{G}$ *or not.*

Proof. Suppose that vertices i and j are not adjacent in $\mathcal{G}$. Because $\mathbf{v}$ is an eigenvector of $\mathcal{G}$, $(d_i - \lambda)\, v_i = \sum_{k\sim i} v_k$. Hence

$$((d_i + 1) - \lambda)\, v_i = v_i + \sum_{k\sim i} v_k = v_j + \sum_{k\sim i} v_k, \tag{3.2}$$

which is the condition that must be met at vertex i for $\mathbf{v}$ to be an eigenvector of $\mathcal{G}'$ affording λ. The eigenvector condition at vertex j is confirmed similarly, and the conditions at the other vertices are the same for $\mathcal{G}'$ as they are for $\mathcal{G}$. Reversing the argument, one establishes the case in which i and j are adjacent in $\mathcal{G}$. □

Suppose $\mathcal{G}_1 = (\mathcal{V}_1, \mathcal{E}_1)$ and $\mathcal{G}_2 = (\mathcal{V}_2, \mathcal{E}_2)$ are graphs on disjoint sets of vertices having eigenvectors $\mathbf{x}$ and $\mathbf{y}$ that afford (the same eigenvalue) λ. Then the valuation $\mathbf{v} : \mathcal{V}_1 \cup \mathcal{V}_2 \longrightarrow \mathbb{R}$ defined by

$$v_k = \begin{cases} x_k, & \text{if } k \in \mathcal{V}_1, \\ y_k, & \text{if } k \in \mathcal{V}_2, \end{cases}$$

is an eigenvector of $\mathcal{G} = \mathcal{G}_1 + \mathcal{G}_2$ that affords λ. If $x_i = y_j$, then, by Thm.7, $\mathbf{v}$ is an eigenvector of the graph $\mathcal{G}'$ obtained from $\mathcal{G}_1 + \mathcal{G}_2$ by adding an edge e_{ij} joining vertex i of $\mathcal{G}_1$ and vertex j of $\mathcal{G}_2$.

Figure 3.2 shows how Thm.7 can be used to extend an eigenvector and its eigenvalue to the transformed graphs by adding edges (represented by red lines) between nodes having the same value. Notice that this transformation does not preserve the regularity of the graph.

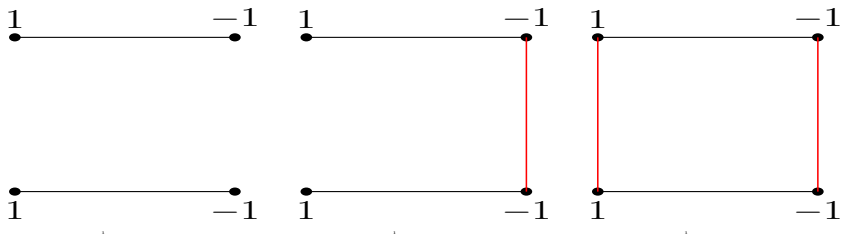

Figure 3.2 – Three graphs obtained by adding or deleting edges between equal nodes, affording (the same eigenvalue) $\lambda = 2$.

Theorem 8 (**Extension/reduction of soft nodes** [47]). *For a graph $\mathcal{G}(\mathcal{V}, \mathcal{E})$ fix a nonempty subset $\mathcal{W}$ of $\mathcal{V}$. Delete all the vertices in $\mathcal{V} \backslash \mathcal{W}$ that are adjacent in $\mathcal{G}$ to no vertex of $\mathcal{W}$. Remove any remaining edges that are incident with no vertex of $\mathcal{W}$. Suppose $\mathbf{v}$ is an eigenvector of the Laplacian of the reduced graph $\mathcal{G}\{\mathcal{W}\}$ that affords λ and is supported by $\mathcal{W}$ in the sense that if $v_i \neq 0$, then $i \in \mathcal{W}$. Then the extension $\mathbf{v}'$ with $v'_j = v_j$ for $j \in \mathcal{W}$ and $v'_j = 0$ otherwise is an eigenvector of $\mathbf{\Delta}(\mathcal{G})$ affording λ.*

Proof. The valuation $\mathbf{v} : \mathcal{V}(\mathcal{G}\{\mathcal{W}\}) \longrightarrow \mathbb{R}$ may be extended to a valuation $\mathbf{v} : \mathcal{V} \longrightarrow \mathbb{R}$ by defining $v_j = 0$ for all $j \in \mathcal{V} \backslash \mathcal{V}(\mathcal{G}\{\mathcal{W}\})$. By Thm.7, this extension is an eigenvector of $\mathcal{G}$ affording λ. □

Thm.8 is illustrated in Figure 3.3

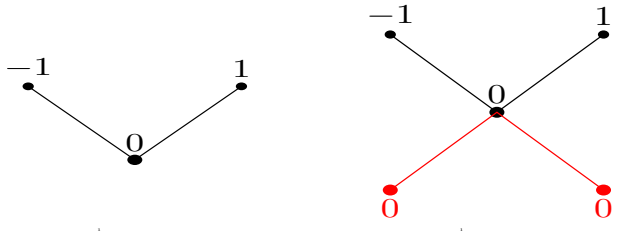

Figure 3.3 – Extension at soft node of the eigenvector $(-1, 0, 1)^T$ by adding soft nodes. The eigenvectors afford (the same eigenvalue) $\lambda = 1$.

Theorem 9 (**Contraction of soft nodes** [47]). *Let $\mathcal{G}$ be a graph on N vertices and $\mathbf{v}$ an eigenvector of $\mathbf{\Delta}(\mathcal{G})$ affording λ. Suppose $i \in \mathcal{V}(\mathcal{G})$, let $\mathcal{N}(i) = \{k \in \mathcal{V}(\mathcal{G}) : e_{ik} \in \mathcal{E}(\mathcal{G})\}$ be the set of its neighbors. Suppose $v_i = 0 = v_j$ where $\mathcal{N}(i) \cap \mathcal{N}(j) = \emptyset$. If e_{ij} is an edge of $\mathcal{G}$, delete it. Let $\mathcal{G}'$ be the graph on $N-1$ vertices obtained by identifying vertices i and j, that is, by contracting them into a single vertex (which is adjacent in $\mathcal{G}'$ to those vertices that are adjacent in $\mathcal{G}$ to i or to j). If $\mathbf{v}'$ is the $(N-1)$-dimensional vector obtained from $\mathbf{v}$ by deleting its j-th coordinate, then $\mathbf{v}'$ is an eigenvector of $\mathbf{\Delta}(\mathcal{G}')$ affording λ.*

Proof. At all but the contracted vertex of $\mathcal{G}'$, the eigenvector condition is the same as

it is for $\mathcal{G}$. Because $\sum_{k\sim i} v_k = 0 = \sum_{k\sim j} v_k$, the eigenvector condition is valid for the contracted vertex of $\mathcal{G}'$ as well. □

Thm.9 is illustrated in Figure 3.4

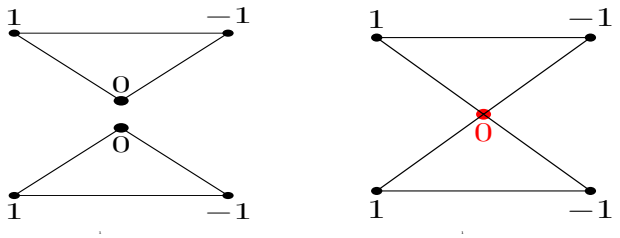

Figure 3.4 – The eigenvector obtained by contracting two soft vertices, affording (the same eigenvalue) $\lambda = 3$.

We introduce the following transformation which preserves the eigenvalues and does not preserve the soft regularity of the graph.

Theorem 10 (**Replace an edge by a soft square** [37])**.** *Let* $\mathbf{v}$ *be an eigenvector of* $\mathbf{\Delta}(\mathcal{G})$ *affording an eigenvalue* λ*. Let* $\mathcal{G}'$ *be the graph obtained from* $\mathcal{G}$ *by deleting an edge* $e_{ij} \in \mathcal{E}(\mathcal{G})$ *such that* $v_i = -v_j$ *and adding two soft nodes* $k, l \in \mathcal{V}(\mathcal{G}')$ *for the extension* $\mathbf{v}'$ *of* $\mathbf{v}$ *(such that* $v'_m = v_m$ *for* $m \in \mathcal{V}(\mathcal{G})$ *and* $v'_k = v'_l = 0$*) and adding four edges* $e_{ik}, e_{kj}, e_{il}, e_{lj} \in \mathcal{E}(\mathcal{G}')$*. Then,* $\mathbf{v}'$ *is an eigenvector of* $\mathbf{\Delta}(\mathcal{G}')$ *for the eigenvalue* λ*.*

Proof. Suppose the edge $e_{ij} \in \mathcal{E}(\mathcal{G})$ joining two nodes having opposite values $v_i = -v_j$, is replaced by a square $e_{ik}, e_{kj}, e_{il}, e_{lj} \in \mathcal{E}(\mathcal{G}')$ of soft nodes $k, l \in \mathcal{V}(\mathcal{G}')$. The eigenvector condition

$$((d_i + 1) - \lambda)\, v_i = v_i + \sum_{m\sim i} v_m = \sum_{m\sim i,\ m\neq j} v_m = 2 \times 0 + \sum_{m\sim i,\ m\neq j} v_m, \qquad (3.3)$$

is the condition that must be met at vertex i for the extension $\mathbf{v}'$ of $\mathbf{v}$, by defining $v'_m = 0$ for $m \in \mathcal{V}(\mathcal{G}') \setminus \mathcal{V}(\mathcal{G})$, to be an eigenvector of $\mathbf{\Delta}(\mathcal{G}')$ affording λ. The eigenvector condition at vertex j is confirmed similarly, and the conditions at the other vertices are the same for $\mathcal{G}'$ as they are for $\mathcal{G}$. □

Figure 3.5 shows how Thm.10 can be used to transform a soft regular graph to a non-soft regular graph without changing the eigenvalue. Note that a square of soft nodes can be replaced by an edge between opposite nodes.

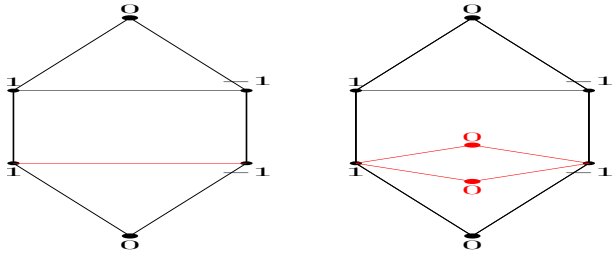

Figure 3.5 – Replacing an edge between opposite nodes by a square of soft nodes. The eigenvectors afford (the same eigenvalue) $\lambda = 3$.

3.2.2 Transformations changing eigenvalues

The following transformation allows us to extend graphs by changing the eigenvalues and preserving the soft regularity of the graph.

Theorem 11 (**Add/Delete an alternate perfect matching** [47])**.** *Let* $\mathbf{v}$ *be an eigenvector of* $\mathbf{\Delta}(\mathcal{G})$ *affording an eigenvalue* λ*. Let* $\mathcal{G}'$ *be the graph obtained from* $\mathcal{G}$ *by adding (resp. deleting) an alternate perfect matching for* $\mathbf{v}$*. Then,* $\mathbf{v}$ *is an eigenvector of* $\mathbf{\Delta}(\mathcal{G}')$ *affording the eigenvalue* $\lambda + 2$ *(resp.* $\lambda - 2$*).*

Proof. Let $i \in \mathcal{V}$ be a fixed but arbitrary vertex. If $v_i = 0$, the eigenvector condition $(d_i - (\lambda + 2))(0) = 0$ is satisfied because the neighbors of i in $\mathcal{G}'$ are the same as its neighbors in $\mathcal{G}$. If $v_i \neq 0$ then it is paired with some j such that $v_i = -v_j$ and the eigenvector condition

$$((d_i \pm 1) - (\lambda \pm 2))\, v_i = (d_i - \lambda)\, v_i \mp v_i = \pm v_j + \sum_{k \sim i} v_k, \tag{3.4}$$

is satisfied in $\mathcal{G}'$. □

Adding an alternate perfect matching is illustrated in Figure 3.6. This transformation preserves the soft regularity of the graph and increases the eigenvalue by 2.

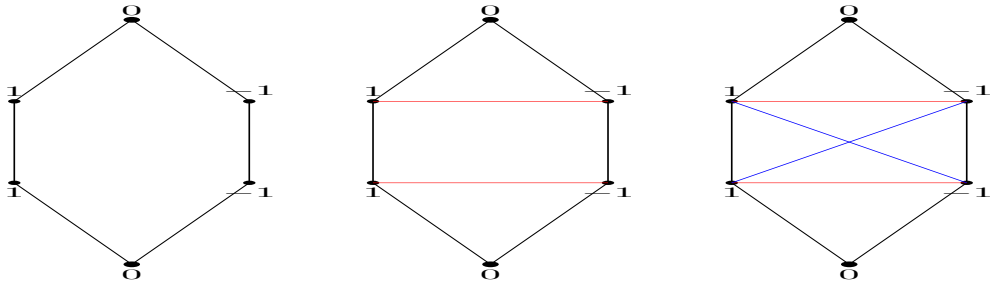

Figure 3.6 – Graphs obtained by adding an alternate perfect matching for the eigenvector $(0,1,1,0,-1,-1)^T$. The eigenvalues are $\lambda = 1$ (left), $\lambda = 3$ (middle) and $\lambda = 5$ (right).

Theorem 12 (**Add soft node** [48])**.** *Let* $\mathbf{v}$ *be an eigenvector of* $\mathbf{\Delta}(\mathcal{G})$ *affording* λ*. Let* $\mathcal{G}'$ *be the graph obtained from* $\mathcal{G}$ *by adding a soft node* k *and edges joining* k *with all the vertices in* $\mathcal{V}(\mathcal{G})$*. Then the extension* $\mathbf{v}'$ *with* $v'_m = v_m$ *for all* $m \in \mathcal{V}(\mathcal{G})$ *and* $v'_k = 0$*, is an eigenvector of* $\mathbf{\Delta}(\mathcal{G}')$ *affording* $\lambda + 1$*.*

Proof. For $i \in \mathcal{V}(\mathcal{G})$, the eigenvector condition

$$((d_i + 1) - (\lambda + 1))\, v_i = (d_i - \lambda)\, v_i = (1)(0) + \sum_{m \sim i} v_m, \tag{3.5}$$

is satisfied in $\mathcal{G}'$. □

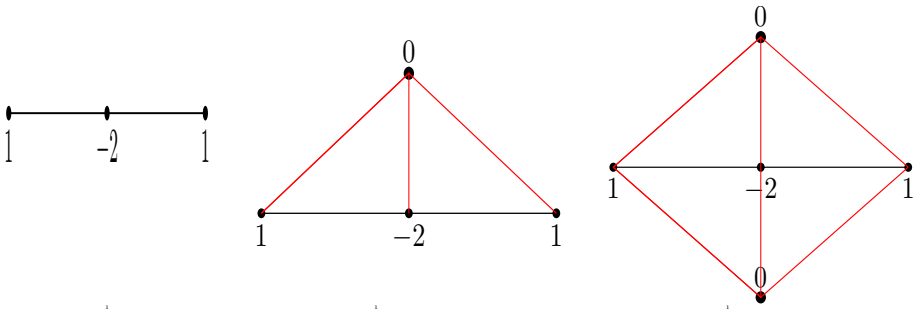

Figure 3.7 – Add of soft node adjacent to all vertices. The eigenvectors afford $\lambda = 3$ (left), $\lambda = 4$ (middle) and $\lambda = 5$ (right).

3.3 Bivalent graphs

The bivalent eigenvector $\mathbf{v}$ must have as many -1 components as $+1$, and thus the bivalent graph must have an even number of nodes. This is a consequence of the orthogonality of $\mathbf{v}$ to the monovalent eigenvector $\mathbf{v}^1$.

Theorem 13 (**Bivalent graphs**). *The bivalent graphs are the regular bipartite graphs and their extensions obtained by adding edges between nodes having the same value for a bivalent eigenvector.*

Proof. Let $\mathcal{G}$ be a graph having a bivalent eigenvector $\mathbf{v}$ affording λ. We reduce $\mathcal{G}$ by deleting all the edges between equal nodes Thm.7, thus obtaining a graph where edges only connect $+1$ to -1. This is a bipartite graph.

We write the eigenvector condition for nodes j (with degree d_j) such that $v_j = 1$

$$(d_j)(1) + \sum_{i \sim j} (-1)(-1) = 2d_j = \lambda. \tag{3.6}$$

Similarly for nodes j such that $v_j = -1$.

The satisfaction of the eigenvector condition for all vertices of $\mathcal{G}$ requires that $\lambda = 2d_j,\ \forall j \in \{1, \ldots, N\}$ so that $d_j = d,\ \forall j \in \{1, \ldots, N\}$. Thus, $\mathcal{G}$ is d-regular graph. Hence a bivalent graph is either a d-regular bipartite graph or obtained from such a graph by adding edges between equal nodes Thm.7.

Reciprocally, a bipartite d-regular graph $\mathcal{G}$ has an even number of nodes and satisfies the eigenvalue condition (3.6) so that $\mathcal{G}$ is bivalent. □

As an example, Figure 3.8 shows the smallest bivalent graph, with eigenvalue $\lambda = 2$. It is a 1-regular graph.

Figure 3.8 – A 1-regular bivalent graph ($d = 1,\ \lambda = 2$).

The extension of two copies of a chain of length 1 seen in Figure 3.8 by adding an alternate perfect matching Thm.11 produces the 2-regular bivalent graph shown in the right of Figure 3.9

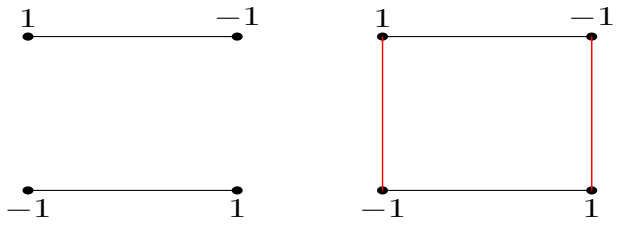

Figure 3.9 – Construction of 2-regular bivalent graph $d = 2,\ \lambda = 4$ (right) from the 1-regular bivalent graph $d = 1,\ \lambda = 2$ (left) by adding an alternate perfect matching.

The extension of three copies of a chain of length 1 seen in Figure 3.8 by adding an alternate perfect matching Thm.11 (two times) gives the 3-regular bivalent graph shown in the right of Figure 3.10

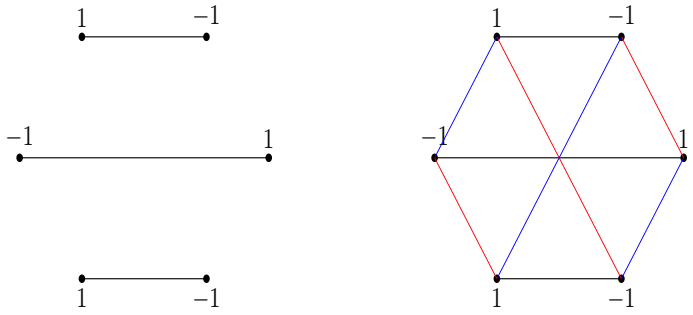

Figure 3.10 – Construction of 3-regular bivalent graph $d = 3,\ \lambda = 6$ (right) from the 1-regular bivalent graph $d = 1,\ \lambda = 2$ (left) by adding two alternate perfect matchings.

Adding edges between equal nodes Thm.7 to three copies of a chain of length 1 seen in Figure 3.8 produces the bivalent eigenvector of the non-regular graphs shown in Figure 3.11 affording the same eigenvalue $\lambda = 2$.

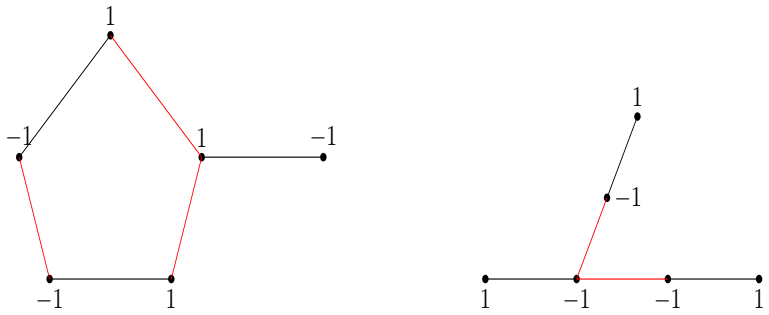

Figure 3.11 – Two bivalent graphs obtained from the 1-regular graph by adding edges between equal nodes, that afford (the same eigenvalue) $\lambda = 2$.

Note that a bivalent eigenvector affords an eigenvalue $\lambda \in \{2, 4, \ldots, 2d_{min}\}$ where d_{min} is the smallest degree of nodes in the graph.

We recover the following result from [50].

Theorem 14 (Bivalent tree)**.** *A tree $\mathcal{T}$ is bivalent if and only if it has a perfect matching.*

Proof. First note that a tree is bipartite and that a 1-regular graph is a perfect matching. Assume $\mathcal{T}$ be a bivalent tree. Then there exists an eigenvector $\mathbf{v}$ with entries solely in $\{1, -1\}$ built from a d-regular bipartite graph by adding edges between nodes of equal

values. Since a tree always has leaves (nodes of degree 1), d must be equal to 1, the subgraph is 1-regular hence a perfect matching.

Conversely, if a tree has a perfect matching, it is easy to construct a bivalent eigenvector by taking opposite values in each edge of the matching, as there are no cycles in a tree, this can be done by Breadth-First Search (BFS) or Depth-First Search (DFS) algorithms [49].

□

For a general graph, the existence of a perfect matching is not a sufficient condition to be bivalent. As examples, we show in Figure 3.12 two asymmetric graphs *i.e.* which have no symmetries.

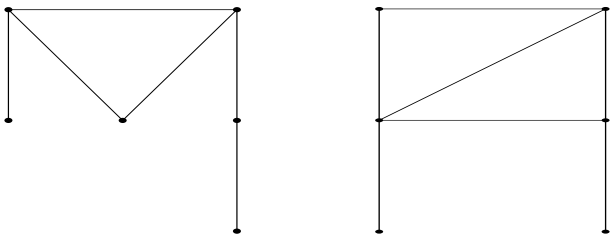

Figure 3.12 – Two asymmetric 6-node graphs. They have a perfect matching but are not bivalent.

3.4 Trivalent graphs

The trivalent eigenvectors have soft nodes, yielding a different dynamical behavior as shown in Chapter 2. The authors in [48] present a classification of graphs whose Laplacian matrices have eigenvectors with soft nodes.

Theorem 15 (**Trivalent graphs**). *Trivalent graphs are obtained from soft regular graphs by applying to the same trivalent eigenvector the transformations:*

- *add a link between two equal nodes,*
- *extension/reduction of soft nodes,*
- *replace an edge by a soft square.*

Proof. Let $\mathcal{G}$ be a graph having a trivalent eigenvector $\mathbf{v}$ affording λ.

We reduce $\mathcal{G}$ by deleting all the edges between equal nodes Thm.7 and deleting soft nodes that are not adjacent to non-soft nodes Thm.8, thus obtaining a graph where edges only connect nodes with different values in $\{1, -1, 0\}$. This is a tripartite graph.

For soft nodes j in the reduced graph, the eigenvector condition

$$(d_j)(0) + \sum_{i\sim j,\ v_i=1} (-1)(1) + \sum_{i\sim j,\ v_i=-1} (-1)(-1) = (\lambda)(0) = 0,$$

requires that

$$\text{card}\,\{i \sim j,\ v_i = +1\} = \text{card}\,\{i \sim j,\ v_i = -1\}\,. \tag{3.7}$$

The eigenvector condition for nodes j such that $v_j = 1$,

$$(d_j)(1) + \sum_{i\sim j,\ v_i\neq 0} (-1)(-1) + \sum_{i\sim j,\ v_i=0} (-1)(0) = (\lambda)(1).$$

A similar condition holds for nodes j such that $v_j = -1$. Thus,

$$\lambda = d_j + \tilde{d}_j = 2d_j - n_j, \quad \forall j \in \mathcal{S}^c, \tag{3.8}$$

where $\mathcal{S} = \{k,\ v_k = 0\}$ the set of the soft nodes, $\mathcal{S}^c = \{1, \ldots, N\}\backslash\mathcal{S}$ the complement of $\mathcal{S}$ *i.e.* the set of the non-soft nodes, $\tilde{d}_j = \text{card}\,\{i \sim j,\ v_i \neq 0\}$ the number of the non-soft neighbors of j and $n_j = \text{card}\,\{i \sim j,\ v_i = 0\}$ the number of the soft neighbors of j.

The eigenvalue formula (3.8) is satisfied for $\mathcal{G}$ being soft regular for $\mathbf{v}$. For trivalent graphs $\mathcal{G}$ that are not soft regular (an example is shown in the left of Figure 3.13), one can transform $\mathcal{G}$ to soft regular graph by applying Thm.10 several times and replacing each edge between nodes of opposite values by a square of two soft nodes (as shown in the right of Figure 3.13).

Conversely, a soft regular tripartite graph $\mathcal{G}$ satisfies the eigenvalue condition (3.8) and any extension of $\mathcal{G}$ of the type above is trivalent.

□

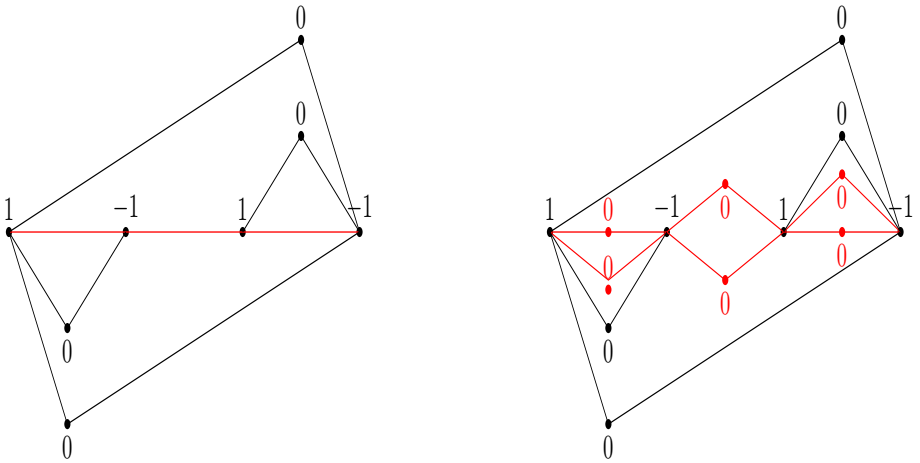

Figure 3.13 – Two trivalent graphs, a non-soft regular graph (left) and a 5-soft regular graph (right), affording (the same eigenvalue) $\lambda = 5$.

Below we give a classification by eigenvalues of the smallest trivalent graphs. Then, the transformations connecting the elements within each class generate trivalent graphs.

The smallest trivalent graph having eigenvalue $\lambda = d_j + \tilde{d}_j = 1$ (where j is a non-soft vertex) satisfies $d_j = 1,\ \tilde{d}_j = 0$. That is the chain of 3 nodes shown in Figure 3.14.

Trivalent trees are constructed from trivalent chain of 3 vertices $(1, 0, -1)^T$ by adding nodes between two equal-valued vertices Thm.7 and extension of soft nodes Thm.8. A characterization of all trees that have 1 as the third smallest Laplacian eigenvalue $\lambda_3 = 1$ is presented in [51].

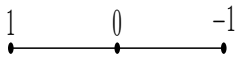

Figure 3.14 – The smallest trivalent graph affording $\lambda = 1$.

The smallest trivalent graphs having eigenvalue $\lambda = d_j + \tilde{d}_j = 2$ (where j is a non-soft vertex) satisfy :

- $d_j = 2,\ \tilde{d}_j = 0$. That is the cycle 4 shown in the left of Figure 3.15,
- $d_j = \tilde{d}_j = 1$. That is the 1-regular bivalent graph.

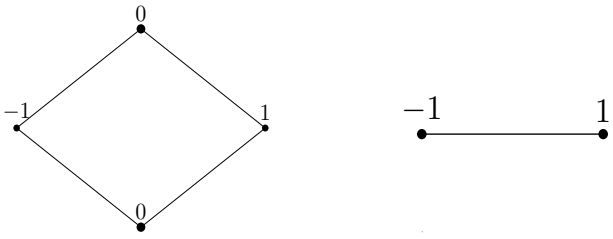

Figure 3.15 – The smallest trivalent graphs affording $\lambda = 2$.

The smallest trivalent graphs having eigenvalue $\lambda = d_j + \tilde{d}_j = 3$ (where j is a non-soft vertex) satisfy :

- $d_j = 3,\ \tilde{d}_j = 0$. That is the graph shown in the left of Figure 3.16,
- $d_j = 2,\ \tilde{d}_j = 1$. That is the graph shown in the right of Figure 3.16.

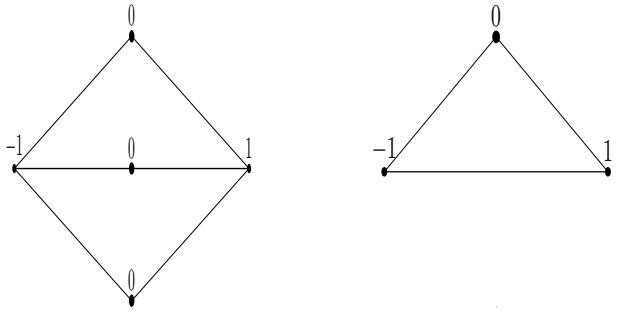

Figure 3.16 – The smallest trivalent graphs affording $\lambda = 3$.

The smallest trivalent graphs having eigenvalue $\lambda = d_j + \tilde{d}_j = 4$ (where j is a non-soft vertex) satisfy :

- $d_j = 4,\ \tilde{d}_j = 0$. That is the graph shown in the left of Figure 3.17,
- $d_j = 3,\ \tilde{d}_j = 1$. That is the graph shown in the middle of Figure 3.17,
- $d_j = \tilde{d}_j = 2$. That is the 2-regular bivalent graph (right of Figure 3.17).

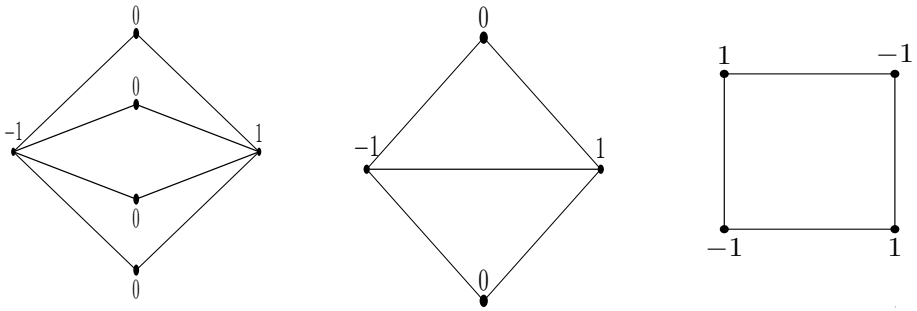

Figure 3.17 – The smallest trivalent graphs affording $\lambda = 4$.

The smallest trivalent graphs having eigenvalue $\lambda = d_j + \tilde{d}_j = 5$ (where j is a non-soft vertex) satisfy :

- $d_j = 5,\ \tilde{d}_j = 0$. That is the graph shown in the left of Figure 3.18,
- $d_j = 4,\ \tilde{d}_j = 1$. That is the graph shown in the middle of Figure 3.18,
- $d_j = 3,\ \tilde{d}_j = 2$. That is the graph shown in the right of Figure 3.18.

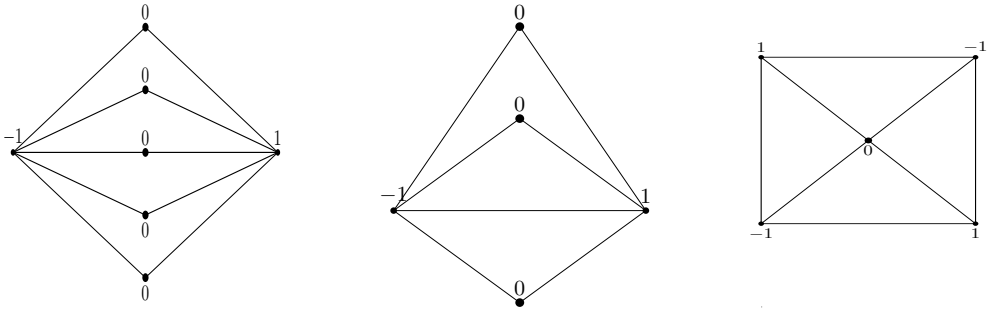

Figure 3.18 – The smallest trivalent graphs affording $\lambda = 5$.

The smallest trivalent graphs having eigenvalue $\lambda = d_j + \tilde{d}_j = 6$ (where j is a non-soft vertex) satisfy :

- $d_j = 6,\ \tilde{d}_j = 0$. That is the first graph in Figure 3.19,
- $d_j = 5,\ \tilde{d}_j = 1$. That is the second graph in Figure 3.19,
- $d_j = 4,\ \tilde{d}_j = 2$. That is the third graph in Figure 3.19,
- $d_j = \tilde{d}_j = 3$. That is the 3-regular bivalent graph (right of Figure 3.19).

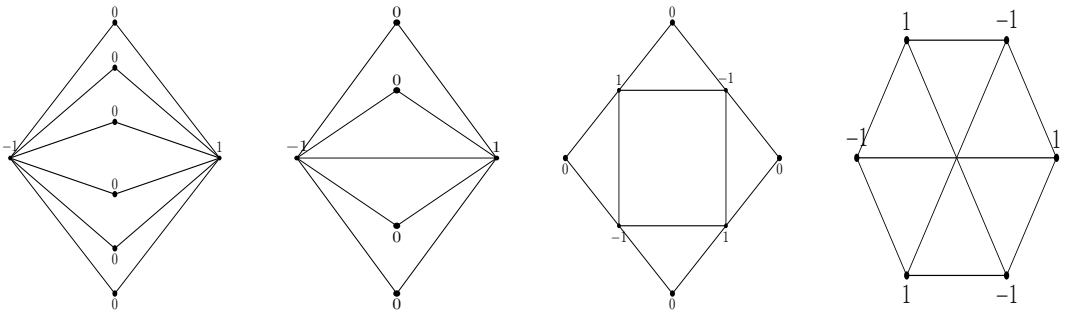

Figure 3.19 – The smallest trivalent graphs affording $\lambda = 6$.

3.5 Conclusion

We have characterized bivalent and trivalent graphs [37] by applying Laplacian eigenvector transformations; these are links between two equal nodes, replacing an edge by a soft square, extension or contraction of soft nodes, adding soft node, and adding or

deleting an alternate perfect matching. These transformations have been also applied in a more general context, that is the classification of graphs whose Laplacian matrices have eigenvectors with soft nodes [48].

We show that bivalent graphs are the regular bipartite graphs and their extensions obtained by adding edges between two equal nodes. We define a soft regular graph as having a Laplacian eigenvector with soft nodes such that each non-soft node has the same degree. Trivalent graphs are shown to be the soft regular graphs and their extensions.

However, the question of whether a given graph is bivalent or trivalent, is difficult and remains open. Wilf [52] asked a similar question: what kind of a graph admits an adjacency matrix eigenvector consisting solely of ± 1 entries? More recently, Stevanović [53] proved that Wilf's problem is NP-complete, and also that the set of graphs having a ± 1 eigenvector of adjacency matrix is quite large. Note that for the regular graphs, our results on the spectrum of the graph Laplacian carry over to the spectrum of the adjacency matrix.

The exploration of these graphs is useful, because they yield periodic orbits for the discrete Φ^4 model and for the Fermi-Pasta-Ulam model.

Chapter 4

Averaging for the nonlinear graph wave equation

In this chapter, we present a first exploration of the averaging method for the simplified version of the discrete Φ^4 model studied in Chapter 2. Our aim was to use this procedure to study the nonlinear couplings of normal modes. However, applying the averaging method to this model is difficult. We explain here the difficulty and how we can solve it.

We write the amplitude equations, by separating the zero frequency (Goldstone) mode and the other modes. For these modes, we perform an averaging and determine the non-resonant terms that do not contribute in the motion. The difficulty is that this procedure cannot be applied for terms containing Goldstone mode, for which we use action angle variables, in order to average those terms around Goldstone orbit. Then, we determine a set of resonance conditions and study it for particular graphs that are complete, cycle and chain graphs. At the end, we highlight the work that remains to be done.

4.1 Amplitude equations

We consider a simplified version of the nonlinear graph wave equation (1.22) with a natural frequency $\omega = 0$ and a coupling coefficient $\epsilon = 1$

$$\ddot{\mathbf{u}} = -\boldsymbol{\Delta}\mathbf{u} - \mathbf{u}^3. \tag{4.1}$$

The amplitude equations of (4.1) are

$$\ddot{a}_j = -\omega_j^2 a_j - \sum_{k,l,n=1}^{N} \Gamma_{jkln}\, a_k a_l a_n, \quad j \in \{1, \dots, N\}, \tag{4.2}$$

where

$$\Gamma_{jkln} = \sum_{m=1}^{N} v_m^j \; v_m^k \; v_m^l \; v_m^n. \tag{4.3}$$

Conversely to the variables $a_j,\ j \in \{2, \ldots, N\}$ in the linear evolution, the zero frequency (Goldstone) mode a_1 is not a periodic oscillation, it is a linear function of time $a_1(t) = \dot{a}_1(0)t + a_1(0)$. Then, it is convenient to separate the variables, a_1 and $a_j,\ j \in \{2, \ldots, N\}$, when considering the nonlinear equations.

For $j = 1$, the amplitude equation is

$$\ddot{a}_1 = -\frac{1}{N} a_1^3 - \frac{3}{N} a_1 \sum_{k=2}^{N} a_k^2 - \frac{1}{\sqrt{N}} \sum_{k,l,n=2}^{N} \gamma_{kln} \; a_k a_l a_n, \tag{4.4}$$

where

$$\gamma_{kln} = \sum_{m=1}^{N} v_m^k \; v_m^l \; v_m^n.$$

The amplitude equations for $j \in \{2, \ldots, N\}$ are

$$\ddot{a}_j + \omega_j^2 a_j = -\frac{3}{N} a_1^2 a_j - \frac{1}{\sqrt{N}} a_1 \sum_{k,l=2}^{N} \gamma_{jkl} \; a_k a_l - \sum_{k,l,n=2}^{N} \Gamma_{jkln} \; a_k a_l a_n. \tag{4.5}$$

To reduce the order of equations (4.5), we use the change of variables

$$z_j = \frac{1}{2} a_j + \frac{\mathrm{i}}{2\omega_j} \dot{a}_j, \quad j \in \{2, \ldots, N\}. \tag{4.6}$$

The equation of Goldstone mode (4.4) becomes

$$\begin{aligned} \ddot{a}_1 = &-\frac{1}{N} a_1^3 - \frac{3}{N} a_1 \sum_{k=2}^{N} \left(z_k^2 + (z_k^*)^2 + 2 z_k z_k^* \right) \\ &- \frac{1}{\sqrt{N}} \sum_{k,l,n=2}^{N} \gamma_{kln} \left(z_k z_l z_n + z_k^* z_l^* z_n^* + 3 z_k^* z_l z_n + 3 z_k^* z_l^* z_n \right). \end{aligned} \tag{4.7}$$

The equations (4.5) for $j \in \{2, \ldots, N\}$ become

$$\begin{aligned} \dot{z}_j + \mathrm{i}\omega_j z_j = &-\frac{3\mathrm{i}}{2\omega_j N} a_1^2 \left(z_j + z_j^* \right) - \frac{\mathrm{i}}{2\omega_j \sqrt{N}} a_1 \sum_{k,l=2}^{N} \gamma_{klj} \left[z_k z_l + 2 z_k^* z_l + z_k^* z_l^* \right] \\ &- \frac{\mathrm{i}}{2\omega_j} \sum_{k,l,n=2}^{N} \Gamma_{klnj} \left(z_k z_l z_n + z_k^* z_l^* z_n^* + 3 z_k^* z_l z_n + 3 z_k^* z_l^* z_n \right). \end{aligned} \tag{4.8}$$

To analyze the equations (4.8), we write

$$z_j = \rho_j \, \mathrm{e}^{-\mathrm{i}\omega_j t}, \quad j \in \{2, \ldots, N\}. \tag{4.9}$$

For a linear system, ρ_j is a constant determined by the initial conditions, and no energy transfer occurs between the modes. When the nonlinearity is present, ρ_j will vary on a time scale large compared to the period $\frac{2\pi}{\omega_j}$. Replacing (4.9) in (4.7), we get

$$\begin{aligned}
\ddot{a}_1 = &-\frac{1}{N} a_1^3 - \frac{3}{N} a_1 \sum_{k=2}^{N} \left[\rho_k^2 \, \mathrm{e}^{-2\mathrm{i}\omega_k t} + (\rho_k^*)^2 \, \mathrm{e}^{2\mathrm{i}\omega_k t} + 2\rho_k \rho_k^* \right] \\
&- \frac{1}{\sqrt{N}} \sum_{k,l,n=2}^{N} \gamma_{kln} \Big[\rho_k \rho_l \rho_n \, \mathrm{e}^{-\mathrm{i}(\omega_k+\omega_l+\omega_n)t} + \rho_k^* \rho_l^* \rho_n^* \, \mathrm{e}^{\mathrm{i}(\omega_k+\omega_l+\omega_n)t} \\
&+ 3\rho_k^* \rho_l \rho_n \, \mathrm{e}^{-\mathrm{i}(-\omega_k+\omega_l+\omega_n)t} + 3\rho_k^* \rho_l^* \rho_n \, \mathrm{e}^{-\mathrm{i}(-\omega_k-\omega_l+\omega_n)t} \Big].
\end{aligned} \tag{4.10}$$

Replacing (4.9) in (4.8), we get

$$\begin{aligned}
\dot{\rho}_j = &-\frac{3\mathrm{i}}{2\omega_j N} a_1^2 \left(\rho_j + \rho_j^* \, \mathrm{e}^{2\mathrm{i}\omega_j t} \right) - \frac{\mathrm{i}}{2\omega_j \sqrt{N}} a_1 \sum_{k,l=2}^{N} \gamma_{klj} \Big[\rho_k \rho_l \, \mathrm{e}^{-\mathrm{i}(\omega_k+\omega_l-\omega_j)t} \\
&+ 2\rho_k^* \rho_l \, \mathrm{e}^{-\mathrm{i}(-\omega_k+\omega_l-\omega_j)t} + \rho_k^* \rho_l^* \, \mathrm{e}^{\mathrm{i}(\omega_k+\omega_l+\omega_j)t} \Big] \\
&- \frac{\mathrm{i}}{2\omega_j} \sum_{k,l,n=2}^{N} \Gamma_{klnj} \Big[\rho_k \rho_l \rho_n \, \mathrm{e}^{-\mathrm{i}(\omega_k+\omega_l+\omega_n-\omega_j)t} + \rho_k^* \rho_l^* \rho_n^* \, \mathrm{e}^{\mathrm{i}(\omega_k+\omega_l+\omega_n+\omega_j)t} \\
&+ 3\rho_k^* \rho_l \rho_n \, \mathrm{e}^{-\mathrm{i}(-\omega_k+\omega_l+\omega_n-\omega_j)t} + 3\rho_k^* \rho_l^* \rho_n \, \mathrm{e}^{-\mathrm{i}(-\omega_k-\omega_l+\omega_n-\omega_j)t} \Big].
\end{aligned} \tag{4.11}$$

In the last sums on the right hand side of (4.10) and (4.11) appear two types of terms, the ones such that the phase

$$\begin{aligned}
&\omega_k + \omega_l + \omega_j \\
&-\omega_k + \omega_l + \omega_j \\
&-\omega_k - \omega_l + \omega_j \\
&\omega_k + \omega_l + \omega_n - \omega_j \\
&\omega_k + \omega_l + \omega_n + \omega_j \\
&-\omega_k + \omega_l + \omega_n - \omega_j \\
&-\omega_k - \omega_l + \omega_n - \omega_j
\end{aligned}$$

is non zero; these are rotating fast and average to zero on the slow time scale [54]. The

other terms -so called- resonant terms are such that

$$\omega_k + \omega_l + \omega_j = 0, \tag{4.12}$$
$$-\omega_k + \omega_l + \omega_j = 0, \tag{4.13}$$
$$-\omega_k - \omega_l + \omega_j = 0, \tag{4.14}$$
$$\omega_k + \omega_l + \omega_n - \omega_j = 0, \tag{4.15}$$
$$\omega_k + \omega_l + \omega_n + \omega_j = 0, \tag{4.16}$$
$$-\omega_k + \omega_l + \omega_n - \omega_j = 0 \tag{4.17}$$
$$-\omega_k - \omega_l + \omega_n - \omega_j = 0. \tag{4.18}$$

They will contribute to the motion of ρ_j. This is the rotating wave approximation ([8] p.813). The study of the Fermi-Pasta-Ulam model [55] yielded a similar resonance conditions.

However, for the rest of cubic terms that contain Goldstone mode a_1, the averaging method cannot be applied, because the terms $a_1 z_j^2$ and $a_1^2 z_j$ are of order t and thus cannot be averaged. Below, we show how we can average these terms containing a_1 around the Goldstone orbit.

4.2 Action-Angle representation for Goldstone mode

For the Goldstone mode it is more convenient to work with action angle variables (I, θ) [56]. The Goldstone orbit is the solution of

$$\ddot{a}_1 = \frac{-1}{N} a_1^3, \tag{4.19}$$

If we define the conjugate $q_1 = a_1, \quad p_1 = \dot{q}_1$, the Hamiltonian $\mathcal{H}_0$ of (4.19) is

$$\mathcal{H}_0(q_1, p_1) = \frac{1}{2}(p_1)^2 + \frac{1}{4N} q_1^4. \tag{4.20}$$

The solutions lie on the level curves of the energy $E_0 = \mathcal{H}_0(q_1, p_1)$ which is a constant of the motion. We set $\alpha = (4N\ E_0)^{\frac{1}{4}}$, then we can write the solution as (Appendix D)

$$q_1(t) = \alpha\ \mathrm{cn}\left(\frac{\alpha}{\sqrt{N}} t, \frac{1}{\sqrt{2}}\right), \tag{4.21}$$

where we have chosen $\dot{q}_1(0) = 0$. The period of oscillations is

$$T = \frac{\sqrt{N}\ \Gamma^2(\frac{1}{4})}{\alpha\sqrt{\pi}}. \tag{4.22}$$

We write the Goldstone mode in terms of action angle variables (see calculations in Appendix E)

$$\begin{cases} q_1 = N^{\frac{1}{6}} \ (3I)^{\frac{1}{3}} \ \mathrm{cn}(\theta), \\ p_1 = -N^{\frac{-1}{6}} \ (3I)^{\frac{2}{3}} \ \mathrm{sn}(\theta) \ \mathrm{dn}(\theta), \end{cases} \tag{4.23}$$

where $(I, \theta) \in \mathbb{R}^+ \times \mathbb{R}$ are conjugate variables. For the elliptic modulus $\kappa = \frac{1}{\sqrt{2}}$, we denote for simplicity the Jacobi elliptic functions, $\mathrm{cn}(\theta) = \mathrm{cn}\left(\theta, \frac{1}{\sqrt{2}}\right)$, $\mathrm{sn}(\theta) = \mathrm{sn}\left(\theta, \frac{1}{\sqrt{2}}\right)$ and $\mathrm{dn}(\theta) = \mathrm{dn}\left(\theta, \frac{1}{\sqrt{2}}\right)$. To show that the coordinates (I, θ) given by (4.23) are canonical it is sufficient to show that one has

$$\{q_1, p_1\} = \frac{\partial q_1}{\partial \theta}\frac{\partial p_1}{\partial I} - \frac{\partial q_1}{\partial I}\frac{\partial p_1}{\partial \theta} = 1, \tag{4.24}$$

where $\{.,.\}$ is the Poisson bracket [54]. Then (4.20) becomes

$$E_0 = \frac{1}{4N^{\frac{1}{3}}} (3I)^{\frac{4}{3}} \equiv \mathcal{H}_0(I). \tag{4.25}$$

The angular frequency is then given by

$$\Omega(I) = \frac{\partial \mathcal{H}_0}{\partial I} = \left(\frac{3I}{N}\right)^{\frac{1}{3}}. \tag{4.26}$$

Notice that

$$p_1 = \frac{\partial q_1}{\partial \theta}\frac{\partial \theta}{\partial t}, \quad \frac{\partial \theta}{\partial t} = \frac{\partial \mathcal{H}_0}{\partial I} = \Omega(I).$$

Similar analytical calculation of the action angle variables for the quartic potential are performed in [57].

Since the transformation in action-angle variables is canonical, we write

$$\begin{cases} \dot{I} = \dfrac{-\partial p_1}{\partial \theta} p_1 + \dfrac{\partial q_1}{\partial \theta}\dot{p}_1, \\ \dot{\theta} = \dfrac{\partial p_1}{\partial I} p_1 - \dfrac{\partial q_1}{\partial I}\dot{p}_1, \end{cases} \tag{4.27}$$

to get the equations in the new variables $I, \ \theta$ when replacing $\dot{p}_1 = \ddot{a}_1$ in (4.27) by (4.10)

$$\begin{aligned} \dot{I} = {} & 3\left(\frac{3I}{N}\right)^{\frac{2}{3}} \mathrm{cn}(\theta) \ \mathrm{sn}(\theta) \ \mathrm{dn}(\theta) \ \sum_{k=2}^{N} \left[\rho_k^2 \ \mathrm{e}^{-2\mathrm{i}\omega_k t} + (\rho_k^*)^2 \ \mathrm{e}^{2\mathrm{i}\omega_k t} + 2\rho_k\rho_k^*\right] \\ & + \left(\frac{3I}{N}\right)^{\frac{1}{3}} \mathrm{sn}(\theta) \ \mathrm{dn}(\theta) \ \sum_{k,l,n=2}^{N} \gamma_{kln} \Big[\rho_k\rho_l\rho_n \ \mathrm{e}^{-\mathrm{i}(\omega_k+\omega_l+\omega_n)t} + \rho_k^*\rho_l^*\rho_n^* \ \mathrm{e}^{\mathrm{i}(\omega_k+\omega_l+\omega_n)t} \\ & + 3\rho_k^*\rho_l\rho_n \ \mathrm{e}^{-\mathrm{i}(-\omega_k+\omega_l+\omega_n)t} + 3\rho_k^*\rho_l^*\rho_n \ \mathrm{e}^{-\mathrm{i}(-\omega_k-\omega_l+\omega_n)t}\Big]. \end{aligned} \tag{4.28}$$

$$\dot{\theta} = \left(\frac{3I}{N}\right)^{\frac{1}{3}} + 3N^{\frac{-2}{3}}\,(3I)^{\frac{-1}{3}}\,\mathrm{cn}^2(\theta)\,\sum_{k=2}^{N}\left[\rho_k^2\,\mathrm{e}^{-2\mathrm{i}\omega_k t} + (\rho_k^*)^2\,\mathrm{e}^{2\mathrm{i}\omega_k t} + 2\rho_k\rho_k^*\right]$$
$$+ N^{\frac{-1}{3}}\,(3I)^{\frac{-2}{3}}\,\mathrm{cn}(\theta)\sum_{k,l,n=2}^{N}\gamma_{kln}\left[\rho_k\rho_l\rho_n\,\mathrm{e}^{-\mathrm{i}(\omega_k+\omega_l+\omega_n)t} + \rho_k^*\rho_l^*\rho_n^*\,\mathrm{e}^{\mathrm{i}(\omega_k+\omega_l+\omega_n)t}\right.$$
$$\left. + 3\rho_k^*\rho_l\rho_n\,\mathrm{e}^{-\mathrm{i}(-\omega_k+\omega_l+\omega_n)t} + 3\rho_k^*\rho_l^*\rho_n\,\mathrm{e}^{-\mathrm{i}(-\omega_k-\omega_l+\omega_n)t}\right]. \tag{4.29}$$

Equations (4.11) become

$$\dot{\rho}_j = -\frac{3\mathrm{i}}{2\omega_j}\left(\frac{3I}{N}\right)^{\frac{2}{3}}\mathrm{cn}^2(\theta)\,\left(\rho_j + \rho_j^*\,\mathrm{e}^{2\mathrm{i}\omega_j t}\right)$$
$$- \frac{\mathrm{i}}{2\omega_j}\left(\frac{3I}{N}\right)^{\frac{1}{3}}\mathrm{cn}(\theta)\sum_{k,l=2}^{N}\gamma_{klj}\left[\rho_k\rho_l\,\mathrm{e}^{-\mathrm{i}(\omega_k+\omega_l-\omega_j)t} + 2\rho_k^*\rho_l\,\mathrm{e}^{-\mathrm{i}(-\omega_k+\omega_l-\omega_j)t}\right.$$
$$\left. + \rho_k^*\rho_l^*\,\mathrm{e}^{\mathrm{i}(\omega_k+\omega_l+\omega_j)t}\right] - \frac{\mathrm{i}}{2\omega_j}\sum_{k,l,n=2}^{N}\Gamma_{klnj}\left[\rho_k\rho_l\rho_n\,\mathrm{e}^{-\mathrm{i}(\omega_k+\omega_l+\omega_n-\omega_j)t}\right.$$
$$\left. + \rho_k^*\rho_l^*\rho_n^*\,\mathrm{e}^{\mathrm{i}(\omega_k+\omega_l+\omega_n+\omega_j)t} + 3\rho_k^*\rho_l\rho_n\,\mathrm{e}^{-\mathrm{i}(-\omega_k+\omega_l+\omega_n-\omega_j)t} + 3\rho_k^*\rho_l^*\rho_n\,\mathrm{e}^{-\mathrm{i}(-\omega_k-\omega_l+\omega_n-\omega_j)t}\right].$$

4.3 Averaging around Goldstone orbit

We fix I_0 and change the variables

$$\begin{cases} J(t) = I(t) - I_0, \\ \Psi(t) = \theta(t) - \omega_0 t, \end{cases} \tag{4.30}$$

where

$$\omega_0 = \Omega(I_0) = \frac{\partial \mathcal{H}_0}{\partial I}(I_0) = \left(\frac{3I_0}{N}\right)^{\frac{1}{3}}, \tag{4.31}$$

is the frequency of the selected periodic orbit I_0. Expanding the action term in the Taylor series

$$(3I)^{\frac{1}{3}} = (3I_0)^{\frac{1}{3}} + (3I_0)^{\frac{-2}{3}}\,J - (3I_0)^{\frac{-5}{3}}\,J^2 + \mathcal{O}(J^3).$$

Then, we write the Hamiltonian (4.25) in the Taylor series

$$\mathcal{H}_0(I) = \mathcal{H}_0(I_0) + \frac{\partial \mathcal{H}_0}{\partial I}(I_0)J + \mathcal{O}(J^2) = h_0 + \omega_0 J + \mathcal{O}(J^2), \tag{4.32}$$

where h_0 is the energy level of the periodic orbit I_0.

Expanding the angle terms in Fourier series formally as

$$\mathrm{cn}(\theta) = \sum_{m\in\mathbb{Z}} C_{2m+1}\ \mathrm{e}^{\mathrm{i}(2m+1)\Omega_0 t}\ \mathrm{e}^{\mathrm{i}(2m+1)\Phi}, \tag{4.33}$$

$$\mathrm{cn}^2(\theta) = \sum_{m\in\mathbb{Z}} D_{2m}\ \mathrm{e}^{\mathrm{i}2m\Omega_0 t}\ \mathrm{e}^{\mathrm{i}2m\Phi}, \tag{4.34}$$

$$\mathrm{sn}(\theta)\ \mathrm{dn}(\theta) = \frac{-\mathrm{d}}{\mathrm{d}\theta}\mathrm{cn}(\theta) = \sum_{m\in\mathbb{Z}} \frac{-\mathrm{i}2\pi(2m+1)}{T_0} C_{2m+1}\ \mathrm{e}^{\mathrm{i}(2m+1)\Phi}\ \mathrm{e}^{\mathrm{i}(2m+1)\Omega_0 t}, \tag{4.35}$$

$$\mathrm{cn}(\theta)\ \mathrm{sn}(\theta)\ \mathrm{dn}(\theta) = \frac{-1}{2}\frac{\mathrm{d}}{\mathrm{d}\theta}\mathrm{cn}^2(\theta) = \sum_{m\in\mathbb{Z}} \frac{-\mathrm{i}\pi 2m}{T_0} D_{2m}\ \mathrm{e}^{\mathrm{i}m\Phi}\ \mathrm{e}^{\mathrm{i}m\Omega_0 t}. \tag{4.36}$$

where $\Omega_0 = \frac{2\pi}{T_0}\omega_0$, $\Phi = \frac{2\pi}{T_0}\Psi$ and $T_0 = \frac{\Gamma^2\left(\frac{1}{4}\right)}{\sqrt{\pi}}$ is the period of the cosine elliptic function. Notice that $\Omega_0 = \frac{2\pi}{T}$ is the nonlinear frequency of the Goldstone orbit of period T given by (4.22).

The final equations are

$$\begin{aligned}
\dot{I} = {} & 3\left(\frac{3I}{N}\right)^{\frac{2}{3}} \sum_{m\in\mathbb{Z}} \frac{-\mathrm{i}\pi 2m}{T_0} D_{2m}\ \mathrm{e}^{\mathrm{i}2m\Phi} \sum_{k=2}^{N} \Big[\rho_k^2\ \mathrm{e}^{-\mathrm{i}(2\omega_k - 2m\Omega_0)t} \\
& + (\rho_k^*)^2\ \mathrm{e}^{\mathrm{i}(2\omega_k + 2m\Omega_0)t} + 2\rho_k\rho_k^*\ \mathrm{e}^{\mathrm{i}2m\Omega_0 t}\Big] \\
& + \left(\frac{3I}{N}\right)^{\frac{1}{3}} \sum_{m\in\mathbb{Z}} \frac{-\mathrm{i}2\pi(2m+1)}{T_0} C_{2m+1}\ \mathrm{e}^{\mathrm{i}(2m+1)\Phi} \sum_{k,l,n=2}^{N} \gamma_{kln} \Big[\rho_k\rho_l\rho_n\ \mathrm{e}^{-\mathrm{i}(\omega_k+\omega_l+\omega_n-(2m+1)\Omega_0)t} \\
& + \rho_k^*\rho_l^*\rho_n^*\ \mathrm{e}^{\mathrm{i}(\omega_k+\omega_l+\omega_n+(2m+1)\Omega_0)t} + 3\rho_k^*\rho_l\rho_n\ \mathrm{e}^{-\mathrm{i}(-\omega_k+\omega_l+\omega_n-(2m+1)\Omega_0)t} \\
& + 3\rho_k^*\rho_l^*\rho_n\ \mathrm{e}^{-\mathrm{i}(-\omega_k-\omega_l+\omega_n-(2m+1)\Omega_0)t}\Big].
\end{aligned} \tag{4.37}$$

$$\begin{aligned}
\dot{\theta} = {} & \left(\frac{3I}{N}\right)^{\frac{1}{3}} + 3N^{\frac{-2}{3}}(3I)^{\frac{-1}{3}} \sum_{m\in\mathbb{Z}} D_{2m}\ \mathrm{e}^{\mathrm{i}2m\Phi} \sum_{k=2}^{N} \Big[\rho_k^2\ \mathrm{e}^{-\mathrm{i}(2\omega_k - 2\Omega_0)t} \\
& + (\rho_k^*)^2\ \mathrm{e}^{\mathrm{i}(2\omega_k + 2m\Omega_0)t} + 2\rho_k\rho_k^*\ \mathrm{e}^{\mathrm{i}2m\Omega_0 t}\Big] \\
& + \frac{1}{N^{\frac{1}{3}}}(3I)^{\frac{-2}{3}} \sum_{m\in\mathbb{Z}} C_{2m+1}\ \mathrm{e}^{\mathrm{i}(2m+1)\Phi} \sum_{k,l,n=2}^{N} \gamma_{kln} \Big[\rho_k\rho_l\rho_n\ \mathrm{e}^{-\mathrm{i}(\omega_k+\omega_l+\omega_n-(2m+1)\Omega_0)t} \\
& + \rho_k^*\rho_l^*\rho_n^*\ \mathrm{e}^{\mathrm{i}(\omega_k+\omega_l+\omega_n+(2m+1)\Omega_0)t} + 3\rho_k^*\rho_l\rho_n\ \mathrm{e}^{-\mathrm{i}(-\omega_k+\omega_l+\omega_n-(2m+1)\Omega_0)t} \\
& + 3\rho_k^*\rho_l^*\rho_n\ \mathrm{e}^{-\mathrm{i}(-\omega_k-\omega_l+\omega_n-(2m+1)\Omega_0)t}\Big].
\end{aligned} \tag{4.38}$$

$$
\begin{aligned}
\dot{\rho}_j = &-\frac{3\mathrm{i}}{2\omega_j}\left(\frac{3I}{N}\right)^{\frac{2}{3}} \sum_{m\in\mathbb{Z}} D_{2m}\ \mathrm{e}^{\mathrm{i}2m\Phi}\ \left(\rho_j\ \mathrm{e}^{\mathrm{i}2m\Omega_0 t} + \rho_j^*\ \mathrm{e}^{\mathrm{i}(2\omega_j+2m\Omega_0)t}\right) \\
&- \frac{\mathrm{i}}{2\omega_j}\left(\frac{3I}{N}\right)^{\frac{1}{3}} \sum_{m\in\mathbb{Z}} C_{2m+1}\ \mathrm{e}^{\mathrm{i}(2m+1)\Phi} \sum_{k,l=2}^{N} \gamma_{klj}\left[\rho_k\rho_l\ \mathrm{e}^{-\mathrm{i}(\omega_k+\omega_l-\omega_j-(2m+1)\Omega_0)t}\right. \\
&\left. + 2\rho_k^*\rho_l\ \mathrm{e}^{-\mathrm{i}(-\omega_k+\omega_l-\omega_j-(2m+1)\Omega_0)t} + \rho_k^*\rho_l^*\ \mathrm{e}^{\mathrm{i}(\omega_k+\omega_l+\omega_j+(2m+1)\Omega_0)t}\right] \\
&- \frac{\mathrm{i}}{2\omega_j} \sum_{k,l,n=2}^{N} \Gamma_{klnj}\left[\rho_k\rho_l\rho_n\ \mathrm{e}^{-\mathrm{i}(\omega_k+\omega_l+\omega_n-\omega_j)t} + \rho_k^*\rho_l^*\rho_n^*\ \mathrm{e}^{\mathrm{i}(\omega_k+\omega_l+\omega_n+\omega_j)t}\right. \\
&\left. + 3\rho_k^*\rho_l\rho_n\ \mathrm{e}^{-\mathrm{i}(-\omega_k+\omega_l+\omega_n-\omega_j)t} + 3\rho_k^*\rho_l^*\rho_n\ \mathrm{e}^{-\mathrm{i}(-\omega_k-\omega_l+\omega_n-\omega_j)t}\right]. \qquad (4.39)
\end{aligned}
$$

In the equations (4.37), (4.38) and (4.39) appear two types of terms, the ones such that the phase is non zero; these are rotating fast and average to zero on the slow time scale. The other terms -so called- resonant terms are such that

$$2\omega_k - m\Omega_0 = 0, \qquad (4.40)$$
$$2\omega_k + m\Omega_0 = 0, \qquad (4.41)$$
$$m\Omega_0 = 0, \qquad (4.42)$$
$$\omega_k + \omega_l + \omega_n - m\Omega_0 = 0, \qquad (4.43)$$
$$\omega_k + \omega_l + \omega_n + m\Omega_0 = 0, \qquad (4.44)$$
$$-\omega_k + \omega_l + \omega_n - m\Omega_0 = 0, \qquad (4.45)$$
$$-\omega_k - \omega_l + \omega_n - m\Omega_0 = 0, \qquad (4.46)$$
$$\omega_k + \omega_l + \omega_n - \omega_j = 0, \qquad (4.47)$$
$$\omega_k + \omega_l + \omega_n + \omega_j = 0, \qquad (4.48)$$
$$-\omega_k + \omega_l + \omega_n - \omega_j = 0, \qquad (4.49)$$
$$-\omega_k - \omega_l + \omega_n - \omega_j = 0, \qquad (4.50)$$

where $k,\ l,\ n,\ j \in \{2,\ldots,N\}$ and $m \in \mathbb{Z}$.

The resonant terms will contribute to the motion of $I,\ \theta$ and ρ_j. This is the rotating wave approximation ([8] p.813). This analysis applies to any graph of arbitrary size N.

4.4 Resonance conditions

Several remarks can be made:

- The resonance conditions (4.40) and (4.43) can hold only for $m \in \mathbb{N}^*$.
- The conditions (4.41) and (4.44) can hold only for $m \in -\mathbb{N}^*$.
- The condition (4.40) is similar to (4.41) when replacing m by $-m$. Similarly for (4.43) and (4.44).
- The condition (4.42) hold only for $m = 0$.
- The condition (4.45) is similar to (4.46) when replacing m by $-m$.
- The condition (4.48) is not satisfied for all $k, l, n, j \in \{2, \dots, N\}$.
- The condition (4.50) is similar to (4.47) with a permutation of indices.
- In following, we study the nonlinear resonances (4.40), (4.43), (4.45), (4.47) and (4.49).
- Since the frequencies ω_k are bounded, then for large m or large Ω_0, we do not have resonances (4.40), (4.43) and (4.45).
- For a general graph $\omega_N \leq \sqrt{N}$, then $m\Omega_0 - 2\omega_k = \mathcal{O}(1)$ if $m\Omega_0 - 2\sqrt{N} = \mathcal{O}(1)$ and this is satisfied when $\Omega_0 \gg \frac{2\sqrt{N}}{m}$. This is a sufficient condition to avoid resonance (4.40).
- For the condition (4.43), $m\Omega_0 - (\omega_k + \omega_l + \omega_n) = \mathcal{O}(1)$ if $m\Omega_0 - 3\sqrt{N} = \mathcal{O}(1)$ and this is satisfied when $\Omega_0 \gg \frac{3\sqrt{N}}{m}$. This is a sufficient condition to avoid resonance (4.43).
- For $m = 0$ in (4.45), we must have $\omega_l + \omega_n = \omega_k$ to get resonance.
- The resonance condition (4.49) is satisfied for
  - $k = l = n = j$ and the corresponding coefficient in the averaged equation is $\Gamma_{klnj} = \sum_{m=1}^{N} (v_m^j)^4$.
  - $l = k,\ n = j$ (or $n = k,\ l = j$) and the corresponding coefficient in the averaged equation is $\Gamma_{klnj} = \sum_{m=1}^{N} (v_m^k)^2 (v_m^j)^2$.

4.4.1 Complete graphs

For a complete graph with N nodes, $\omega_j = \sqrt{N},\ \forall j \in \{2, \dots, N\}$.

Resonance $2\ \omega_k - m\ \Omega_0 = 0$

A sufficient condition to avoid the resonance (4.40) is

$$\Omega_0 \neq \frac{2\sqrt{N}}{m}, \quad \forall m \in \mathbb{N}^*.$$

Resonance $\omega_k + \omega_l + \omega_n - m\Omega_0 = 0$

A sufficient condition to avoid the resonance (4.43) is

$$\Omega_0 \neq \frac{3\sqrt{N}}{m}, \quad \forall m \in \mathbb{N}^*.$$

Resonance $-\omega_k + \omega_l + \omega_n - m\Omega_0 = 0$

A sufficient condition to avoid the resonance (4.45) is

$$\Omega_0 \neq \frac{\sqrt{N}}{m}, \quad \forall m \in \mathbb{N}^*.$$

Resonance $\omega_k + \omega_l + \omega_n - \omega_j = 0$

The condition (4.47) is not satisfied, $\omega_k + \omega_l + \omega_n - \omega_j \neq 0, \quad \forall k, l, n, j \in \{2, \ldots, N\}$.

Resonance $-\omega_k + \omega_l + \omega_n - \omega_j = 0$

For a fix $j \in \{2, \ldots, N\}$, the resonance (4.49) is satisfied for the $(N-1)^3$ permutations of indices $k, l, n \in \{2, \ldots, N\}$.

4.4.2 Cycles

For cycles with N nodes, we have $\omega_N \leq 2$

Resonance $2\ \omega_k - m\ \Omega_0 = 0$

A sufficient condition to avoid the resonance (4.40) is $\Omega_0 > 4$.

Resonance $\omega_k + \omega_l + \omega_n - m\Omega_0 = 0$

A sufficient condition to avoid the resonance (4.43) is $\Omega_0 > 6$.

Resonance $-\omega_n + \omega_k + \omega_l - m\Omega_0 = 0$

First, we study the case $m = 0$ where the resonance condition (4.45) reduces to $\omega_k + \omega_l = \omega_n$ which is given by

$$\sin\left(\frac{k\pi}{N}\right) + \sin\left(\frac{l\pi}{N}\right) = \sin\left(\frac{n\pi}{N}\right), \tag{4.51}$$

for $k, l, n \in \{1, \ldots, N-1\}$. Numerical computations of the trigonometric identity (4.51) show that solutions of (4.51) occur for $N = 3p$ and $p \geq 2$. They are

$$N = 3p, \quad \sin\left(\frac{k\pi}{N}\right) + \sin\left(\frac{(p-k)\pi}{N}\right) = \sin\left(\frac{(p+k)\pi}{N}\right), \tag{4.52}$$

where $p \geq 2$ and $1 \leq k \leq \frac{N}{6}$. The relation (4.52) is easily checked using the trigonometric formula $\sin(\alpha+\beta) - \sin(\alpha-\beta) = 2\cos(\alpha)\sin(\beta)$ with $\alpha = \frac{\pi}{3}$ and $\beta = \frac{k\pi}{N}$.
An additional solution exists for $N = 30p$ and $p \geq 1$

$$N = 30p, \quad \sin\left(\frac{3p\pi}{N}\right) + \sin\left(\frac{5p\pi}{N}\right) = \sin\left(\frac{9p\pi}{N}\right), \tag{4.53}$$

for $p \geq 1$. The second solution (4.53) is easily verified because $\sin(3\alpha) = 3\sin(\alpha) - 4\sin^3(\alpha)$ and $\sin\left(\frac{\pi}{10}\right) = \frac{1}{4}\left(\sqrt{5}-1\right)$.

Resonance $\omega_k + \omega_l + \omega_n - \omega_j = 0$

The resonance condition (4.47) for cycle with N nodes is

$$\sin\left(\frac{k\pi}{N}\right) + \sin\left(\frac{l\pi}{N}\right) + \sin\left(\frac{n\pi}{N}\right) = \sin\left(\frac{j\pi}{N}\right), \quad k, l, n, j \in \{1, \ldots, N-1\}.$$

For $N = 30p,\ k = p$, we have the solution

$$N = 30p, \quad \sin\left(\frac{p\pi}{N}\right) + \sin\left(\frac{3p\pi}{N}\right) + \sin\left(\frac{5p\pi}{N}\right) = \sin\left(\frac{11p\pi}{N}\right). \tag{4.54}$$

Notice that (4.54) is obtained by combining (4.52) with $N = 30p,\ k = p$ and (4.53).

4.4.3 Chains

For chains with N nodes, we have $\omega_N \leq 2$.

Resonance $2\ \omega_k - m\ \Omega_0 = 0$

A sufficient condition to avoid the resonance (4.40) is $\Omega_0 > 4$.

Resonance $\omega_k + \omega_l + \omega_n - m\Omega_0 = 0$

A sufficient condition to avoid the resonance (4.43) is $\Omega_0 > 6$.

Resonance $-\omega_n + \omega_k + \omega_l - m\Omega_0 = 0$

First, we study the case $m = 0$ where the resonance condition (4.45) reduces to $\omega_k + \omega_l = \omega_n$ which is given by

$$\sin\left(\frac{k\pi}{2N}\right) + \sin\left(\frac{l\pi}{2N}\right) = \sin\left(\frac{n\pi}{2N}\right), \tag{4.55}$$

for $k, l, n \in \{1, \ldots, N-1\}$. This trigonometric identity is similar to (4.51) when replacing N by $2N$. Resonances occur for $N = 3p$ and $p \geq 2$. They are

$$N = 3p, \quad \sin\left(\frac{k\pi}{2N}\right) + \sin\left(\frac{(2p-k)\pi}{2N}\right) = \sin\left(\frac{(2p+k)\pi}{2N}\right), \tag{4.56}$$

where $1 \leq k \leq \frac{N}{3} - 1$.
An additional solution exists for $N = 15p$ and $p \geq 1$

$$N = 15p, \quad \sin\left(\frac{3p\pi}{2N}\right) + \sin\left(\frac{5p\pi}{2N}\right) = \sin\left(\frac{9p\pi}{2N}\right). \tag{4.57}$$

Resonance $\omega_k + \omega_l + \omega_n - \omega_j = 0$

The resonance condition (4.47) for chain with N nodes is

$$\sin\left(\frac{k\pi}{2N}\right) + \sin\left(\frac{l\pi}{2N}\right) + \sin\left(\frac{n\pi}{2N}\right) = \sin\left(\frac{j\pi}{2N}\right), \quad k, l, n, j \in \{1, \ldots, N-1\}.$$

For $N = 15p,\ k = p$, we have the solution

$$N = 15p, \quad \sin\left(\frac{p\pi}{2N}\right) + \sin\left(\frac{3p\pi}{2N}\right) + \sin\left(\frac{5p\pi}{2N}\right) = \sin\left(\frac{11p\pi}{2N}\right). \tag{4.58}$$

Notice that (4.58) is obtained by combining (4.56) with $N = 30p,\ k = p$ and (4.57).

4.5 Perspective

This procedure can determine the nonlinear stability of the averaged system in the case where all the terms are non-resonant. Moreover, one can explain analytically the instabilities of the Goldstone mode shown in Figure 2.2, by correlating linear instability of the Goldstone orbit with resonances in the averaged system.

Chapter 5

Localized solutions of nonlinear wave equations on networks

Abstract. We study localized solutions for the discrete Φ^4 model on finite arbitrary networks. Assuming a large amplitude localized initial condition on one node of the graph, we approximate its evolution by the Duffing equation. The rest of the network satisfies a linear system forced by the excited node. This approximation is validated by reducing the discrete Φ^4 model to the discrete nonlinear Schrödinger equation and by Fourier analysis. Finally, we examine numerically the condition for localization in the parameter plane, coupling versus amplitude and show that the localization amplitude depends on the maximal normal eigenfrequency.

The chapter is organized as follows: We give the localized modes for the discrete ϕ^4 equation in section 5.1. In section 5.2, we reduce the graph nonlinear wave equation for a non-zero natural frequency to a discrete nonlinear Schrödinger equation and determine nonlinear localized solutions. Section 5.3 confirms this analysis by studying the dynamics in real and Fourier space of two main networks; in particular we examine the localization vs delocalization regimes in the parameter plane coupling vs amplitude.

5.1 The graph nonlinear wave equation : Localized modes

We study the discrete ϕ^4 equation (1.22) on a finite network

$$\ddot{\mathbf{u}} = -\left(\epsilon\mathbf{\Delta} + \omega^2\mathbf{I}\right)\mathbf{u} - \mathbf{u}^3, \tag{5.1}$$

In the Chapter 2, we constructed nonlinear periodic orbits which are extension of some linear normal modes of the graph Laplacian. In this chapter instead, we take a different approach, we assume a large amplitude localized initial condition and search for

nonlinear localized solutions (see [58]). An important remark is that this work can be generalized to any odd power of the nonlinearity.

5.1.1 Natural frequency $\omega = 0$

We consider a large amplitude initial condition localized at node j and examine its evolution. First, we consider the anti-continuum limit, $\epsilon = 0$, the evolution of u_j satisfies the Duffing equation

$$\ddot{u}_j = -u_j^3, \tag{5.2}$$

where $u_j(0) = \rho$. The other nodes u_k, verify $u_k(0) = 0$ and therefore $u_k(t) = 0$. The solution of (5.2) can be written in terms of the cosine Jacobi elliptic function [41]

$$u_j(t) = \rho \ \mathrm{cn}\left(\rho t, \frac{1}{\sqrt{2}}\right), \tag{5.3}$$

where the modulus of cn is $\kappa = \frac{1}{\sqrt{2}}$ (Appendix C) and where we assumed $\dot{u}_j(0) = 0$. The period of oscillations (Appendix D) is

$$T_0 = \frac{\Gamma^2\left(\frac{1}{4}\right)}{\rho\sqrt{\pi}}. \tag{5.4}$$

The frequency of oscillations is

$$\Omega_0 = \frac{2\pi}{T_0} = \frac{2\pi\sqrt{\pi}}{\Gamma^2\left(\frac{1}{4}\right)}\rho, \tag{5.5}$$

Now examine the weak coupling limit $\epsilon \ll 1$. The nearest neighbors k of j solve the forced system

$$\ddot{u}_k = -\epsilon \sum_{p=1}^{N} \Delta_{kp} u_p - u_k^3 = -\epsilon d_k u_k + \epsilon u_j + \epsilon \sum_{p\sim k,\ p\neq j} u_p - u_k^3, \tag{5.6}$$

where d_k is the degree of the node k, the notation $p \sim k$ indicates the adjacency of vertices and the sum is taken over the other neighbors p of k. We assume that u_k is small and will find a condition on ρ for this to hold. If u_k is small, it is natural to neglect the cubic term u_k^3. The part of the solution for u_k due to the forcing is

$$\ddot{u}_k^f = \epsilon u_j(t) = \epsilon\rho \ \mathrm{cn}\left(\rho t, \frac{1}{\sqrt{2}}\right), \tag{5.7}$$

where the forcing u_j is periodic of frequency Ω_0 and amplitude ρ. Then, the response u_k to this periodic forcing will be of amplitude

$$\left|u_k^f\right| = \mathcal{O}\left(\frac{\epsilon}{\rho}\right). \tag{5.8}$$

This amplitude is small if $\rho \geq 1$. Similarly, the next nearest neighbors l of node j exhibit a forced oscillation given by $\ddot{u}_l^f = \epsilon u_k(t)$ and this gives

$$\left| u_l^f \right| = \mathcal{O}\left(\frac{\epsilon^2}{\rho^3} \right). \tag{5.9}$$

For simplicity and without loss of generality, we assume an initial excitation of node $j = 1$. The evolution of the nodes $\{2, \ldots, N\}$ is described by the forced system of linear ordinary differential equations

$$\ddot{\mathbf{v}} = -\epsilon \ \mathbf{\Delta}^1 \ \mathbf{v} + \mathbf{f}, \tag{5.10}$$

where $\mathbf{v} = (u_2, u_3, \ldots, u_N)^T$, $\mathbf{\Delta}^1$ is the matrix obtained by removing the first line and the first column from the graph Laplacian $\mathbf{\Delta}$ and where $\mathbf{f} = (f_1, f_2, \ldots, f_{N-1})^T$ is the forcing term such that $f_k = \epsilon u_1$ if k adjacent to 1 ($k \sim 1$) and 0 otherwise. The matrix $\mathbf{\Delta}^1$ is a reduction of the graph Laplacian $\mathbf{\Delta}$. It is therefore real symmetric and positive, then $\mathbf{\Delta}^1$ has real eigenvalues $0 < \sigma_1^2 \leq \sigma_2^2 \leq \cdots \leq \sigma_{N-1}^2$ and a basis of orthonormal eigenvectors $\mathbf{z}^1, \mathbf{z}^2, \ldots \mathbf{z}^{N-1}$. These verify

$$\mathbf{\Delta}^1 \ \mathbf{z}^m = \sigma_m^2 \ \mathbf{z}^m, \tag{5.11}$$

for $m \in \{1, \ldots, N-1\}$. We expand $\mathbf{v}$ using a basis of the eigenvectors $\mathbf{z}^m$ as

$$\mathbf{v} = \sum_{m=1}^{N-1} \alpha_m \ \mathbf{z}^m. \tag{5.12}$$

Substituting (5.12) into (5.10) and projecting on each eigenvector $\mathbf{z}^m$, we get

$$\ddot{\alpha}_m = -\epsilon \sigma_m^2 \alpha_m + \sum_{p=1}^{N-1} f_p z_p^m, \tag{5.13}$$

where we have used the orthonormality of the eigenvectors of $\mathbf{\Delta}^1$. The sum can be written as

$$\sum_{p=1}^{N-1} f_p z_p^m = \epsilon u_1 \sum_{k \sim 1} z_{k-1}^m.$$

We then get a set of $(N-1)$ second order inhomogeneous ordinary differential equations

$$\ddot{\alpha}_m = -\epsilon \sigma_m^2 \alpha_m + \epsilon u_1 \sum_{k \sim 1} z_{k-1}^m, \tag{5.14}$$

where $m \in \{1, \ldots, N-1\}$. At this level, we just rewrote equation (5.10) in the basis $\mathbf{z}^m$. Initially, $\alpha_m(0) = \dot{\alpha}_m(0) = 0$ so that we only observe the forced response of the system. In particular, the modes α_m such that $\sum_{k \sim 1} z_{k-1}^m = 0$ will remain zero. This reveals that the harmonic frequencies of the solutions $u_2, \ldots, u_N$ that will be observed are

$$\sqrt{\epsilon} \ \sigma_m, \tag{5.15}$$

for $m \in \{1, \ldots, N-1\}$ such that $\sum_{k\sim 1} z_{k-1}^m \neq 0$.

In general, for initial excitation of node j, the harmonic frequencies (5.15) of the matrix $\mathbf{\Delta}^j$ (obtained by removing the j line and the j column from the graph Laplacian $\mathbf{\Delta}$) will be observed if

$$\sum_{k\sim j,\ k<j} z_k^m + \sum_{k\sim j,\ k>j} z_{k-1}^m \neq 0, \tag{5.16}$$

where $\mathbf{z}^m$ are the eigenvectors of $\mathbf{\Delta}^j$.

5.1.2 Natural frequency $\omega \neq 0$

Now, we consider the equation (5.1) with a natural frequency $\omega \neq 0$. The evolution at the excited node j to a first approximation satisfies the Duffing equation

$$\ddot{u}_j = -\omega^2 u_j - u_j^3, \tag{5.17}$$

where $u_j(0) = \rho$. The solution can be written in terms of cosine elliptic functions

$$u_j(t) = \rho \ \mathrm{cn}\left(\sqrt{\omega^2 + \rho^2}\ t,\ \kappa\right), \tag{5.18}$$

where the modulus $\kappa = \sqrt{\frac{\rho^2}{2(\omega^2+\rho^2)}}$ and we assumed $\dot{u}_j(0) = 0$.

As above, we assume an excitation at node $j = 1$. The evolution at nodes $\{2, \ldots, N\}$ is described by the forced system of linear ordinary differential equations

$$\ddot{\mathbf{v}} = -\left(\epsilon\ \mathbf{\Delta}^1 + \omega^2\ \mathbf{I}\right)\mathbf{v} + \mathbf{f}, \tag{5.19}$$

Substituting (5.12) into (5.19) and projecting on each eigenvector $\mathbf{z}^m$ of $\mathbf{\Delta}^1$, we get

$$\ddot{\alpha}_m = -\left(\epsilon\sigma_m^2 + \omega^2\right)\alpha_m + \epsilon u_1 \sum_{k\sim 1} z_{k-1}^m, \tag{5.20}$$

where $m \in \{1, \ldots, N-1\}$. The harmonic frequencies are

$$\sqrt{\epsilon\sigma_m^2 + \omega^2}, \tag{5.21}$$

for $m \in \{1, \ldots, N-1\}$ such that $\sum_{k\sim 1} z_{k-1}^m \neq 0$.

5.2 Modulation theory $\omega \neq 0$

When the natural frequency is not zero, following [59], we reduce the discrete Φ^4 equation (5.1) to the discrete nonlinear Schrödinger equation. We write

$$\mathbf{u}(t) = \sqrt{\epsilon}\boldsymbol{\psi}(T)\mathrm{e}^{\mathrm{i}\omega \mathrm{t}} + \sqrt{\epsilon}\boldsymbol{\psi}^*(\mathrm{T})\mathrm{e}^{-\mathrm{i}\omega \mathrm{t}}\ , \tag{5.22}$$

where $T = \epsilon t$, $\boldsymbol{\psi} = (\psi_1(t), \psi_2(t), \ldots, \psi_N(t))^T$ is the field vector and $\boldsymbol{\psi}^*$ is the complex conjugate of $\boldsymbol{\psi}$. Plugging (5.22) into (5.1) and collecting terms in order of $\epsilon^{\frac{1}{2}}, \epsilon^{\frac{3}{2}}, \ldots$, we obtain for the order $\epsilon^{\frac{3}{2}}$ the graph nonlinear Schrödinger equation (see Appendix F)

$$\frac{2\mathrm{i}\omega}{\epsilon}\dot{\boldsymbol{\psi}} = -\boldsymbol{\Delta}\boldsymbol{\psi} - 3\left|\boldsymbol{\psi}\right|^2\boldsymbol{\psi}\ . \tag{5.23}$$

This model describes the coupling between waveguides in an optical array. In [60], the authors examined how linear normal modes couple due to the cubic nonlinearity in (5.23). Here instead, we assume a large amplitude localized initial condition. This is a natural and relevant consideration that parallels classical studies of discrete solitons in the nonlinear Schrödinger equation and light localization in nonlinear photonic structures.

We assume that $|\psi_j| = r = \frac{\rho}{2\sqrt{\epsilon}} \geq 1$ constant at a given node where $\rho = u_j(0)$, and $|\psi_k| = 0,\ \forall k \neq j$. The evolution of the excited node j is given by

$$\frac{2\mathrm{i}\omega}{\epsilon}\dot{\psi}_j = -3r^2\psi_j. \tag{5.24}$$

The solution of (5.24) is

$$\psi_j(t) = r\ \mathrm{e}^{\mathrm{i}\frac{3\epsilon r^2}{2\omega}t} = \frac{\rho}{2\sqrt{\epsilon}}\mathrm{e}^{\frac{\mathrm{i}3\rho^2}{8\omega}t}. \tag{5.25}$$

Thus, the solution u_j can be approximated using (5.22) by

$$u_j(t) \approx \rho\ \cos\left(\left(\frac{3\rho^2}{8\omega} + \omega\right)t\right), \tag{5.26}$$

where the nonlinear frequency is

$$\Omega \approx \frac{3\rho^2}{8\omega} + \omega. \tag{5.27}$$

This regime is valid when the correction to the frequency of oscillation due to the nonlinearity is smaller than the natural frequency

$$\frac{3}{8\omega}\rho^2 \ll \omega. \tag{5.28}$$

This means ω large enough. Discrete breathers for (5.23) in chains were studied in [34], using the continuation arguments in ϵ starting from the anticontinuous limit, to show the local existence of discrete breathers.

The nearest neighbors k of j solve a forced system

$$\frac{2\mathrm{i}\omega}{\epsilon}\dot{\psi}_k = -\sum_{p=1}^{N}\Delta_{kp}\psi_p = -d_k\psi_k + \psi_j + \sum_{p\sim k,\ p\neq j}\psi_p, \tag{5.29}$$

where we neglected the cubic terms. A particular solution of the forced part $\frac{2\mathrm{i}\omega}{\epsilon}\dot{\psi}_k^f = \psi_j$ is

$$\psi_k^f(t) = \frac{1}{3r}\left(1 - \mathrm{e}^{\mathrm{i}\frac{3\epsilon r^2}{2\omega}t}\right) = \frac{2\sqrt{\epsilon}}{3\rho}\left(1 - \mathrm{e}^{\mathrm{i}\frac{3\rho^2}{8\omega}t}\right). \tag{5.30}$$

Similarly, the evolution of the next nearest neighbors l is given by

$$\frac{2\mathrm{i}\omega}{\epsilon}\dot{\psi}_l = -\sum_{p=1}^{N}\Delta_{lp}\psi_p = -d_l\psi_l + \psi_k + \sum_{p\sim l,\ p\neq k}\psi_p. \tag{5.31}$$

We have the proportional scalings for ψ_k and ψ_l

$$|\psi_k| = \mathcal{O}\left(\frac{\sqrt{\epsilon}}{\rho}\right)\ , \quad |\psi_l| = \mathcal{O}\left(\frac{\epsilon\sqrt{\epsilon}}{\rho^3}\right), \tag{5.32}$$

corresponding to the scalings for u_k and u_l

$$|u_k| = \mathcal{O}\left(\frac{\epsilon}{\rho}\right)\ , \quad |u_l| = \mathcal{O}\left(\frac{\epsilon^2}{\rho^3}\right),$$

similarly to the scalings for $\omega = 0$ (5.8,5.9).

As above, for simplicity and without loss of generality, we assume an excitation of node $j = 1$. The evolution of the nodes $\{2, \ldots, N\}$ is described by the forced system of linear ordinary differential equations

$$\dot{\boldsymbol{\varphi}} = \frac{\mathrm{i}\epsilon}{2\omega}\ \left(\boldsymbol{\Delta}^1\ \boldsymbol{\varphi} - \mathbf{f}\right), \tag{5.33}$$

where $\boldsymbol{\varphi} = (\psi_2, \psi_3, \ldots, \psi_N)^T$, and where $\mathbf{f} = (f_1, f_2, \ldots, f_{N-1})^T$ is the forcing term such that $f_k = \psi_1$ if k adjacent to 1 ($k \sim 1$) and 0 otherwise.

We expand $\boldsymbol{\varphi}$ using a basis of the eigenvectors $\mathbf{z}^m$ of $\boldsymbol{\Delta}^1$

$$\boldsymbol{\varphi} = \sum_{m=1}^{N-1}\beta_m\ \mathbf{z}^m. \tag{5.34}$$

Substituting (5.34) into (5.33) and projecting on each eigenvector $\mathbf{z}^m$, we get

$$\dot{\beta}_m = \mathrm{i}\frac{\epsilon}{2\omega}\sigma_m^2\beta_m - \mathrm{i}\frac{\epsilon}{2\omega}\psi_1\sum_{k\sim 1} z_{k-1}^m. \tag{5.35}$$

The harmonic frequencies of $\boldsymbol{\varphi}$ are $\sqrt{\frac{\epsilon}{2\omega}}\sigma_m$ for $m \in \{1, \ldots, N-1\}$ such that $\sum_{k\sim 1} z_{k-1}^m \neq 0$. The harmonic frequencies of $\mathbf{v} = (u_2, u_3, \ldots, u_N)^T$ using (5.22) are

$$\sqrt{\frac{\epsilon}{2\omega}}\ \sigma_m + \omega, \tag{5.36}$$

for $m \in \{1, \ldots, N-1\}$ such that $\sum_{k\sim 1} z_{k-1}^m \neq 0$. Notice that (5.36) and (5.21) are almost equal for large ω and small ϵ, and these are the conditions of validity of the approximation by modulation theory.

5.3 Numerical results

We illustrate our findings on two graphs: a cycle 3 joined to a single isolated node known as the paw graph (Figure 5.1), and the cycle 6 (Figure 5.7). The first graph is not regular and has one symmetry, the permutation of nodes 3 and 4. The second is a cycle invariant under cyclic permutations. We will see how symmetries affect the observed modes and how localized solutions destabilize.

The system of ordinary differential equations (5.1) is solved in double precision, using a Runge-Kutta 4-5 method with a time step 10^{-2} and a relative error of 10^{-8}. To check the validity of the solutions, we calculated the Fourier transform $\widehat{u}_k$ of each $u_k,\ k \in \{1, \ldots, N\}$. This revealed the frequencies of the motion and allowed a detailed comparison with the analysis of sections 5.2 and 5.3. In practise, we used the fast Fourier transform (FFT) of Matlab on a time-series of $n = 20000$ points on a time $t_f = 200$ to approximate the continuum Fourier transform. The data was multiplied by a Hamming window

$$u_k(m) \times \left(0.54 - 0.46 \cos\left(2\pi \frac{(m-1)}{n}\right)\right),$$

for $m \in \{1, \ldots, n\},\ k \in \{1, \ldots, N\}$.

5.3.1 Paw graph

We consider the paw graph studied in [60].

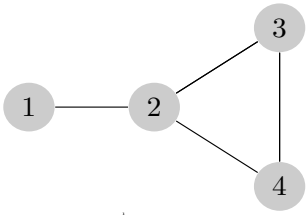

Figure 5.1 – Paw graph.

Natural frequency $\omega = 0$

Exciting node 1

We solve equation (5.1) with $\omega = 0,\ \epsilon = 0.2$ for the paw graph. The left panel of Figure 5.2 shows the time evolution of the solutions $u_k,\ k \in \{1, \ldots, 4\}$ when exciting the system at node $j = 1$ with initial amplitude $u_1(0) = \rho = 3$. We see clearly a localized solution;

it can be observed over more than a thousand periods with no significant decay. The logarithm with base 10 of the modulus of the discrete Fourier transform of the solutions $\log_{10}\left(|\widehat{u}_k|\right),\quad k\in\{1,\ldots,4\}$ are shown on the right panel of Figure 5.2. The Fourier components of the neighbor u_2 corresponding to the linear mode and the nonlinear mode are about equal. As we go to the next nearest neighbor the Fourier component due to the nonlinear excitation of node 1 is a 100 times smaller than the linear response of the network. This is a general feature that we see on all the systems we have analyzed. It confirms the exponential localization of the nonlinear mode.

From the Fourier spectrum, we determine that u_1 oscillates at the nonlinear frequency (5.5) $\Omega_0=\frac{6\pi\sqrt{\pi}}{\Gamma^2\left(\frac{1}{4}\right)}\approx 2.54$ and at the odd harmonics of Ω_0 ($3\Omega_0$ and weakly at $5\Omega_0$) due to the Fourier expansion of the solution (5.3) (formula (D.4) Appendix C)

$$u_1(t)=\rho\ \mathrm{cn}\left(\rho t,\frac{1}{\sqrt{2}}\right)\approx 4\sqrt{2}\ \Omega_0\left[b_1\cos\left(\Omega_0 t\right)+b_3\cos\left(3\Omega_0 t\right)+b_5\cos\left(5\Omega_0 t\right)+\ldots\right], \tag{5.37}$$

where

$$b_1=\frac{\mathrm{e}^{\frac{-\pi}{2}}}{1+\mathrm{e}^{-\pi}},\ b_3=\frac{\mathrm{e}^{\frac{-3\pi}{2}}}{1+\mathrm{e}^{-3\pi}},\ b_5=\frac{\mathrm{e}^{\frac{-5\pi}{2}}}{1+\mathrm{e}^{-5\pi}}.$$

The solutions shown in Figure 5.2 are such that $u_1=\mathcal{O}\left(\rho\right)$ and $|u_2|=\mathcal{O}\left(\frac{\epsilon}{\rho}\right),\ |u_3|=|u_4|=\mathcal{O}\left(\frac{\epsilon}{\rho^3}\right)$. To describe the evolution of u_2,u_3 and u_4, it is then natural to reduce the system (5.1) to the linear system forced by u_1

$$\ddot{u}_1=-u_1^3. \tag{5.38}$$

$$\begin{pmatrix}\ddot{u}_2\\ \ddot{u}_3\\ \ddot{u}_4\end{pmatrix}=-\epsilon\begin{pmatrix}3&-1&-1\\-1&2&-1\\-1&-1&2\end{pmatrix}\begin{pmatrix}u_2\\u_3\\u_4\end{pmatrix}+\epsilon u_1\begin{pmatrix}1\\0\\0\end{pmatrix}. \tag{5.39}$$

The Fourier representation shows that the nearest neighbor u_2 and similarly the next nearest neighbors u_3 and u_4 oscillate at the nonlinear frequency Ω_0 and at the eigenfrequencies (5.15) of the matrix $\epsilon\mathbf{\Delta}^1$

$$\sqrt{\epsilon}\sigma_1=\sqrt{0.2\left(2-\sqrt{3}\right)}\approx 0.23,$$
$$\sqrt{\epsilon}\sigma_3=\sqrt{0.2\left(2+\sqrt{3}\right)}\approx 0.86,$$

where

$$\mathbf{\Delta}^1=\begin{pmatrix}3&-1&-1\\-1&2&-1\\-1&-1&2\end{pmatrix}. \tag{5.40}$$

The eigenvectors of $\mathbf{\Delta}^1$ are

$$\mathbf{z}^1 = \frac{1}{\sqrt{6-2\sqrt{3}}}\begin{pmatrix}\sqrt{3}-1\\1\\1\end{pmatrix},\ \mathbf{z}^2 = \frac{1}{\sqrt{2}}\begin{pmatrix}0\\1\\-1\end{pmatrix},\ \mathbf{z}^3 = \frac{1}{\sqrt{6+2\sqrt{3}}}\begin{pmatrix}\sqrt{3}+1\\-1\\-1\end{pmatrix}. \tag{5.41}$$

The absence of the eigenfrequency $\sqrt{\epsilon}\sigma_2 = \sqrt{0.2\times 3} \approx 0.77$ is due to

$$\sum_{k\sim 1} z_{k-1}^2 = z_1^2 = 0.$$

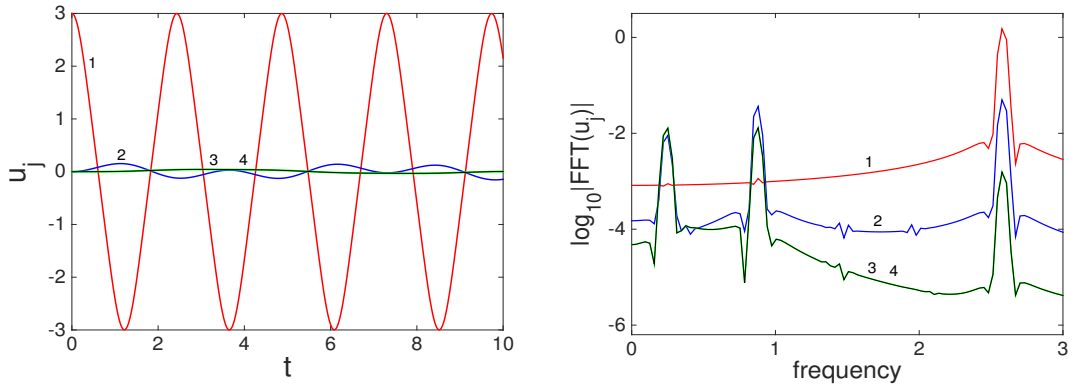

Figure 5.2 – Solution of equation (5.1) for the paw graph and an initial condition $u_1(0) = 3,\ u_2(0) = u_3(0) = u_4(0) = 0$. Left panel: time evolution of u_1 (red online), u_2 (blue online), u_3 (green online) and u_4 (black online). Right panel: Fourier transform of the solutions $\widehat{u}_1$ (red online), $\widehat{u}_2$ (blue online), $\widehat{u}_3$ (green online) and $\widehat{u}_4$ (black online). The parameters are $\omega = 0,\ \epsilon = 0.2$.

The equations (5.14) are then

$$\ddot{\alpha}_1 = -0.2\left(2-\sqrt{3}\right)\alpha_1 + \frac{0.2\left(\sqrt{3}-1\right)}{\sqrt{6-2\sqrt{3}}}u_1, \tag{5.42}$$

$$\ddot{\alpha}_3 = -0.2\left(2+\sqrt{3}\right)\alpha_3 + \frac{0.2\left(\sqrt{3}+1\right)}{\sqrt{6+2\sqrt{3}}}u_1, \tag{5.43}$$

To conclude, when exciting node 1 with a large amplitude ρ, the evolution of u_1 is given by (5.3) and the evolution of $u_2,\ u_3$ and u_4 by

$$\begin{pmatrix}u_2(t)\\u_3(t)\\u_4(t)\end{pmatrix} = \alpha_1(t)\mathbf{z}^1 + \alpha_3(t)\mathbf{z}^3, \tag{5.44}$$

where α_1 and α_3 are solutions of equations (5.42,5.43). Note that solving the reduced system (5.38,5.39) yields the same results as the ones shown in Figure 5.2.

Exciting node 2

To observe the different response of the system, we now excite node $j = 2$ with initial amplitude $u_2(0) = \rho = 3$ and $\omega = 0,\ \epsilon = 0.2$. The left panel of Figure 5.3 shows the time evolution of the solutions $u_k,\ k \in \{1, \ldots, 4\}$. The logarithm with base 10 of the modulus of the discrete Fourier transform of the solutions $\log_{10}(|\widehat{u}_k|),\ \ k \in \{1, \ldots, 4\}$ are shown on the right panel of Figure 5.3.

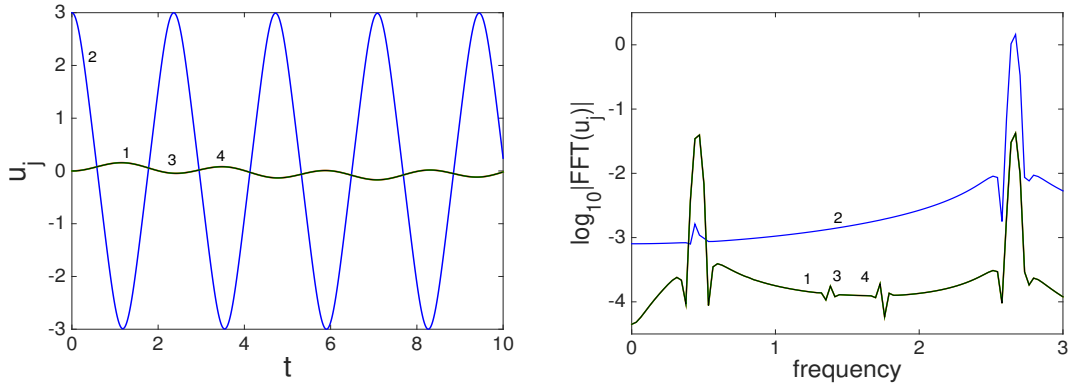

Figure 5.3 – Solution of equation (5.1) for the paw graph and an initial condition $u_2(0) = 3,\ u_1(0) = u_3(0) = u_4(0) = 0$. Left panel: time evolution of u_1 (red online), u_2 (blue online), u_3 (green online) and u_4 (black online). Right panel: Fourier transform of the solutions $\widehat{u}_1$ (red online), $\widehat{u}_2$ (blue online), $\widehat{u}_3$ (green online) and $\widehat{u}_4$ (black online). The parameters are $\omega = 0,\ \epsilon = 0.2$.

The Fourier spectrum shows that u_2 oscillates at the nonlinear frequency (5.5) $\Omega_0 = \frac{6\pi\sqrt{\pi}}{\Gamma^2\left(\frac{1}{4}\right)} \approx 2.54$ and at the odd harmonics of Ω_0 ($3\Omega_0$ and weakly at $5\Omega_0$). The solutions shown in Figure 5.3 are such that $u_2 = \mathcal{O}(\rho)$ and $|u_k| \ll \rho$ for $k = 1, 3$ and 4. To describe the evolution of u_1, u_3 and u_4, it is then natural to reduce the system (5.1) to the linear system forced by u_2

$$\begin{pmatrix} \ddot{u}_1 \\ \ddot{u}_3 \\ \ddot{u}_4 \end{pmatrix} = -\epsilon \begin{pmatrix} 1 & 0 & 0 \\ 0 & 2 & -1 \\ 0 & -1 & 2 \end{pmatrix} \begin{pmatrix} u_1 \\ u_3 \\ u_4 \end{pmatrix} + \epsilon u_2 \begin{pmatrix} 1 \\ 1 \\ 1 \end{pmatrix}. \tag{5.45}$$

The Fourier representation shows that the nearest neighbors $u_1,\ u_3$ and u_4 oscillate at the nonlinear frequency Ω_0 and at the eigenfrequencies (5.15) of the matrix $\epsilon\mathbf{\Delta}^2$

$$\sqrt{\epsilon}\sigma_1 = \sqrt{\epsilon}\sigma_2 = \sqrt{0.2} \times 1 \approx 0.447, \tag{5.46}$$

where

$$\mathbf{\Delta}^2 = \begin{pmatrix} 1 & 0 & 0 \\ 0 & 2 & -1 \\ 0 & -1 & 2 \end{pmatrix}. \tag{5.47}$$

The eigenvectors of $\mathbf{\Delta}^2$ are

$$\mathbf{z}^1 = \frac{1}{\sqrt{2}} \begin{pmatrix} 0 \\ 1 \\ 1 \end{pmatrix}, \quad \mathbf{z}^2 = \begin{pmatrix} 1 \\ 0 \\ 0 \end{pmatrix}, \quad \mathbf{z}^3 = \frac{1}{\sqrt{2}} \begin{pmatrix} 0 \\ 1 \\ -1 \end{pmatrix}.$$

Here, only one linear frequency exists. The absence of the eigenfrequency $\sqrt{\epsilon}\sigma_3 = \sqrt{0.2 \times 3}$ is due to

$$\sum_{k\sim 2, k<2} z_k^3 + \sum_{k\sim 2, k>2} z_{k-1}^3 = z_1^3 + z_2^3 + z_3^3 = 0.$$

Exciting node 3

We now excite node 3 with initial amplitude $u_3(0) = \rho = 3$ and $\omega = 0,\ \epsilon = 0.2$. The left panel of Figure 5.4 shows the time evolution of the solutions $u_k,\ k \in \{1, \ldots, 4\}$. The logarithm with base 10 of the modulus of the discrete Fourier transform of the solutions $\log_{10}(|\widehat{u}_k|),\ \ k \in \{1, \ldots, 4\}$ are shown on the right panel of Figure 5.4.

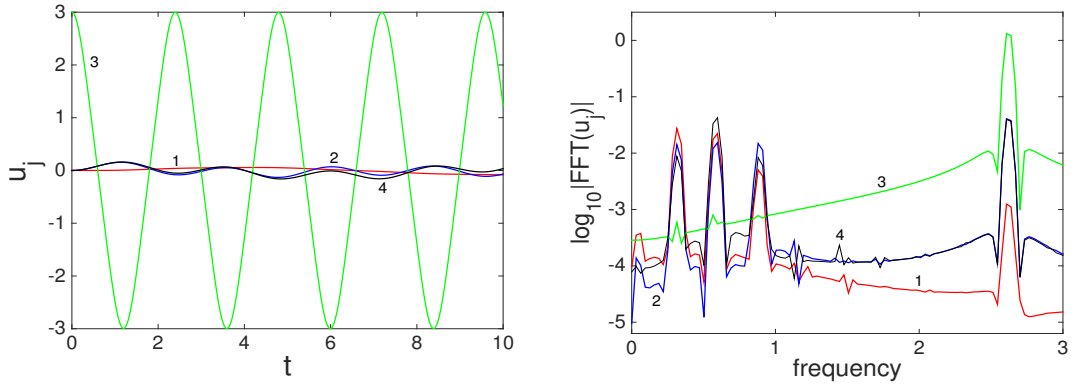

Figure 5.4 – Solution of equation (5.1) for the paw graph and an initial condition $u_3(0) = 3,\ u_1(0) = u_2(0) = u_4(0) = 0$. Left panel: time evolution of u_1 (red online), u_2 (blue online), u_3 (green, online) and u_4 (black online). Right panel: Fourier transform of the solutions $\widehat{u}_1$ (red online), $\widehat{u}_2$ (blue online), $\widehat{u}_3$ (green online) and $\widehat{u}_4$ (black online). The parameters are $\omega = 0,\ \epsilon = 0.2$.

From the Fourier spectrum, we can determine that u_3 oscillates at the nonlinear frequency (5.5) $\Omega_0 = \frac{6\pi\sqrt{\pi}}{\Gamma^2\left(\frac{1}{4}\right)} \approx 2.54$ and at the odd harmonics of Ω_0 ($3\Omega_0$ and weakly at $5\Omega_0$). The solutions shown in Figure 5.4 are such that $u_3 = \mathcal{O}(\rho)$ and $|u_k| \ll \rho$ for $k = 1, 2$ and 4. To describe the evolution of u_1, u_2 and u_4, it is then natural to reduce

the system (5.1) to the linear system forced by u_3

$$\begin{pmatrix} \ddot{u}_1 \\ \ddot{u}_2 \\ \ddot{u}_4 \end{pmatrix} = -\epsilon \begin{pmatrix} 1 & -1 & 0 \\ -1 & 3 & -1 \\ 0 & -1 & 2 \end{pmatrix} \begin{pmatrix} u_1 \\ u_2 \\ u_4 \end{pmatrix} + \epsilon u_3 \begin{pmatrix} 0 \\ 1 \\ 1 \end{pmatrix} \tag{5.48}$$

The Fourier representation shows that the nearest neighbors u_2 and u_4 (and similarly the next nearest neighbor u_1) oscillate at the nonlinear frequency Ω_0 and at the eigenfrequencies (5.15) of the matrix $\epsilon\mathbf{\Delta}^3$

$$\begin{aligned} \sqrt{\epsilon}\sigma_1 &= \sqrt{0.2\left(2 - 2\cos\left(\frac{2\pi}{9}\right)\right)} \approx 0.3059, \\ \sqrt{\epsilon}\sigma_2 &= \sqrt{0.2\left(2 - 2\cos\left(\frac{4\pi}{9}\right)\right)} \approx 0.5749, \\ \sqrt{\epsilon}\sigma_3 &= \sqrt{0.2\left(2 + 2\cos\left(\frac{\pi}{9}\right)\right)} \approx 0.8808. \end{aligned}$$

where

$$\mathbf{\Delta}^3 = \begin{pmatrix} 1 & -1 & 0 \\ -1 & 3 & -1 \\ 0 & -1 & 2 \end{pmatrix}. \tag{5.49}$$

The eigenvectors of $\mathbf{\Delta}^3$ are

$$\mathbf{z}^1 = \begin{pmatrix} 0.844 \\ 0.449 \\ 0.293 \end{pmatrix}, \quad \mathbf{z}^2 = \begin{pmatrix} 0.449 \\ -0.293 \\ -0.844 \end{pmatrix}, \quad \mathbf{z}^3 = \begin{pmatrix} 0.293 \\ -0.844 \\ 0.449 \end{pmatrix}.$$

Natural frequency $\omega \neq 0$

We now analyze a non zero natural frequency, choose $\omega = 3$ and $\epsilon = 0.2$ and solve the graph nonlinear wave equation (5.1) for the paw graph. The left of Figure 5.5 shows the time evolution of the localized solutions at $j = 1$ with amplitude $u_1(0) = 3$. Again this has been observed for over a thousand periods with no significant decay. The right of Figure 5.5 shows the logarithm with base 10 of the modulus of the discrete Fourier transform of the solutions $\log_{10}\left(|\widehat{u}_k|\right), \quad k \in \{1, \ldots, 4\}$.

Note that u_1 oscillates at frequencies Ω, 3Ω and weakly at 5Ω where $\Omega \approx 4$. The nearest neighbor u_2 (and similarly the next nearest neighbors u_3 and u_4) oscillate at the nonlinear frequency Ω and at eigenfrequencies (5.21) which are almost equal to those in

(5.36)

$$\sqrt{\epsilon\sigma_1^2+\omega^2} \approx \sqrt{\frac{\epsilon}{2\omega}}\sigma_1 + \omega \approx 3,$$
$$\sqrt{\epsilon\sigma_3^2+\omega^2} \approx \sqrt{\frac{\epsilon}{2\omega}}\sigma_3 + \omega \approx 3.12.$$

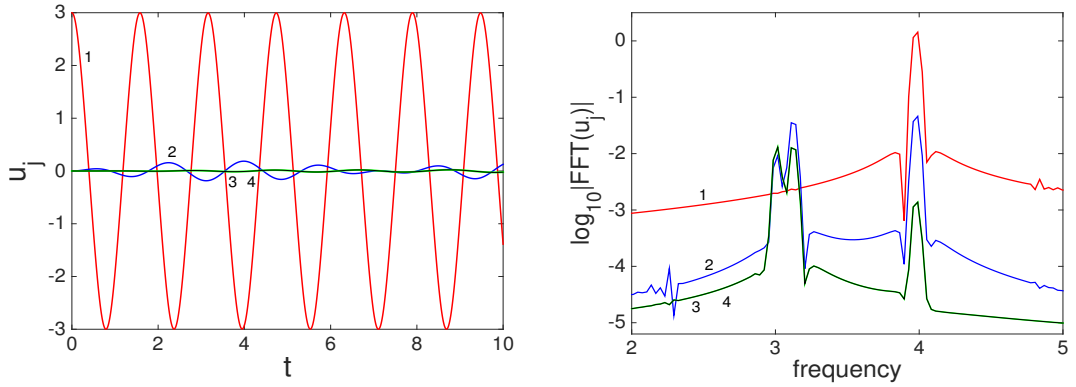

Figure 5.5 – Solution of equation (5.1) for the paw graph and an initial condition $u_1(0) = 3,\ u_2(0) = u_3(0) = u_4(0) = 0$. Left panel: time evolution of u_1 (red online), u_2 (blue online), u_3 (green online) and u_4 (black online). Right panel: Fourier transform of the solutions $\widehat{u}_1$ (red online), $\widehat{u}_2$ (blue online), $\widehat{u}_3$ (green online) and $\widehat{u}_4$ (black online). The parameters are $\omega = 3,\ \epsilon = 0.2$.

We proceed to validate the modulation theory by solving the graph nonlinear Schrödinger equation (5.23) with $\omega = 3$ and $\epsilon = 0.2$. From this solution, we calculate $\mathbf{u}$ using the change of variables (5.22). The comparison of Figs. 5.5 and 5.6 confirm the approximation by the modulation theory.

When exciting initially node 2, we note that u_2 oscillates at frequencies $\Omega,\ 3\Omega$ and weakly at 5Ω where $\Omega \approx 4$. The nearest neighbors $u_1,\ u_3$ and u_4 oscillate at the nonlinear frequency Ω and at eigenfrequencies (5.21)

$$\sqrt{\epsilon\sigma_1^2+\omega^2} = \sqrt{\epsilon\sigma_2^2+\omega^2} \approx 3.033.$$

Similarly, exciting initially node 3, we observe that u_3 oscillates at frequencies $\Omega,\ 3\Omega$ and weakly at 5Ω where $\Omega \approx 4$. The nearest neighbors u_2 and u_4 (and similarly the next

nearest neighbor u_1) oscillate at the nonlinear frequency Ω and at eigenfrequencies (5.21)

$$\sqrt{\epsilon\sigma_1^2+\omega^2} \approx 3.0156,$$
$$\sqrt{\epsilon\sigma_2^2+\omega^2} \approx 3.0546,$$
$$\sqrt{\epsilon\sigma_3^2+\omega^2} \approx 3.1266.$$

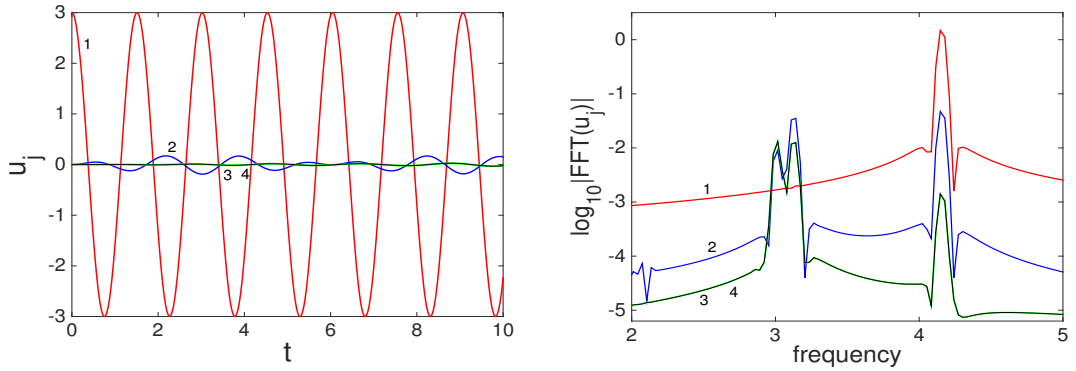

Figure 5.6 – Solution of equation (5.23) for the paw graph plotted in the u variables using (5.22) for an initial condition $u_1(0) = 3$, $u_2(0) = u_3(0) = u_4(0) = 0$. Left panel: time evolution of u_1 (red online), u_2 (blue online), u_3 (green online) and u_4 (black online). Right panel: Fourier transform of the solutions $\widehat{u}_1$ (red online), $\widehat{u}_2$ (blue online), $\widehat{u}_3$ (green online) and $\widehat{u}_4$ (black online). Same parameters as in Figure 5.5.

5.3.2 Cycle 6

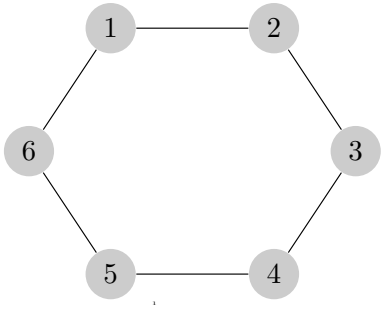

Figure 5.7 – Cycle 6

Natural frequency $\omega = 0$

We now consider the cycle 6 where all the nodes are invariant under cyclic permutations, so that they behave the same way. We solve equation (5.1) with $\omega = 0$ and $\epsilon = 0.2$ when exciting the system at site $j = 1$ with initial amplitude $u_1(0) = 3$. The left panel of Figure 5.8 shows the time evolution of the solutions $u_k,\ k \in \{1, \ldots, 6\}$. Notice how u_1 is large while $u_2,\ u_3$ and u_4 are small, indicating a localized oscillation. The right panel of Figure 5.8 shows the logarithm with base 10 of the modulus $\log_{10}(|\widehat{u}_k|),\ \ k \in \{1, \ldots, 6\}$ of the discrete Fourier transform of the solutions. The permutation symmetry of nodes $2 \leftrightarrow 6$ and $3 \leftrightarrow 5$ is reflected in the solutions $u_2 = u_6$ and $u_3 = u_5$. This network should show five linear modes, nevertheless due to the symmetry only three linear modes are present.

The dynamics at nodes $\{2, \ldots, 6\}$ is described by the linear system

$$\begin{pmatrix} \ddot{u}_2 \\ \ddot{u}_3 \\ \ddot{u}_4 \\ \ddot{u}_5 \\ \ddot{u}_6 \end{pmatrix} = -\epsilon \begin{pmatrix} 2 & -1 & 0 & 0 & 0 \\ -1 & 2 & -1 & 0 & 0 \\ 0 & -1 & 2 & -1 & 0 \\ 0 & 0 & -1 & 2 & -1 \\ 0 & 0 & 0 & -1 & 2 \end{pmatrix} \begin{pmatrix} u_2 \\ u_3 \\ u_4 \\ u_5 \\ u_6 \end{pmatrix} + \epsilon u_1 \begin{pmatrix} 1 \\ 0 \\ 0 \\ 0 \\ 1 \end{pmatrix} \tag{5.50}$$

Using the result of the Fourier spectrum, we can determine that u_1 oscillates at frequencies $\Omega_0 \approx 2.54$, $3\Omega_0$ and weakly at $5\Omega_0$. The nearest neighbors (u_2 and u_6) and next nearest neighbors (u_3 and u_5) oscillate at frequencies Ω_0 and at the eigenfrequencies (5.15) of the matrix $\epsilon\mathbf{\Delta}^1$

$$\begin{aligned} \sqrt{\epsilon}\sigma_1 &= \sqrt{0.2\left(2 - \sqrt{3}\right)} \approx 0.23, \\ \sqrt{\epsilon}\sigma_3 &= \sqrt{0.2 \times 2} \approx 0.63, \\ \sqrt{\epsilon}\sigma_5 &= \sqrt{0.2\left(2 + \sqrt{3}\right)} \approx 0.86, \end{aligned}$$

where

$$\mathbf{\Delta}^1 = \begin{pmatrix} 2 & -1 & 0 & 0 & 0 \\ -1 & 2 & -1 & 0 & 0 \\ 0 & -1 & 2 & -1 & 0 \\ 0 & 0 & -1 & 2 & -1 \\ 0 & 0 & 0 & -1 & 2 \end{pmatrix}. \tag{5.51}$$

The eigenvectors of $\mathbf{\Delta}^1$ are

$$\mathbf{z}^1 = \frac{-1}{2\sqrt{3}}\left(1, \sqrt{3}, 2, \sqrt{3}, 1\right)^T,$$
$$\mathbf{z}^2 = \frac{1}{2}\left(1, 1, 0, -1, -1\right)^T,$$
$$\mathbf{z}^3 = \frac{1}{\sqrt{3}}\left(1, 0, -1, 0, 1\right)^T,$$
$$\mathbf{z}^4 = \frac{1}{2}\left(-1, 1, 0, -1, 1\right)^T,$$
$$\mathbf{z}^5 = \frac{1}{2\sqrt{3}}\left(-1, \sqrt{3}, -2, \sqrt{3}, -1\right)^T.$$

The absence of the frequencies $\sqrt{\epsilon}\sigma_2$ and $\sqrt{\epsilon}\sigma_4$ is due to

$$\sum_{l\sim 1} z_{l-1}^2 = z_1^2 + z_5^2 = 0,$$
$$\sum_{l\sim 1} z_{l-1}^4 = z_1^4 + z_5^4 = 0.$$

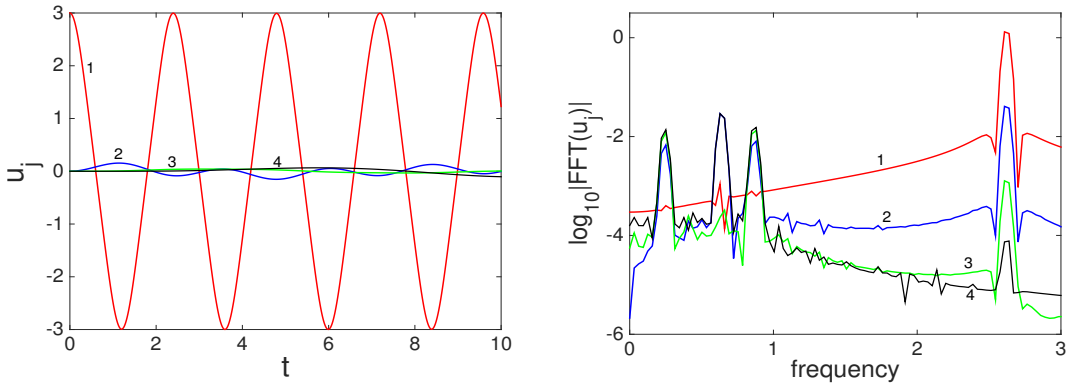

Figure 5.8 – Solution of equation (5.1) for the cycle 6 for initial amplitudes $u_1(0) = 3,\ u_2(0) = u_3(0) = u_4(0) = u_5(0) = u_6(0) = 0$. Left panel: time evolution of u_1 (red online), u_2 (blue online), u_3 (green online) and u_4 (black online). Right panel: Fourier transform of the solutions $\widehat{u}_1$ (red online), $\widehat{u}_2$ (blue online), $\widehat{u}_3$ (green online) and $\widehat{u}_4$ (black online). The parameters are $\omega = 0,\ \epsilon = 0.2$.

Natural frequency $\omega \neq 0$

We consider the equation (5.1) with $\omega = 3$ and $\epsilon = 0.2$ for cycle 6 when exciting the system at site $j = 1$ with initial amplitude $u_1(0) = 3$.

Note that u_1 oscillates at frequencies Ω, 3Ω and weakly at 5Ω where $\Omega \approx 4$. The nearest neighbors and next nearest neighbors oscillate at frequency Ω and at the eigenfrequencies (5.21) of the matrix $\epsilon\mathbf{\Delta}^1 + \omega^2\mathbf{I}$

$$\sqrt{\epsilon\sigma_1^2 + \omega^2} \approx 3, \quad \sqrt{\epsilon\sigma_3^2 + \omega^2} \approx 3.06, \quad \sqrt{\epsilon\sigma_5^2 + \omega^2} \approx 3.12.$$

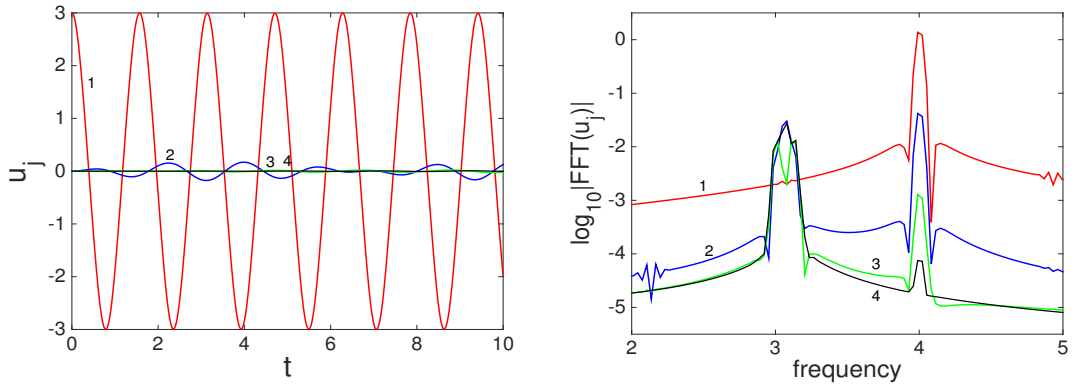

Figure 5.9 – Solution of equation (5.1) for the cycle 6 for initial amplitudes $u_1(0) = 3$, $u_2(0) = u_3(0) = u_4(0) = u_5(0) = u_6(0) = 0$. Left panel: time evolution of u_1 (red online), u_2 (blue online), u_3 (green online) and u_4 (black online). Right panel: Fourier transform of the solutions $\widehat{u}_1$ (red online), $\widehat{u}_2$ (blue online), $\widehat{u}_3$ (green online) and $\widehat{u}_4$ (black online). The parameters are $\omega = 3$, $\epsilon = 0.2$.

Solving the graph nonlinear Schrödinger equation (5.23) with $\omega = 3$ and $\epsilon = 0.2$ for cycle 6 and calculating $\mathbf{u}$ using the change of variables (5.22), yields the same results as the ones shown in Figure 5.9.

5.3.3 Localization vs delocalization

Up to now, we choose a large amplitude ρ and a small coupling ϵ. This leads to a localized solution. For a fixed amplitude, if we increase the coupling, the linear spectrum of the matrix $\mathbf{\Delta}^j$ will collide with the nonlinear frequency Ω_0. For lattices, this is the well-known modulational instability, see for example [59] and [24]. For general networks, the localized solution disappears and there is a strong coupling with the neighboring nodes. Also, the spectrum does not show well defined frequencies. To illustrate the delocalization regime, we choose $\omega = 0$, $\epsilon = 0.5$ and solve equation (5.1) for the paw graph with initial amplitude $u_1(0) = 2$. Figure 5.10 shows the time evolution of the solutions, there is a strong exchange of energy between nodes.

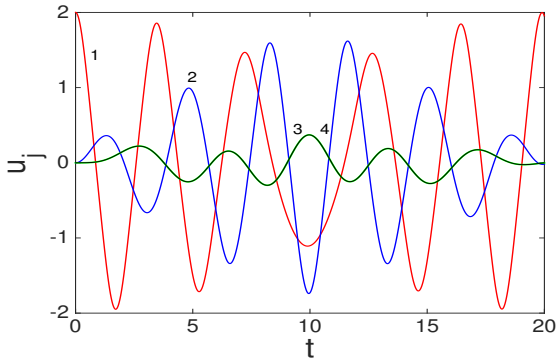

Figure 5.10 – Time evolution of u_1 (red online), u_2 (blue online), u_3 (green online) and u_4 (black online) solutions of (5.1) with $\omega = 0,\ \epsilon = 0.5$ in the paw graph for initial amplitudes $u_1(0) = 2,\ u_2(0) = u_3(0) = u_4(0) = 0$.

Using the localized character of the solution and the Fourier spectrum as indicators, we examined the parameter plane (ϵ, ρ) and plotted the regions of localization versus delocalization. First we consider the paw graph and plot these regions for initial excitations of nodes 1, 2 and 3. This is shown in Figure 5.11.

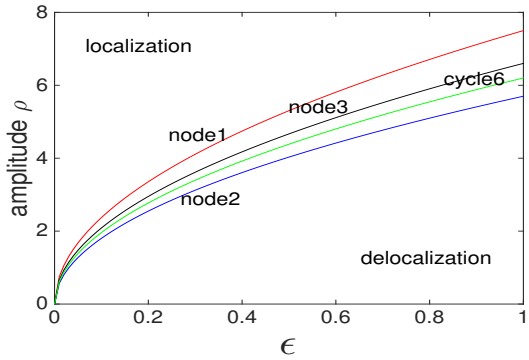

Figure 5.11 – Regions of delocalization in the (ϵ, ρ) plane with $\omega = 0$, exciting initially nodes 1, 2 and 3 for the paw graph and any node for cycle 6 with amplitude ρ. The lines separates the regions of localization (large ρ) and the regions of delocalization (small ρ).

The separation curve is $\mathcal{O}(\sqrt{\epsilon})$ since the eigenfrequencies of $\epsilon\mathbf{\Delta}^j$ scale like $\sqrt{\epsilon}$. As one can see, the amplitudes for localization are larger for node 1 then node 3 and finally node 2. The maximal linear frequencies are $\sqrt{\epsilon}\sigma_{N-1}$ where $\sigma_{N-1} = 1.93$, 1.96 and 1, respectively for nodes 1,3 and 2. Then the linear spectrum is closer to the nonlinear frequency Ω_0 for nodes 1 and 3 and farther for node 2. Nevertheless, we observe a difference between nodes 1 and 3 in Figure 5.11 and this could be due to their different

degrees, $d_1 = 1$ and $d_3 = 2$.

To investigate the effect of the degree on the localization region we compare in Figure 5.11 the paw graph, exciting node 3 (black online) where $d_3 = 2$, and any node of cycle 6 (green online), where all nodes have degree 2, for $\omega = 0$. Note that both curves are very close. The curve for node 1 of the paw graph is above the one for node 3. It is apart from the one for cycle 6 despite the fact that the two maximum frequencies are equal $\sigma_{N-1} = 1.93$.

Taking $\omega \neq 0$ leads to very close results as the linear spectrum and the nonlinear frequency are both approximately shifted by ω. When choosing a quintic nonlinearity in equation (5.1), the nonlinear frequency is much larger while the linear spectrum is unchanged. Then, we need to increase ϵ considerably to observe coupling to the linear modes.

5.4 Conclusion

We studied localized solutions for a nonlinear graph wave equation. These are approximated by the Duffing equation for the excited node and a forced linear system for the neighboring nodes. We validate this approximation by calculating the Fourier spectrum of the numerical solution. This shows the nonlinear frequency of the excited node together with the normal eigenfrequencies of the linear system describing the neighboring nodes.

The existence of these localized solutions is confirmed using numerical simulations and modulation theory. We also examined the localization / delocalization regions in the parameter plane (ϵ, ρ). We confirm that localization holds when the nonlinear frequency is well above the linear spectrum which is bounded by $\mathcal{O}(\sqrt{\epsilon})$. The localization curve $\rho(\epsilon)$ depends on the maximal normal eigenfrequency.

Conclusion and Perspectives

The graph wave equation arises naturally from conservation laws on a network. There, the usual continuum Laplacian is replaced by the graph Laplacian. We consider such a wave equation with a cubic on-site nonlinearity on a general network. This system models complex physical networks in mechanical and electrical engineering.

First, we identified normal modes of the linear theory that extend nonlinear periodic orbits. These are the Goldstone mode and other special modes. The corresponding eigenvectors have components in $\{1\}$, $\{-1, 1\}$ or $\{-1, 0, 1\}$; we call them monovalent, bivalent and trivalent respectively. These orbits and their stability were analyzed numerically. It would be interesting to confirm that the stability results we obtained, can be extended to general graphs. We could also try to find bi-periodic orbits that involve two nonlinear normal modes and examine their linear stability. The main model in this thesis was the nonlinear graph wave equation with on-site nonlinearity. It would be interesting to study models with intersite nonlinearity, in particular the Fermi-Pasta-Ulam model.

Bivalent graphs have been characterized as regular bi-partite graphs and their extensions obtained by adding edges between vertices with the same value for the considered eigenvector. Trivalent graphs are obtained from -what we call- soft regular graphs by applying transformations of graphs (addition of an edge between nodes of same value, extension/reduction of soft nodes, replace an edge by a soft square). To determine if a given graph is bivalent or trivalent is a difficult question; some answers can be given for special configurations.

We examined localized periodic solutions stemming from the interplay between nonlinearity and discreteness. We approximated these by a Duffing oscillator for the excited node and a forced linear system for the rest of the network. This approximation was validated by Fourier analysis and modulation theory. It would be interesting to examine the evolution of two excited nodes.

Appendix A

Spectrum of cycles and chains

Spectrum of cycles

For cycles, the graph Laplacian $\mathbf{\Delta}$ is a circulant matrix where each row is shifted to the right by one element relative to the preceding row

$$\mathbf{\Delta} = \begin{pmatrix} 2 & -1 & 0 & \dots & 0 & -1 \\ -1 & 2 & -1 & 0 & \dots & 0 \\ 0 & \ddots & \ddots & \ddots & \ddots & \vdots \\ \vdots & \ddots & \ddots & \ddots & \ddots & 0 \\ 0 & \dots & 0 & -1 & 2 & -1 \\ -1 & 0 & \dots & 0 & -1 & 2 \end{pmatrix}. \tag{A.1}$$

The spectrum of $\mathbf{\Delta}$ is well known [61]. The repeated eigenvalues are

$$\omega_{2k}^2 = \omega_{2k+1}^2 = 4\sin^2\left(\frac{k\pi}{N}\right), \tag{A.2}$$

for $k = 1, \dots, \frac{N-1}{2}$ (resp. $k = 1, \dots, \frac{N-2}{2}$) if N is odd (resp. N is even). The first eigenvalue $\omega_1^2 = 0$ is simple. When N is even, the last one $\omega_N^2 = 4$ is also simple. The components of Goldstone eigenvector $v_m^1 = \frac{1}{\sqrt{N}},\ m \in \{1, ..., N\}$. The components of the corresponding orthonormal eigenvectors $\mathbf{v}^j,\ j \in \{2, \dots, N\}$ are

$$v_m^j = \sqrt{\frac{2}{N}} \begin{cases} \cos\left(\frac{j\pi}{N}(m-1)\right),\ m \in \{1, \dots, N\},\ \ j \text{ even}, \\ \\ \sin\left(\frac{(j-1)\pi}{N}(m-1)\right),\ m \in \{1, \dots, N\},\ \ j \text{ odd}. \end{cases} \tag{A.3}$$

Spectrum of chains

For a chain of length $N-1$ (N nodes), the graph Laplacian is a tridiagonal matrix

$$\mathbf{\Delta} = \begin{pmatrix} 1 & -1 & 0 & \dots & 0 \\ -1 & 2 & -1 & \ddots & \vdots \\ 0 & \ddots & \ddots & \ddots & 0 \\ \vdots & \ddots & -1 & 2 & -1 \\ 0 & \dots & 0 & -1 & 1 \end{pmatrix}. \tag{A.4}$$

The spectrum of $\mathbf{\Delta}$ is well known [61]. The eigenvalues are simple:

$$\omega_j^2 = 4\sin^2\left(\frac{(j-1)\pi}{2N}\right), \quad j \in \{1, ..., N\}. \tag{A.5}$$

The component m of the corresponding orthonormal eigenvector $\mathbf{v}^j$ is

$$v_m^j = \sqrt{\frac{2}{N}}\cos\left(\frac{(j-1)\pi}{N}\left(m - \frac{1}{2}\right)\right), \quad j, m \in \{1, ..., N\}. \tag{A.6}$$

Appendix B

Stability of periodic orbits

Suppose that $\mathbf{x}(t) = \boldsymbol{\gamma}(t) = \boldsymbol{\gamma}(t+T)$ is a periodic orbit of period T for the differential equation $\frac{\mathrm{d}\mathbf{x}}{\mathrm{d}t} = \mathbf{f}(\mathbf{x})$. If the vector field $\mathbf{f} \in C^1$ we can linearize the ODE about $\boldsymbol{\gamma}$ by setting $\mathbf{x}(t) = \boldsymbol{\gamma}(t) + \mathbf{y}(t)$ and expanding $\mathbf{f}$ in a Taylor series to obtain

$$\frac{\mathrm{d}}{\mathrm{d}t}(\mathbf{x}+\mathbf{y}) = \mathbf{f}(\boldsymbol{\gamma}(t)) + \frac{\mathrm{d}\mathbf{y}}{\mathrm{d}t} = \mathbf{f}(\boldsymbol{\gamma}(t)+\mathbf{y}) = \mathbf{f}(\boldsymbol{\gamma}(t)) + \mathbf{Df}(\boldsymbol{\gamma}(t))\,\mathbf{y} + o(\mathbf{y}). \tag{B.1}$$

If we neglect the $o(\mathbf{y})$ term we obtain the linearization

$$\frac{\mathrm{d}\mathbf{y}}{\mathrm{d}t} = \mathbf{Df}(\boldsymbol{\gamma}(t))\,\mathbf{y} = \mathbf{B}(t)\mathbf{y}, \tag{B.2}$$

where the matrix $\mathbf{B}(t)$ is periodic in time. Such systems can be analyzed using Floquet theory ([39] p.174, see also [62]). The fundamental matrix solution of (B.2) is $\mathbf{M}(t)$ whose columns are linearly independent solutions of (B.2) for the initial conditions given by the columns of the identity matrix. For $t = T$, the period of $\boldsymbol{\gamma}$, the matrix $\mathbf{M} = \mathbf{M}(T)$ is called the monodromy matrix. The eigenvalues of $\mathbf{M}$ are the Floquet multipliers, and Floquet's theorem shows that all the solutions of (B.2) are bounded whenever the Floquet multipliers have magnitude small than one. For the case (B.2), one of the Floquet multipliers is trivially one.

If linear Hamiltonian system has characteristic multiplier ρ_i then it also has the multipliers ρ_i^* and ρ_i^{-1}. Then, linear periodic Hamiltonian system is stable if and only if all characteristic multipliers lie on unit circle.

Appendix C

Basic properties of the elliptic functions

Consider the upper limit ϕ of the integral

$$x = \int_0^{\phi} \frac{\mathrm{d}y}{\sqrt{1-\kappa^2 \sin^2 y}}, \tag{C.1}$$

as a function of x. The functions

$$\begin{aligned} \mathrm{cn}\,(x,\kappa) &= \cos(\phi)\,, \\ \mathrm{sn}\,(x,\kappa) &= \sin(\phi)\,, \\ \mathrm{dn}\,(x,\kappa) &= \sqrt{1-\kappa^2 \sin^2 \phi}, \end{aligned}$$

are the Jacobi elliptic functions cosine, sine and delta, respectively; see [41] p.567. Here $\kappa \in [0,1]$ is the elliptic modulus, and $\kappa' = \sqrt{1-\kappa^2}$ is the complementary modulus. The functions cn and sn are periodic functions with period $4K$, while dn is periodic with period $2K$, where

$$K \equiv K(\kappa) = \int_0^{\frac{\pi}{2}} \frac{\mathrm{d}\theta}{\sqrt{1-\kappa^2 \sin(\theta)^2}}, \qquad K' \equiv K'(\kappa) = K(\kappa'), \tag{C.2}$$

which for $\kappa = \frac{1}{\sqrt{2}}$ gives

$$K\left(\frac{1}{\sqrt{2}}\right) = K'\left(\frac{1}{\sqrt{2}}\right) = \frac{\Gamma^2\left(\frac{1}{4}\right)}{4\sqrt{\pi}} \approx 1.8541,$$

where $\Gamma(.)$ is the gamma function and $\Gamma\left(\frac{1}{4}\right) \approx 3.6256$.

One has

$$\mathrm{cn}\left(-x,\kappa\right)=\mathrm{cn}\left(x,\kappa\right),\quad \mathrm{sn}\left(-x,\kappa\right)=-\mathrm{sn}\left(x,\kappa\right),\quad \mathrm{dn}\left(-x,\kappa\right)=\mathrm{dn}\left(x,\kappa\right).$$

We have

$$\frac{\mathrm{d}}{\mathrm{d}x}\mathrm{cn}\left(x,\kappa\right)=-\mathrm{sn}\left(x,\kappa\right)\ \mathrm{dn}\left(x,\kappa\right),$$

$$\frac{\mathrm{d}}{\mathrm{d}x}\mathrm{sn}\left(x,\kappa\right)=\mathrm{cn}\left(x,\kappa\right)\ \mathrm{dn}\left(x,\kappa\right),$$

$$\frac{\mathrm{d}}{\mathrm{d}x}\mathrm{dn}\left(x,\kappa\right)=-\kappa^{2}\ \mathrm{sn}\left(x,\kappa\right)\ \mathrm{cn}\left(x,\kappa\right).$$

Moreover the following identities hold:

$$\begin{aligned}&\mathrm{cn}^{2}\left(x,\kappa\right)+\mathrm{sn}^{2}\left(x,\kappa\right)=1,\\&\mathrm{dn}^{2}\left(x,\kappa\right)+\kappa^{2}\mathrm{sn}^{2}\left(x,\kappa\right)=1,\\&\mathrm{dn}^{2}\left(x,\kappa\right)-\kappa^{2}\mathrm{cn}^{2}\left(x,\kappa\right)=1-\kappa^{2}.\end{aligned}$$

The Fourier series of the cosine elliptic function is given by

$$\mathrm{cn}\left(x,\kappa\right)=\frac{2\pi}{\kappa K}\sum_{m=0}^{\infty}\frac{q^{m+\frac{1}{2}}}{1+q^{2m+1}}\cos\left(\left(2m+1\right)\frac{\pi x}{2K}\right),\tag{C.3}$$

$$\mathrm{sn}\left(x,\kappa\right)=\frac{2\pi}{\kappa K}\sum_{m=0}^{\infty}\frac{q^{m+\frac{1}{2}}}{1+q^{2m+1}}\sin\left(\left(2m+1\right)\frac{\pi x}{2K}\right),\tag{C.4}$$

$$\mathrm{dn}\left(x,\kappa\right)=\frac{\pi}{2K}+\frac{2\pi}{K}\sum_{m=1}^{\infty}\frac{q^{m}}{1-q^{2m}}\cos\left(\frac{2m\pi x}{2K}\right),\tag{C.5}$$

where $q=\mathrm{e}^{\frac{-\pi K'}{K}}$ so that $q=\mathrm{e}^{-\pi}$ for $\kappa=\frac{1}{\sqrt{2}}$.

Appendix D

The Duffing oscillator

The period of u solution of

$$\frac{\mathrm{d}^2 u}{\mathrm{d}t^2} = -\beta u^3. \tag{D.1}$$

Integrating the equation, we get

$$\left(\frac{\mathrm{d}u}{\mathrm{d}t}\right)^2 = \frac{\beta}{2}\left(\rho^4 - u^4\right),$$

where we assumed $u(0) = \rho$ and $\frac{\mathrm{d}u}{\mathrm{d}t}(0) = 0$. This yields

$$\mathrm{d}t = \pm\sqrt{\frac{2}{\beta}}\frac{\mathrm{d}u}{\sqrt{\rho^4 - u^4}}.$$

The period T_0 of $u(t)$ is then given by the elliptic integral

$$T_0 = 4\sqrt{\frac{2}{\beta}}\int_0^\rho \frac{\mathrm{d}u}{\sqrt{\rho^4 - u^4}} = \frac{4\sqrt{2}}{\rho\sqrt{\beta}}\int_0^1 \frac{\mathrm{d}z}{\sqrt{1 - z^4}}.$$

We know that

$$\int_0^1 \frac{\mathrm{d}z}{\sqrt{1 - z^4}} = \frac{\Gamma^2\left(\frac{1}{4}\right)}{4\sqrt{2\pi}}.$$

Then, the period of oscillations is

$$T_0 = \frac{\Gamma^2\left(\frac{1}{4}\right)}{\rho\sqrt{\beta\pi}}. \tag{D.2}$$

The solution of (D.1) can be written in terms of the cosine Jacobi elliptic function

$$u(t) = \rho\ \mathrm{cn}\left(\rho\sqrt{\beta}t, \frac{1}{\sqrt{2}}\right). \tag{D.3}$$

The period of the cosine elliptic function is $T_0 = \frac{4K\left(\frac{1}{\sqrt{2}}\right)}{\rho\sqrt{\beta}} = \frac{\Gamma^2\left(\frac{1}{4}\right)}{\rho\sqrt{\beta\pi}}$. This confirms the calculation above for (D.2).

The Fourier series (C.3) of the solution (D.3) is

$$u(t) = \frac{8\pi\sqrt{2}}{\sqrt{\beta}T_0} \sum_{m=0}^{\infty} b_{2m+1} \cos\left[(2m+1)\Omega_0 t\right], \tag{D.4}$$

where

$$\Omega_0 = \frac{2\pi}{T_0}, \quad b_{2m+1} = \frac{\mathrm{e}^{-\pi\left(m+\frac{1}{2}\right)}}{1+\mathrm{e}^{-\pi(2m+1)}}.$$

Appendix E

Action-angle variables for the quartic potential

The Hamiltonian of the quartic potential

$$\mathcal{H}_{\mathcal{G}}(q,p) = \frac{1}{2}(p)^2 + \frac{1}{4N}q^4. \tag{E.1}$$

The action variable as a function of the energy ([56] p.103-116) is

$$I \equiv \frac{1}{T_0}\oint p\,(q_1, E_0)\ \mathrm{d}q_1 = \frac{2}{T_0}\int_{-\alpha}^{\alpha}\sqrt{2\left(E_0 - \frac{(q_1)^4}{4N}\right)}\ \mathrm{d}q_1 = \frac{2\alpha\sqrt{2E_0}}{T_0}\int_{-1}^{1}\sqrt{1-x^4}\ \mathrm{d}x, \tag{E.2}$$

where $\alpha = (4NE_0)^{\frac{1}{4}}$, the angle θ is defined modulo T_0 instead than 2π where $T_0 = \frac{\Gamma^2\left(\frac{1}{4}\right)}{\sqrt{\pi}}$ is the period of the cosine elliptic function $\mathrm{cn}\left(t, \frac{1}{\sqrt{2}}\right)$. Evaluation of the integral gives

$$\int_{-1}^{1}\sqrt{1-x^4}\ \mathrm{d}x = \frac{T_0\sqrt{2}}{6}.$$

The action is thus

$$I = \frac{1}{3\sqrt{N}}\left(4NE_0\right)^{\frac{3}{4}}. \tag{E.3}$$

By inverting, we obtain the energy $E_0(I)$ as a function of the action

$$E_0 = \frac{1}{4N^{\frac{1}{3}}}\left(3I\right)^{\frac{4}{3}} \equiv \mathcal{H}_G(I). \tag{E.4}$$

Appendix F

Derivation of the Graph nonlinear Schrödinger equation

We consider the continuum equation of (1.22) (see [63])

$$\frac{\mathrm{d}^2\mathbf{u}}{\mathrm{d}t^2} + \omega^2\mathbf{u} = -\epsilon\boldsymbol{\Delta}\mathbf{u} - \mathbf{u}^3. \tag{F.1}$$

To eliminate the term $\omega^2\mathbf{u}$, we write

$$\mathbf{u} = \sqrt{\epsilon}\boldsymbol{\psi}(T)\mathrm{e}^{\mathrm{i}\omega t} + \sqrt{\epsilon}\boldsymbol{\psi}^*(T)\mathrm{e}^{-\mathrm{i}\omega t}, \tag{F.2}$$

where $T = \epsilon t$ and $\boldsymbol{\psi}^*$ is the complex conjugate of $\boldsymbol{\psi}$. We have

$$\begin{aligned}\frac{\mathrm{d}^2\mathbf{u}}{\mathrm{d}t^2} = \epsilon^{\frac{5}{2}}\left(\frac{\mathrm{d}^2\boldsymbol{\psi}}{\mathrm{d}T^2}\mathrm{e}^{\mathrm{i}\omega t} + \frac{\mathrm{d}^2\boldsymbol{\psi}^*}{\mathrm{d}T^2}\mathrm{e}^{-\mathrm{i}\omega t}\right) + 2\mathrm{i}\omega\epsilon^{\frac{3}{2}}\left(\frac{\mathrm{d}\boldsymbol{\psi}}{\mathrm{d}T}\mathrm{e}^{\mathrm{i}\omega t} - \frac{\mathrm{d}\boldsymbol{\psi}^*}{\mathrm{d}T}\mathrm{e}^{-\mathrm{i}\omega t}\right)\\ - \omega^2\sqrt{\epsilon}\left(\boldsymbol{\psi}\mathrm{e}^{\mathrm{i}\omega t} + \boldsymbol{\psi}^*\mathrm{e}^{-\mathrm{i}\omega t}\right).\end{aligned}$$

The left hand side of the equation (F.1) is

$$\frac{\mathrm{d}^2\mathbf{u}}{\mathrm{d}t^2} + \omega^2\mathbf{u} = \epsilon^{\frac{5}{2}}\left(\frac{\mathrm{d}^2\boldsymbol{\psi}}{\mathrm{d}T^2}\mathrm{e}^{\mathrm{i}\omega t} + \frac{\mathrm{d}^2\boldsymbol{\psi}^*}{\mathrm{d}T^2}\mathrm{e}^{-\mathrm{i}\omega t}\right) + 2\mathrm{i}\omega\epsilon^{\frac{3}{2}}\left(\frac{\mathrm{d}\boldsymbol{\psi}}{\mathrm{d}T}\mathrm{e}^{\mathrm{i}\omega t} - \frac{\mathrm{d}\boldsymbol{\psi}^*}{\mathrm{d}T}\mathrm{e}^{-\mathrm{i}\omega t}\right).$$

The right hand side of the equation (F.1) gives

$$\begin{aligned}-\epsilon\boldsymbol{\Delta}\mathbf{u} - \mathbf{u}^3 = -\epsilon^{\frac{3}{2}}\Big(&\boldsymbol{\Delta}\boldsymbol{\psi}\mathrm{e}^{\mathrm{i}\omega t} + \boldsymbol{\Delta}\boldsymbol{\psi}^*\mathrm{e}^{-\mathrm{i}\omega t} + \boldsymbol{\psi}^3\mathrm{e}^{3\mathrm{i}\omega t} + (\boldsymbol{\psi}^*)^3\,\mathrm{e}^{-3\mathrm{i}\omega t} + 3\,|\boldsymbol{\psi}|^2\,\boldsymbol{\psi}\mathrm{e}^{\mathrm{i}\omega t}\\ &+ 3\,|\boldsymbol{\psi}|^2\,\boldsymbol{\psi}^*\mathrm{e}^{-\mathrm{i}\omega t}\Big).\end{aligned}$$

We obtain for the order $\mathcal{O}\left(\epsilon^{\frac{3}{2}}\right)$

$$\begin{aligned}2\mathrm{i}\omega\frac{\mathrm{d}\boldsymbol{\psi}}{\mathrm{d}T}\mathrm{e}^{\mathrm{i}\omega t} - 2\mathrm{i}\omega\frac{\mathrm{d}\boldsymbol{\psi}^*}{\mathrm{d}T}\mathrm{e}^{-\mathrm{i}\omega t} = &-\boldsymbol{\Delta}\boldsymbol{\psi}\mathrm{e}^{\mathrm{i}\omega t} - \boldsymbol{\Delta}\boldsymbol{\psi}^*\mathrm{e}^{-\mathrm{i}\omega t} - \boldsymbol{\psi}^3\mathrm{e}^{3\mathrm{i}\omega t} - (\boldsymbol{\psi}^*)^3\,\mathrm{e}^{-3\mathrm{i}\omega t}\\ &- 3\,|\boldsymbol{\psi}|^2\,\boldsymbol{\psi}\mathrm{e}^{\mathrm{i}\omega t} - 3\,|\boldsymbol{\psi}|^2\,\boldsymbol{\psi}^*\mathrm{e}^{-\mathrm{i}\omega t}.\end{aligned}$$

Multiplying by $\mathrm{e}^{-\mathrm{i}\omega t}$, we get

$$2\mathrm{i}\omega\frac{\mathrm{d}\boldsymbol{\psi}}{\mathrm{d}T} - 2\mathrm{i}\omega\frac{\mathrm{d}\boldsymbol{\psi}^*}{\mathrm{d}T}\mathrm{e}^{-2\mathrm{i}\omega t} = -\boldsymbol{\Delta}\boldsymbol{\psi} - \boldsymbol{\Delta}\boldsymbol{\psi}^*\mathrm{e}^{-2\mathrm{i}\omega t} - \boldsymbol{\psi}^3\mathrm{e}^{2\mathrm{i}\omega t} - (\boldsymbol{\psi}^*)^3\,\mathrm{e}^{-4\mathrm{i}\omega t} - 3\,|\boldsymbol{\psi}|^2\,\boldsymbol{\psi} - 3\,|\boldsymbol{\psi}|^2\,\boldsymbol{\psi}^*\mathrm{e}^{-2\mathrm{i}\omega t}.$$

The terms with a non zero phase are rotating fast and average to zero on the slow time scale. Only the terms that have 0 phase contribute. This is the *rotating wave approximation* ([8] p.813). We obtain the nonlinear Schrödinger equation

$$2\mathrm{i}\omega\frac{\mathrm{d}\boldsymbol{\psi}}{\mathrm{d}T} = -\boldsymbol{\Delta}\boldsymbol{\psi} - 3\,|\boldsymbol{\psi}|^2\,\boldsymbol{\psi}. \tag{F.3}$$

Bibliography

[1] G. Kirchhoff, *Über die Auflösung der Gleichungen, auf welche man bei der Untersuchung der linearen Verteilung galvanischer Ströme geführt wird.* Ann. Phys. Chem. 72, 497-508 (1847). Translated by J. B. O'Toole in IRE Transactions on Circuit Theory, Volume 5, Issue 1,4-7 (1958).

[2] C. Maas, *Transportation in graphs and the admittance spectrum.* Discr. Appl. Math. 16, 31-49 (1987).

[3] J. Friedman and J-P. Tillich, *Wave equations for graphs and the edge-based Laplacian.* Pacific Journal of Mathematics, Vol. 216, No. 2 (2004).

[4] D. Cvetkovic, P. Rowlinson and S. Simic, *An Introduction to the Theory of Graph Spectra.* London Mathematical Society Student Texts 75, Cambridge: Cambridge University Press (2010).

[5] R. Merris, *Laplacian matrices and graphs: a survey.* Linear Algebra and its Applications 197/198, 143-176 (1994).

[6] M. Fiedler, *Algebraic connectivity of graphs.* Czechoslovak Mathematical Journal, 23(98), 298-305 (1973).

[7] J-G. Caputo, A. Knippel and E. Simo, *Oscillations of networks: the role of soft nodes.* J. Phys. A: Math. Theor. 46, 035101 (2013).

[8] A. C. Scott, *Encyclopedia of nonlinear science.* London: Routledge, Taylor and Francis Group (2005).

[9] R. M. Rosenberg, *On nonlinear vibrations of systems with many degrees of freedom.* Advances in applied mechanics 9, 155-242 (1966).

[10] W. Strauss, *Nonlinear invariant wave equations.* Lecture notes in physics, G. Velo and A. Wightman, New York: Springer (1978).

[11] A. C. Scott, *Nonlinear Science: Emergence and Dynamics of Coherent Structures.* Oxford Texts in Applied and Engineering Mathematics, 2nd edn, Oxford-New York: Oxford University Press (2003).

[12] A. Grolet, N. Hoffmann, F. Thouverez C. Schwingshackl, *Travelling and standing envelope solitons in discrete non-linear cyclic structures.* Mechanical Systems and Signal Processing, Vol 81, 75-87 (2016).

[13] E. Fermi, J. Pasta and S. Ulam, *Collected Papers of Enrico Fermi*, Chicago, IL: University of Chicago Press (1965).

[14] B. Juanico, Y. H. Sanejouand, F. Piazza, P. De Los Rios, *Discrete breathers in nonlinear network models of proteins.* Phys. Rev. Lett. 99, 238104 (2007).

[15] F. Martínez-Farías, P. Panayotaros and A. Olvera, *Weakly nonlinear localization for a 1-D FPU chain with clustering zones.* European Physical Journal - Special Topics - 223, 2943-2952 (2014).

[16] K. V. Avramov and Y. V. Mikhlin, *Review of applications of nonlinear normal modes for vibrating mechanical systems.* Appl. Mech. Rev. 65, 020801 (2013).

[17] A. Lyapunov, *Problème général de la stabitité du mouvement.* Ann. Fac. Sci., Toulouse (2), 203-474 (1907).

[18] K. R. Meyer, G. R. Hall and D. Offin, *Introduction to Hamiltonian Dynamical Systems and the N-Body Problem.* 2nd edn, Springer, New York (2009).

[19] A. Weinstein, *Normal modes for non-linear Hamiltonian systems.* Invent. Math. 20, 47-57 (1973).

[20] J. Moser, *Periodic orbits near an equilibrium and a theorem by Alan Weinstein.* Comm. Pure Appl. Math. 29, 727-747 (1976).

[21] A. J. Sievers and S. Takeno, *Intrinsic localized modes in anharmonic crystals.* Phys. Rev. Lett. 61, 970-973 (1988).

[22] J. B. Page, *Asymptotic solutions for localized vibrational modes in strongly anharmonic periodic systems.* Phys. Rev. B 41, 7835-7838 (1990).

[23] R. S. MacKay and S. Aubry, *Proof of existence of breathers for time-reversible or Hamiltonian networks of weakly coupled oscillators.* Nonlinearity 7, 1623-1643 (1994).

[24] S. Flach, *Conditions on the existence of localized excitations in nonlinear discrete systems.* Phys. Rev. E 50, 3134 (1994).

[25] S. Flach and C. R Willis, *Discrete breathers*, Physics reports 295, 181-264 (1998); S. Flach and A. V. Gorbach, *Discrete breathers - Advances in theory and applications*, Physics Reports 467, 1-116 (2008).

[26] P. Binder, D. Abraimov, A. V. Ustinov, S. Flach and Y. Zolotaryuk, *Observation of breathers in Josephson ladders.* Phys. Rev. Lett. 84, 745 (2000).

[27] A. B. Aceves, C. De Angelis, T. Peschel, R. Muschall, F. Lederer, S. Trillo, and S. Wabnitz, *Discrete self-trapping, soliton interactions, and beam steering in nonlinear waveguide arrays*. Phys. Rev. E 53, 1172 (1996).

[28] H. S. Eisenberg, Y. Silberberg, R. Morandotti, A. R. Boyd, and J. S. Aitchison, *Discrete spatial optical solitons in waveguide arrays*. Phys. Rev. Lett. 81, 3383-3386 (1998).

[29] J. W. Fleischer, M. Segev, N. K. Efremidis, and D. N. Christodoulides, *Observation of two-dimensional discrete solitons in optically induced nonlinear photonic lattices*. Nature (London) 422, 147 (2003).

[30] M. Peyrard, *Nonlinear dynamics and statistical physics of DNA*. Nonlinearity 17 R1 (2004).

[31] M. Sato, B. E. Hubbard, A. J. Sievers, B. Ilic, D. A. Czaplewski, and H. G. Craighead, *Observation of locked intrinsic localized vibrational modes in a micromechanical oscillator array*. Phys. Rev. Lett. 90, 044102 (2003).

[32] M. Sato, S. Yasui, M. Kimura, T. Hikihara and A. J. Sievers, *Management of localized energy in discrete nonlinear transmission lines*. Europhysics Letters 80, 30002 (2007).

[33] S. Flach and A. Gorbach, *Discrete breathers in Fermi-Pasta-Ulam lattices*. Chaos 15, 015112 (2005).

[34] P. Panayotaros, *Continuation of normal modes in finite NLS lattices*. Physics Letters A 374, 3912–3919 (2010).

[35] Kenichiro Aoki, *Stable and unstable periodic orbits in the one-dimensional lattice ϕ^4 theory*. Phys. Rev. E 94, 042209 (2016).

[36] J-G. Caputo, I. Khames, A. Knippel and P. Panayotaros, *Periodic orbits in nonlinear wave equations on networks*. J. Phys. A: Math. Theor. 50, 375101 (2017).

[37] J-G. Caputo, I. Khames and A. Knippel, *On graph Laplacians eigenvectors with components in* $\{1, -1, 0\}$, submitted article (2018). http://arxiv.org/abs/1806.00072

[38] ISGCI: Information System on Graph Classes and their Inclusions. "List of Small Graphs". http://www.graphclasses.org/smallgraphs.html

E. W. Weisstein, *Graph theory*, MathWorld.
http://mathworld.wolfram.com/topics/SimpleGraphs.html

[39] James D. Meiss, *Differential Dynamical Systems*. SIAM (2007).

[40] The Mathworks, www.mathworks.com

[41] M. Abramowitz and I. A. Stegun, *Handbook of Mathematical Functions*. New York: Dover (1965).

[42] E. L. Ince, *Ordinary differential equations*. New York, Dover Publications (1956).

[43] Andrei V. Frolov, *Non-linear Dynamics and Primordial Curvature Perturbations from Preheating*. Classical and Quantum Gravity 27(12):124006 (2010).

[44] G. M. Chechin and D. S. Ryabov, *Stability of nonlinear normal modes in the Fermi-Pasta-Ulam β chain in the thermodynamic limit*. Phys. Rev. E 85, 056601 (2012).

[45] T. Bountis, G. Chechin, and V. Sakhnenko, *Discrete symmetry and stability in Hamiltonian dynamics*. Int. J. Bif. Chaos 21, 1539 (2011).

[46] M. Fiedler, *A property of eigenvectors of nonnegative symmetric matrices and its application to graph theory*. Czech Math. J. 25, 619-633 (1975).

[47] R. Merris, *Laplacian graph eigenvectors*. Linear Algebra and its Applications 278, 221-236 (1998).

[48] J-G. Caputo and A. Knippel, *On graph Laplacians with eigenvectors having zero entries*, working paper (2018).

[49] R. Faure, B. Lemaire et C. Picouleau, *Précis de recherche opérationnelle : Méthodes et exercices d'application*. Collection: Sciences Sup, Dunod (2014).

[50] J. J. Molitierno and M. Neumann, *On trees with perfect matchings*. Linear Algebra and its Applications 362, 75-85 (2003).

[51] S. Barik , A. K. Lal and S. Pati, *On trees with Laplacian eigenvalue one*. Journal Linear and Multilinear Algebra, Vol.56, No.6, 597-610 (2008).

[52] H. S. Wilf, *Spectral bounds for the clique and independence numbers of graphs*. Journal of Combinatorial Theory, Series B 40, 113-117 (1986).

[53] D. Stevanović, *On ± 1 eigenvectors of graphs*. Ars Mathematica Contemporanea Vol 11, No 2, 415-423 (2016).

[54] Jan A. Sanders, Ferdinand Verhulst and James Murdock, *Averaging Methods in Nonlinear Dynamical Systems*. Springer (2007).

[55] F. Martinez-Farias and P. Panayotaros, *Breather solutions for inhomogeneous FPU models using Birkhoff normal forms*. Physica D 335, 10-25 (2016).

[56] I. Percival and D. Richards, *Introduction to Dynamics*. Cambridge: Cambridge University Press (1982).

[57] M. V. Bartuccelli, A. Berretti, J. H. B. Deane, G. Gentile and S. A. Gourley, *Selection rules for periodic orbits and scaling laws for a driven damped quartic oscillator*. Nonlinear Analysis: Real World Applications 9, 1966-1988 (2008).

[58] J-G. Caputo, I. Khames, A. Knippel and A. B. Aceves, *Localized solutions of nonlinear wave equations on networks*, submitted article (2018). https://arxiv.org/abs/1804.07628

[59] Y. S. Kivshar and M. Peyrard, *Modulational instabilities in discrete lattices*, Phys. Rev. A 46 3198-3205 (1992); Y. S. Kivshar, *Localized modes in a chain with nonlinear on-site potential*, Physics Letters A, volume 173, Issue 2, 172-178 (1993).

[60] A. B. Aceves and J-G. Caputo, *Mode dynamics in nonuniform waveguide arrays: A graph Laplacian approach*. Journal of Optics, Volume 16, Issue 3, article id. 035202 (2014).

[61] D. Cvetkovic, M. Doob, H. Sachs, *Spectra of Graphs*. Academic Press, New York (1979).

[62] J. Guckenheimer and P. Holmes, *Nonlinear Oscillations, Dynamical Systems, and Bifurcations of Vector Fields*. Springer (1983).

[63] R. K. Dodd, J. C. Eilbeck, J. D. Gibbon and H. C. Morris, *Solitons and nonlinear wave equations*. Academic Press, New York, 1982.